E.O. Paton Electric Welding Institute of the National Academy of Sciences of Ukraine

International Scientific-Technical and Production Journal

The Paton WELDING JOURNAL

Issue 01 2019

Published Monthly Since 2000

English translation of the monthly «Avtomaticheskaya Svarka» (Automatic Welding) journal published in Russian since 1948

Founders
E.O. Paton Electric Welding Institute, NASU
International Association «Welding»

Publisher
International Association «Welding»

Translators
A.A. Fomin, O.S. Kurochko, I.N. Kutianova
Editor
N.G. Khomenko
Electron galley
D.I. Sereda, T.Yu. Snegiryova

Address
E.O. Paton Electric Welding Institute,
International Association «Welding»
11 Kazimir Malevich Str. (former Bozhenko Str.),
03150, Kyiv, Ukraine
Tel.: (38044) 200 60 16, 200 82 77
Fax: (38044) 200 82 77, 200 81 45
E-mail: journal@paton.kiev.ua
www.patonpublishinghouse.com

State Registration Certificate
KV 4790 of 09.01.2001
ISSN 0957-798X
DOI: http://dx.doi.org/10.15407/tpwj

Subscriptions
$384, 12 issues per year,
air postage and packaging included.
Back issues available.

CONTENTS

SCIENTIFIC AND TECHNICAL

INDUSTRIAL

NEWS

INFORMATION

DOI: http://dx.doi.org/10.15407/tpwj2019.01.01

ON THE PROBLEM OF CONTACT ELECTRIC RESISTANCE OF DIFFERENT-SIZED SURFACES

D.M. KALEKO
E.O. Paton Electric Welding Institute of the NAS of Ukraine
11 Kazimir Malevich Str., 03150, Kyiv, Ukraine. E-mail: office@paton.kiev.ua

The theory of electric contacts assumes an experimentally-verified inverse proportionality of electric transient resistance to applied load. The paper shows that this condition is not fulfilled at small compression forces of different-sized contacts, which take place, in particular, in excitation of electric arc by contact or breakup of thin conductor. Measurements of electric resistance of near-contact area between thin (0.75 mm diameter) conductor and sheet of steels St37 (steel 10) and 1.4301 (08Kh18N10), brass CuZn37 (L63) and aluminium alloy AlMg3 (AMg3) showed that there is an increase of electric resistance due to elastic deformation of contact surface under the effect of local load at the rise of force to specific limits. Under experimental conditions the boundary force was equal to 2–3 daN, depending on the mechanical characteristics of metal. Beyond these limits a generally accepted functional dependence becomes effective. 12 Ref., 1 Table, 8 Figures.

Keywords: *transient electric resistance, electric contacts, elastic deformation, stud welding*

Role of contact resistance as a nonlinear element of electric circuits is very large and extensive literature is devoted to it. A fundamental source is the book by R. Holm [1], in which the contact region is considered as that of electric current contraction, determined by the real area of surfaces coming into electric contact. Here, considering that roughness microprotrusions on the contacting surfaces have random distribution of height, it is assumed that they are plastically deformed under the impact of applied load, and, thus, the real area of contacting surfaces is determined by the compression force and mechanical characteristics of contact materials.

All the works related to study of transient resistance in electric contacts [1], electric resistance at resistance welding [2], development of physical contact at cold [3] and diffusion welding [4], as well as in mechanical engineering [5], consider the contact between flat (or spherical and cylindrical [1]) surfaces under the conditions of plastic deformation of the surface of an absolutely rigid body.

Considering the deformation of microprotrusions of various shapes, one of the surfaces is considered to be smooth and undeformable. Otherwise it would be necessary to take into account the probabilistic nature of conditions on the contact surface. By the data of work [5], the pitch of microroughnesses, which make up the roughness in their totality, changes from 2 up to 800, and their height varies from 0.03 up to 400 μm. At modeling attempts the real pattern is approximated by spherical, conical, pyramidal and prismatic protrusions, and their actual distribution over the surface is replaced by a scheme, where the notions of «contour» and «apparent» area are introduced. As is shown in work [6], the contour area is equal to 5–10 %, and the actual one is to 0.01–0.1 % of the nominal one.

At the same time, the indeterminateness of microprotrusion geometry and their topography, of randomness of unevenness meeting on the mated surfaces, and of their deformation conditions respectively makes any strict scheme unreal. The only proven by practice conclusion from the numerous models comes down to proportionality of the contact area and electric transient resistance to the applied load $1/P^{\alpha}$, where P is the force of compression of the contacting surfaces, and α is the empirical coefficient varying within 0.3–0.8. It follows from here that the contact electric resistance is independent on the apparent area of contact, i.e. on pressure, applied to the contacting surfaces. As will be shown below, this is valid only at relatively high loads, when elastic deformation in the contact area has been exhausted.

Review of attempts to derive a formula for calculation of contact resistance [7] showed the inapplicability of the known formulas without additional experiment.

Unlike the studied conditions of contacting of solids, at arc excitation by a melting thin conductor, which is in place in arc welding [8], and arc-contact stud welding, as well as at resistance spot welding, the shape of the contacting surfaces in electrode-part contact is characterized by a great difference of the areas of interacting surfaces and of their texture.

This aroused interest in the study of functional dependence of transient electric resistance on the applied force under the conditions, different from those studied earlier, namely, in contact of surfaces different in size.

To study the influence of load on electric resistance in the field of contacting, it turned out to be rational to use the method of arc-contact stud welding as the base. This is due to mass production of studs of an original shape, having a thin protrusion on the welded end. Studs are made by cold heading and that is why the scatter of protrusion diameters and their lengths is practically absent in one batch.

In arc-contact capacitor-type stud welding by the «preliminary contact» method, the process starts from the stud contacting the sheet (Figure 1), as the name suggests, without switching on the capacitor discharge current. Then discharge current is switched on, heating of the thin protrusion starts right up to its breakup with subsequent transition of the process to the arc stage. Such a process is realized with application of a welding gun with an adjustable force of stud pressing down within 1–10 daN.

Experiments were conducted in a device, consisting of a post, with RMK-2 welding gun fastened on it (Figure 2, *a*). As the stud is pressed to the sheet by the welding gun spring, the extension of the protrusion edge relative to the plane of gun supports is kept constant on the level of 2 mm. Resistance was measured by microhmmeter of GOM-802 type with 10 μOhm accuracy. Here, the instrument probes were located as shown in Figure 2, *b*. Resistance of sheet area between stud contact and measuring probe was equal from 61 μOhm (brass L63) to 130 (alloy AMg3).

Experiments (Figure 3) were conducted with M6 studs and sheets from steels St35 (steel 10) and 1.4301 (steel 08Kh18N10), brass CuZn37 (L63), aluminium alloy AlMg3 (AMg3), manufactured by Heinz Soyer Bolzenschweisstechnik GmbH Company. Here, 3 samples from one batch of the respective material were taken.

A characteristic feature of the change of contact resistance, noted by us at load increase, is the difference from the above inversely proportional dependence, namely, increase of the resistance at increase of compression force from 1 to 2–3 daN. Here, as shown by comparison of the graphs, the relative increment of resistance is the greater the higher the hardness of the stud material* and the sensitivity to work hardening at stud manufacturing by cold heading. The latter pertains to steel 1.4301 and two-phase brass CuZn37 [9].

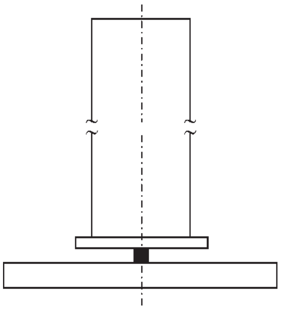

Figure 1. Scheme of the initial stage of the process of stud welding with preliminary contact

For stainless steel the maximum of resistance shifted to the 3 daN mark, whereas for other metals it is on the level of 2 daN (allowing for discreteness of sample compression force).

From the works known to us, only in paper [10] it is shown (Figure 4) that in electrode-part contact at spot welding the electric resistance first grows at increase of compression force, and starts decreasing only after a certain load has been achieved. Here, the dependence was obtained for aluminium alloy. Therefore, in materials characterized by higher elastic resistance than that of aluminium alloys, it was to be expected that this effect will be even more pronounced.

Qualitative increase of contact resistance can be explained, taking into account the difference in the textures of contacting samples (Figure 5). As shear modulus $G = \frac{E}{2(1+\vartheta)}$, where E is the Young's modulus, and ϑ is the Poisson's ratio, having a positive value in metals, it is clear that at elastic compression of parts, having mutually perpendicular texture, the first to deform is the part having a texture, normal relative to the load direction. Here, a gap forms and the area of loaded part contact becomes smaller, and electric resistance grows, accordingly.

Solution of the problem of elastic deformation of a semi-infinite body under the impact of pressure P, uniformly distributed over the end plane of a cylinder of radius r, is given in [11]. Assuming flatness of the contacting surfaces on the micro- and macrolevel, i.e.

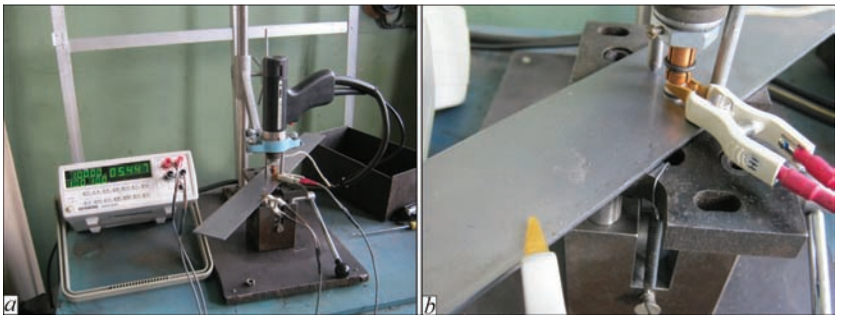

Figure 2. General view of the device (*a*) and arrangement of the probes of GOM-802 instrument (*b*) at measurement of electric resistance of the contact region of a 0.75 mm dia protrusion on the stud and the sheet

*Normed hardness values of steel 10–1170 MPa (GOST 4041), steel 08Kh18N10 — 1700 MPa (GOST 25054), brass L64 — 700 MPa (GOST 13726), alloy AMg3 — 450 MPa (GOST 2208)

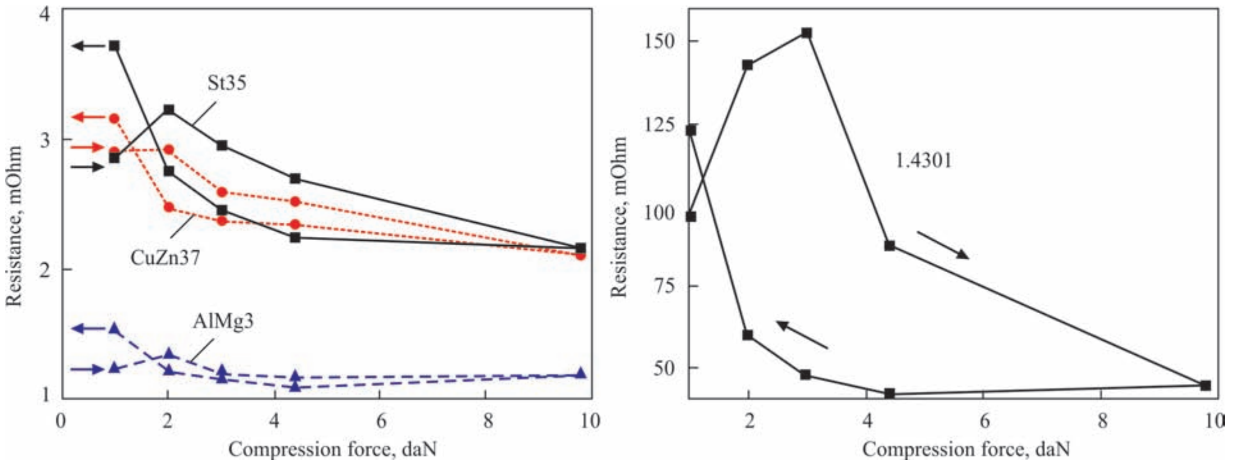

Figure 3. Dependence of electric resistance of the contact zone between the protrusion of 0.75 mm diameter and the sheet on the applied compression force at different scales

absence of their initial loose fit and impact of just the forces normal to the interface, as well as, in keeping with the above remarks, absolute rigidity of the cylinder, the equation of elastic movement of the surface of a semi-infinite body under load within the loaded surface is as follows:

$$u_z = \frac{4(1-\vartheta^2)}{\pi E} \Pr E\left(\frac{R}{r}\right),$$

where $E(R/r)$ is the full elliptic integral of the 2nd kind modulo (R/r), tabulated in [12].

This equation does not allow for movement of a rigid cylinder following the deformation of a plate outside the loaded region in such a way that the outer circumference of the cylinder base rests continuously on the plate.

Calculation of deformation in the central meridional plane of the studied metals, the characteristics of which are given in the Table, yields the value of deviation from the sheet plane (gap between the contacting surfaces), shown in the graphs (Figure 6). This Figure, of course, is just illustrative, as the structural changes in the sheet material at rolling were not taken into account in calculations, in particular, strengthening of the metal surface layer, and a purely elastic and only normal interaction of the compressed surfaces was assumed (we neglected the tangential stresses in this idealized scheme). This is justified by the fact that the protrusion does not have a sharp edge at cold heading (see Figure 7 below), stress concentration on the edge and its plastic deformation at small loads are absent, respectively. Considering what was said about the outer boundary of cylindrical contact resting on the edges of the deformation pit on the sheet, the final values of the gap between the contacting surfaces should be reduced.

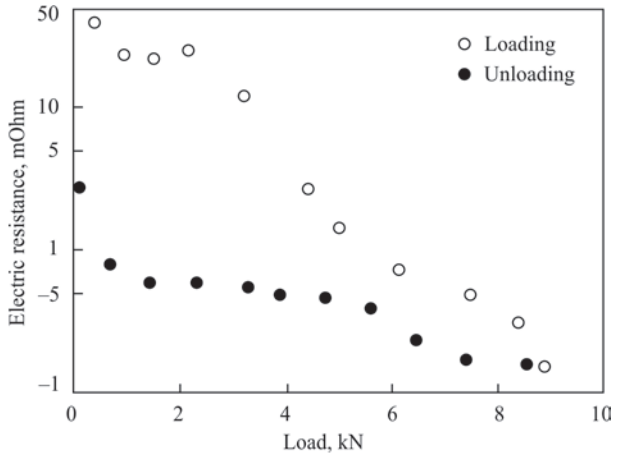

Figure 4. Dependence of electric resistance on the load in the contact of electrode-part from aluminium alloy 5482 in as-delivered condition. Electrode diameter is 7.5 mm [10]

With load increase deformation goes from purely elastic one into the elastoplastic region. This is noticeable from comparison of graphs in Figures 3 and 6 and the remark given above at analysis of graphs in Figure 3.

Note also that at low pressures just the surface layer of the compressed metal is deformed and, judging by the photos of metal cross-section after load, given in the above-cited work [10], the roughness microprotrusions at initial loading do not change their shape and do not affect the change of contact zone resistance.

With load increase, ever deeper-lying layers of sheet metal are involved in shear deformation, causing increase of reactive stress. When this stress reaches a certain level, dependent on elastic characteristics of metal and degree of its work hardening, first elastic and then plastic deformation of roughnesses starts at the protrusion end face. Such a behaviour of metal in

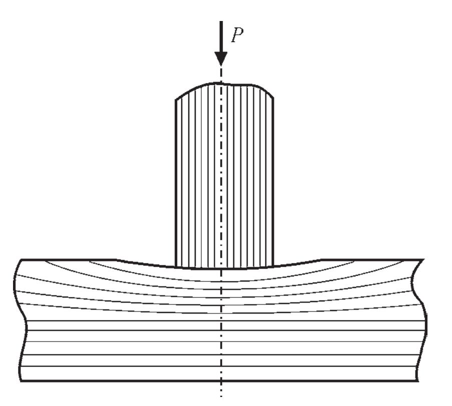

Figure 5. Scheme of loading of the contact of stud protrusion with the sheet

Characteristics of elastic properties of the studied materials

Metal	Modulus of elasticity, MPa	Poisson's ratio [6]
Steel 10 [5]	206	0.24–0.28
08Kh1810T [5]	196	0.25–0.30
Brass L63 [7]	100	0.33–0.42
Alloy AMg3 [7]	71	0.32–0.36

the contact influences lowering of contact resistance, when exceeding the respective boundary compression force (Figure 3). Plastic deformation results in drawing together of contacting surfaces and greater contact area at coincidence of their shape.

Further analysis of graphs in Figure 3 shows the presence of hysteresis, which is the greater, the lower the ductility of the studied metal. Hysteresis is indicative of the elastic nature of behaviour of near-contact zone metal at unloading. At load dropping below 4.5 daN, the electric resistance grows as a result of elastic change of the surface with appearance (or preservation) of second level roughnesses [2]. At final unloading (in our case to 1 daN), the electric resistance of the contact area turns out to be higher than the initial one for all the samples.

Analysis of the final shape of the protrusion contact surface at the stud end face was conducted in order to clarify the increase of contact resistance above the initial one after the loading-unloading cycle. For this purpose M4 stud with a protrusion ($d \times h$ = 0.55×0.65) was loaded by 10 daN force by the spring of RMK-2 gun. Studs were selected randomly from one batch of each materi-

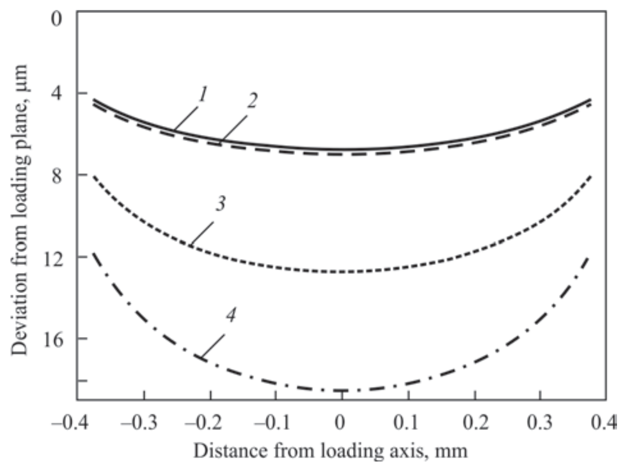

Figure 6. Deformation of sheet plane under the pressure of the protrusion on M6 stud with 2 dN force: *1* — carbon steel 10; *2* — 08Kh18N10T; *3* — brass L63; *4* — alloy AMg3

al. The end face was photographed from the eyepiece of MBS-10 microscope at 56.3 magnification (Figure 7).

The presented photographs show that the initial relief obtained at cold heading of studs, changed after loading and subsequent unloading, becoming rougher as a result of plastic deformation, accompanied by material shifting, because of uncontrolled deviation from parallelism of the contacting surfaces and the thus caused appearance of tangential stresses. Judging by curves in Figure 3 and photos in Figure 7, such a plastic change of near-contact volume occurs at the loading stage, and the work-hardened metal is elastically deformed, restoring its shape at unloading. This is exactly what explains the fact that in all the exper-

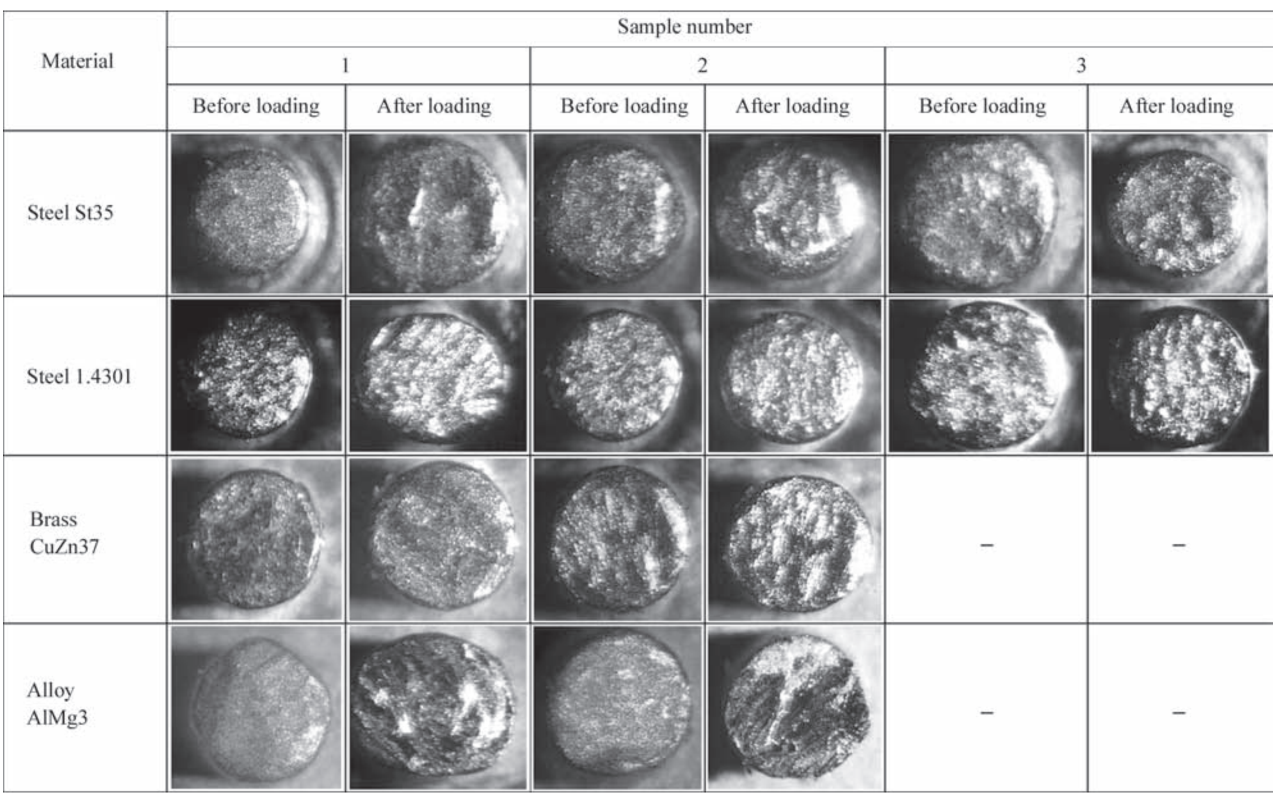

Figure 7. Shape of the protrusion contact surface before and after loading by 10 daN force

iments the contact zone resistance after unloading is greater than before loading.

An essential influence of plastic deformation on contact region resistance is demonstrated by Figure 8, which shows the change of electric resistance of the contact region at loading of M3 and M6 studs from steel 1.4301 with protrusion diameters of 0.6 (M3) and 0.75 (M6) mm, respectively. Pressure in the contact between the protrusion at the stud end face and the sheet at loading of M3 stud is 1.5 times greater, than at loading of M6 studs. As a result, plastic deformation in the near-contact region occurs at a lower force at loading of M3 stud, than at loading of M6 stud, and no above-mentioned increase of electric resistance at initial loading of the protrusion on M3 stud is observed in the graph. At 5–10 daN loading the graphs for M3 and M6 studs practically coincide. Therefore, here, the higher pressure on the protrusion of M3 stud results in the actual contact area due to plastic deformation being comparable to that of M6 stud, and the dependence of transient resistance on load being independent on the nominal contact area and following the inverse proportionality law, in keeping with the above Holm formula. On the other hand, the higher pressure and the thus caused strengthening, leads to the elastic component of deformation of the contacting surface on M3 stud being higher than that on M6 stud. This is indicated by the discrepancy of the graphs at relieving of the load from the above-mentioned 4.5 daN.

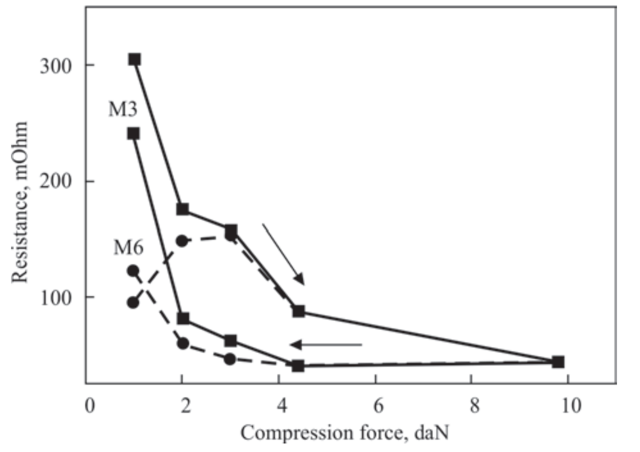

Figure 8. Dependence of electric resistance of the zone of contact between the protrusions of 0.6 (M3) and 0.75 mm (M6) diameter and sheet of steel 1.4301 on the applied compression force

Conclusions

1. The known inversely proportional dependence of electric contact resistance on the compression force of current-supplying surfaces is disturbed in the region of small forces, applied in the contact of areas of different size. A hypothesis was proposed about taking into account in this case not so much the plastic deformation of the contacting surfaces, but rather the elastic deformation of the surface layer of one of the elements under the impact of the load, distributed over the region of this surface limited by the area of the second element of the contacting pair.

2. At small compression forces of different-sized contacts, occurring, in particular, at excitation of the arc by touching or by exploding thin conductor, load increase leads to increase of electric contact resistance, as a result of elastic deformation of the surface and appearance of a local gap between the contacting surfaces, commensurate with the height of microroughnesses on the contacting surfaces. This results in decrease of the area of electric contact and increase of its electric resistance without current interruption.

3. Boundary value of load, at which the functional dependence of transient electric resistance of different-sized contacts from the applied force becomes inversely proportional, and the nominal current-conducting area looses its influence, depends on mechanical characteristics of material and the more the higher are its elastic properties.

4. At variation of the load from the maximum to minimum one, the inversely proportional dependence of electric transient resistance on the compression force of the current-carrying surfaces is preserved. But here plastic deformation of the contact interface at the loading stage leads to increase of its electric resistance at minimum compression force compared to the initial one.

5. Additional research specifying the dependence of electric resistance of different-sized contacts on mechanical properties of material and the ratio of areas of the contacting surfaces is of interest.

1. Holm, R. (1961) *Electric contacts*. Moscow, IL [in Russian].
2. Kochergin, K.A. (1972) *Pressure welding*. Leningrad, Mashinostroenie [in Russian].
3. Sakhatsky, G.V. (1979) *Technology of cold welding*. Kiev, Naukova Dumka [in Russian].
4. Karakozov, E.S. (1986) *Pressure welding of metals*. Moscow, Mashinostroenie [in Russian].
5. Demkin, N.V., Ryzhov, E.V. (1981) *Quality of surface and contact of machine parts*. Moscow, Mashinostroenie [in Russian].
6. Kragelsky, I.V., Dobychin, N.M., Kombalov, V.S. (1977) *Principles of calculation for friction and wear*. Moscow, Mashinostroenie [in Russian].
7. Slobodyan, M.S. (2013) Analysis of procedures for evaluation of electric resistance of electrode-electrode and part-part areas before spot resistance microwelding. *Svarochnoye Proizvodstvo*, **8**, 20–24 [in Russian].
8. Leskov, G.I. (1970) *Electric welding arc*. Moscow, Mashinostroenie [in Russian].
9. Askeland, D.R., Fulay, P.P., Wright, W.J. (2011) *The science and engineering of materials*. Cengage Learning.
10. Thornton, P.H., Krause, A.R., Davies, R.G. (1996) Contact resistance in spot welding. *Welding J.*, **12**, 402–412.
11. Johnson, G.L. (1989) *Mechanics of contact interaction*. Moscow, Mir [in Russian].
12. Yanke, E., Emde, F., Lyosh, F. (1977) *Special functions. Formulas, plots, tables*. Moscow, Nauka [in Russian].

Received 26.08.2018

DOI: http://dx.doi.org/10.15407/tpwj2019.01.02

RESTORATIVE HEAT TREATMENT OF STEAM PIPELINES AND THEIR WELDED JOINTS (REVIEW)

V.V. DMITRIK[1], **E.S. GARASHCHENKO**[1], **A.V. GLUSHKO**[1], **V.N. SOKOLOVA**[2] and **T.A. SYRENKO**[1]
[1]NTU «Kharkiv Polytechnic Institute»
2 Kirpicheva Str., 61002, Kharkiv, Ukraine
[2]Kharkiv Heat and Power Plant-3
3 Energeticheskaya Str., 61036, Kharkiv, Ukraine. E-mail: svarka126@ukr.net

The state and key directions of development of technologies for restorative heat treatment of steam pipeline welded joints are considered. The technologies of heat treatment and their advantages and disadvantages are presented. The first part of the review presents a summary of the development of restorative heat treatment. The directions of development of restorative heat treatment of welded joints, the most promising for extension of service life of steam pipelines according to the opinion of the authors, were formulated and justified. The justification of the possibility of using heat treatment of long-operating elements of steam pipelines with a degraded structure and presence of damages is given. The possibility of producing a metal of a steam pipeline with a structural state and properties, meeting the service requirements is justified. 23 Ref., 3 Figures.

Keywords: *restorative heat treatment, steam pipeline, welded joints, metal structure, operation, damageability*

Structural changes, taking place in the metal of steam pipelines of heat-resistant pearlite steels 15Kh1M1F and 12Kh1MF, operating for a long time under creep and low-cycle fatigue, lead to a decrease in its properties and a reduction in the service life. Welded joints of steam pipelines are characterized by the presence of a certain structural, chemical and mechanical heterogeneity, formed as a result of welding heating. The presence of heterogeneity provides a greater intensity of structural transformations in the metal of welded joints as compared with similar transformations of the base metal of steam pipelines. Accordingly, the service life of metal of welded joints of steam pipelines is limited by structural transformations, taking place in their metal.

During the long process of operation of steam pipelines (more than 250 thou h) under creep conditions, their initial structure, recommended by standard documentation [1–3], turns into a ferrite-carbide mixture. At the same time, the metal is damaged by creep pores and fatigue cracks. Structural changes in the metal of the heat-affected-zone (HAZ) regions of welded joints, as well as its damageability, occur with the greater intensity than similar changes and damageability of the weld metal and base metal. Structural changes and damageability are more typical to certain HAZ regions of welded joints of steels 15Kh1M1F and 12Kh1MF [4, 5]: partial recrystallization, where the new products of austenite decay present a globular pearlite (Figure 1); overheating, where the number of austenitic grain is less than 5th (GOST 5639–82); fusions, where relatively large ferrite grains can be formed, grouped in chains, arranged symmetrically to the weld metal (Figure 2).

In connection with the constantly increasing number of steam pipelines having a degraded structure, as well as a certain degree of damageability, it is important to use a restorative heat treatment (RHT) to extend their service life [7–13]. The use of RHT can provide restoration of the degraded structure and properties to a level close to the initial state, as well as eliminate the damageability, formed by the creep mechanism.

The aim of the work is to clarify the possibility of using RHT for long-operating elements of steam pipelines with different degree of degradation of the structure and a certain level of damageability, to obtain their structural state and properties, which meet the operational requirements.

Replacement of steam pipelines, having a degraded structure and damages, by new ones, is a very laborious and expensive operation. In some cases, such an operation can be prevented by using local RHT. When performing RHT, it is necessary to take into account the peculiarities of the distribution of stresses formed during releasing the support-suspension system [14].

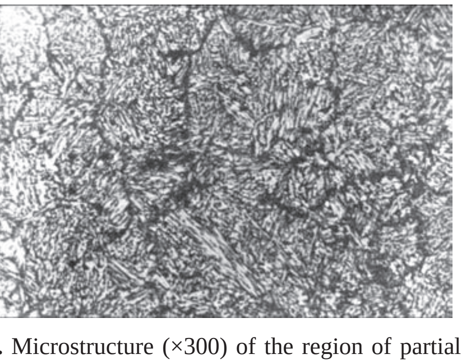

Figure 1. Microstructure (×300) of the region of partial recrystallization of HAZ metal of welded joint of steel 15Kh1M1F [6]

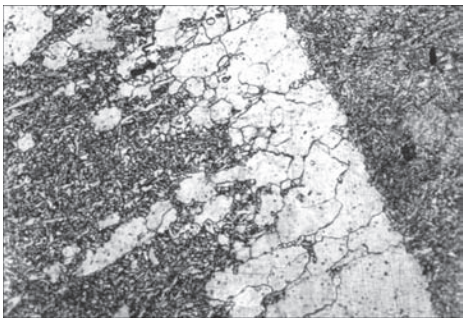

Figure 2. Microstructure (×100) of the region of fusion of the HAZ metal of steel 15Kh1M1F [5] welded joint

To optimize the performance of RHT, it is advisable to consider the features of structural changes, occurring in the metal of steam pipelines, operating for a long time under creep conditions. The transformation of the initial structure into ferrite-carbide mixture provides physical and chemical processes, taking place at different intensity in the metal of HAZ regions of welded joints and at a constant (less intensive) one in the weld metal and in the base metal of the steam pipelines. Physicochemical processes can be represented by the sequence of passing their stages [15–17]: diffusion movement of chromium and molybdenum from central zones of α-phase crystals to their near-boundary zones, which leads to the formation of segregations; transition of chromium, molybdenum, and vanadium from crystals of α-phase into carbides, as well as the formation of new carbides of group II (Mo_2C and VC); running of carbide reactions $M_3C \rightarrow M_7C_3 \rightarrow M_{23}C_6$; coagulation of carbide phases, mainly $M_{23}C_6$ and M_7C_3; formation of discontinuous chains, mainly from carbides $M_{23}C_6$ along the grain boundaries of α-phase; formation of polygonal structure (areas of overheating and partial recrystallization of HAZ); local elimination of grain boundaries (initial stage of recrystallization); coalescence of vacancies, nucleation and development of creep pores; separation of grain boundaries from carbides; initiation and propagation of fatigue microcracks.

Operation of power units in the maneuverable mode is characterized by the presence of variable (cyclic) stresses, as well as the presence of local regions of their concentrations. For example, in backing rings of joints, being butt welded; in places of contact of

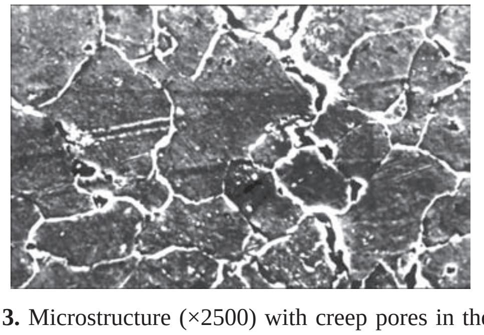

Figure 3. Microstructure (×2500) with creep pores in the structure of the region of partial recrystallization of the HAZ metal of steel 15Kh1M1F [21] welded joints

steam pipelines of different thicknesses; in the region of HAZ fusion (inner surface of steam pipeline); in places of lacks of penetration, lacks of fusion along the walls of a gap, etc.

Structural changes lead to a decrease in strength and impact toughness of the metal of steam pipelines. In the process of long-term operation under creep conditions, deformation processes occur, which are interconnected with structural transformations, for example, such as formation of a subgrain structure, increase in the density of dislocations near obstacles, etc. It is known that deformation processes are associated with the formation of creep pores [18], which requires further clarification.

In the process of RHT (normal mode), the pores, having a diameter of less than 2 mm, are eliminated (healed) [7–13]. It is noted that in the presence of accumulation of damageability of higher than 20–25 % of the state of fracture, applying RHT, heat resistance of the elements of steam pipelines increases insufficiently. The healing of pores as a result of diffusion of substitution and interstitial elements occurs under the influence of the following factors: temperature of isothermal exposure in the austenitic state; exposure duration; polymorphic transformations. It is advisable to reveal the shape and limiting dimensions of creep pores and fatigue cracks, which can be eliminated using RHT.

The double normalization proposed by P.A. Antikain [19, 20] deserves attention: the first one is at a temperature of $T \geq 1050–1100$ °C, which provides elimination of relatively large pores and homogenization of γ-phase; the second one is at the temperatures recommended by standard documentation and used for treatment of steels in the initial state, which allows increasing the number of austenitic grain.

High-temperature cyclic thermal treatment (HCHT), which provides a multiple cyclic heating above the temperature of polymorphous transformation and subsequent cooling, requires clarification. It is also advisable to study the peculiarities of healing pores located over the body and along the boundaries of α-phase grains, as well as to clarify how healing of pores is associated with the segregation of chromium and molybdenum.

Heating and corresponding exposure above the critical point A_{c3} provides the decay of carbides of I and partially II groups. The reverse transition of alloying elements of chromium, molybdenum and vanadium occurs from carbides into crystals of the α-phase.

It is advisable to clarify: how the exposure at the temperatures above A_{c3} is associated with the austenitic grain size; influence of the exposure duration on the homogeneity of austenitic grains, i.e., the uniform distribution in the γ-phase of the substitution and interstitial elements; how the heat treatment provides elimination of creep pores, having a rounded and branched shape, shown in Figure 3; effect of RHT on fatigue cracks.

A considerable practical interest is represented by restorative heat treatment of welded joints. As is noted above, the structural transformations and damageability of welded joints occur most intensely in the regions of fusion, overheating, and partial recrystallization of their HAZ [4, 5].

The metal of the region of partial recrystallization is subjected to welding heating during manufacture of joints in the temperature range of A_{c1}–A_{c3}. The region can have a lower hardness than in the other regions of HAZ, as well as weld metal and base metal. During long-term operation of welded joints, the hardness of the region of partial recrystallization decreases to a greater degree than the hardness of other HAZ regions, as well as that of weld metal and base metal [6, 18, 21]. The structure of the partial recrystallization region can represent the globularized pearlite as a rejection component [4, 5]. Double RHT, as well as HCHT, provide a more complete elimination of rejection structures and damageability, caused during welding in the HAZ, as well as in the weld metal regions [7–15, 22, 23]. Double normalization and tempering [8] deserves attention when using heat treatment, which provides the possibility of relatively complete elimination of structural, chemical and mechanical heterogeneity, as well as dispersion strengthening of welded joint metal. It is urgent to establish the possibility of induction heating during heat treatment of steam pipelines, including their welded joints without dismantling the steam pipelines themselves. The improvement of heat treatment of steam pipelines, having a degraded structure and a certain level of damageability, will allow obtaining the structural state of their metal and properties, meeting the operational requirements, which will provide an increase in their service life.

Conclusions

It was found that for introduction of restorative heat treatment of metal of steam pipelines and their welded joints, having a degraded structure and a certain damageability, it is necessary to investigate:

• effect of heating on the value of austenitic grain;

• relationship between the heating and homogeneity of the austenitic structure, as well as dependence of structural state on heating;

• possibility of elimination of creep pores of a certain size and shape applying heat treatment.

1. (2003) *Standard instruction on control of metal and extension of metal life of basic components of boilers, turbines and pipelines of thermal power plants* (RD 10-577-03). Moscow, GUP NTTs, Gostekhnadzor Rossii [in Russian].
2. (2004) *Instruction on examination procedure and extension of service life of steam pipelines extending beyond economic life* (SO 153-34.17.470). Moscow, TsPTI ORGRES [in Russian].
3. (2003) *Instruction on restorative heat treatment of components of heat power equipment* (SO 153-34.17.459–2003). Moscow, Minenergo RF [in Russian].
4. Dmitrik, V.V., Baumer, V.N. (2007) Carbide phases and damageability of welded joints in long-term operation. *Metallofizika, Novejshie Tekhnologii*, **7**, 937–948 [in Russian].
5. Dmitrik, V.V., Bratash, S.N. (2010) On damageability of welded joints of steam pipelines by creep mechanism. *Ibid*., 32(2), 1657–1663 [in Russian].
6. Dmytryk, V.V., Syrenko, T.A., Bartash, S.N., Glushko, A.V. (2015) Specification of metal damageability mechanism of long-operated steam line welds. *Eastern-European J. of Enterprise Technologies*, 6(1), **78**, 13–18.
7. Gladshtejn, V.I., Ermolaev, V.V., Shklyar, A.I. et al. (2007) Restorative heat treatment of casing parts during turbine renovation. *Teploenergetika*, **4**, 8–12 [in Russian].
8. Khromchenko, F.A., Lappa, V.A. (1997) Life of welded joints of steam pipelines after restorative heat treatment. *Svarochn. Proizvodstvo*, **6**, 32–35 [in Russian].
9. Shvetsova, T.A., Krejtser, K.K. (2007) About experience of restorative heat treatment of steam pipelines and results of their subsequent operation. *Energetik*, **5**, 7–9 [in Russian].
10. Loskutov, S.A., Koryagin, Yu.D., Bukin, Yu.A. (2014) Optimization of structure and properties of long-operated metal of steam pipelines from 12Kh1MF steel by restorative heat treatment. *Vestnik YuUrGU. Seriya Metallurgiya*, 14(**4**), 45–51 [in Russian].
11. Trusov, L.P., Berezina, T.G., Bogatyrev, Yu.M. et al. (1973) Restoration of thin structure and properties of 12Kh1MF steel after long-term operation. *Problemy Prochnosti*, **1**, 67–71 [in Russian].
12. Ivanova, V.S., Antikajn, P.A., Sabitova, N.S. (1965) Healing of damages accumulated under cyclic overloads of steel. *Metallovedenie i Termich. Obrab. Metallov*, **1**, 7–9 [in Russian].
13. Shklyarov, M.I., Osmakov, V.N., Alekseev, S.V. et al. (1995) Extension of life of power equipment parts using restorative heat treatment. *Teploenergetika*, **4**, 2–7 [in Russian].
14. Popov, A.B., Chebotarev, O.M. (2003) Problems appearing in conducting of restorative heat treatment of steam pipelines. *Ibid*., **3**, 42–45 [in Russian].
15. Dolzhansky, P.R. (2005) Peculiarities of evaluation of life of steam line pipes under operation extending beyond economic life. *Ibid*., **8**, 35–39 [in Russian].
16. Dityashchev, B.D., Popov, A.B. (2007) Complex approach to determination of residual life of TPP steam pipelines. *Ibid*., **2**, 21–25 [in Russian].
17. Semenov, V.K., Belyaev, A.A. (2010) Prediction of amount of damages of pipeline systems and steam pipelines of TPPs. *Ibid*., **1**, 37–39 [in Russian].
18. Dmitrik, V.V., Glushko, A.V., Syrenko, T.A. (2018) Peculiarities of welded joints weakening in operating steam pipelines. *The Paton Welding J*., **5**, 7–11.
19. Antikajn, P.A. (1990) *Metals and strength calculation of boilers and pipelines*. Moscow, Energoatomizdat [in Russian].
20. Antikajn, P.A. (1977) Restorative heat treatment of welded joints of TPP steam lines. *Teploenergetika*, **10**, 34–38 [in Russian].
21. Glushko, A. (2016) Researching of welded steam pipe joints operated for a long time. *Eastern-European J. of Enterprise Technologies*, 1(**84**), 14–20.
22. Zislin, G.S., Kamenskaya, N.I., Shabal, V.N. et al. (1995) Restorative heat treatment of pipes of steam main at Cherepovetsky hydropower plant. *Teploenergetika*, **4**, 8–11 [in Russian].
23. Popov, A.B. (2002) Some peculiarities of technical support of restorative heat treatment procedures of steam pipelines. *Ibid*., **4**, 15–17 [in Russian].

Received 20.10.2018

DOI: http://dx.doi.org/10.15407/tpwj2019.01.03

STRENGTH AND FATIGUE LIFE OF JOINTS OF HIGH-STRENGTH ALLOY AA7056-T351, MADE BY ELECTRON BEAM WELDING

I.M. KLOCHKOV, V.M. NESTERENKOV, O.M. BERDNIKOVA and **S.I. MOTRUNICH**
E.O. Paton Electric Welding Institute of the NAS of Ukraine
11 Kazimir Malevich Str., 03150, Kyiv, Ukraine. E-mail: office@paton.kiev.ua

Application of modern aluminium alloys when designing elements and structures for aircraft and rocket construction, sea vessels and ground transportation, is ensured by high values of their strength and ductility. New welding technologies allow reducing the structure weight and lowering the operating costs, respectively, while providing the required values of strength and fatigue life. Here, producing sound welded joints of heat-hardenable aluminium alloys is an urgent science and technology problem. Application of welding technologies with a small temperature contribution, such as electron beam welding, compared to traditional welding processes, is promising for aircraft and rocket construction. The objective of this work is studying the level of softening, structural features, magnitude of residual postweld stresses, mechanical properties and regularities of fatigue resistance of joints of heat-hardenable aluminium alloy AA7056-T351 with higher zinc content, produced by electron beam welding. 8 Ref., 2 Tables, 5 Figures.

Keywords: *welded joints, fatigue resistance, residual stresses, aluminium alloy, electron beam welding*

Heat-hardenable aluminium alloys, owing to their high specific weight, considerable corrosion resistance, high values of fatigue resistance and fatigue crack growth, are widely applied for manufacturing components of carrier rockets and space vehicles, launch complexes, vessels, air and ground transportation, agricultural machinery, chemical equipment and other welded structures, which, as a rule, are operated under very complex conditions [1, 2].

At the current stage of development of subsonic and supersonic aviation, aluminium alloys are the main structural materials in aircraft construction [3]. Selection of the alloy for the structure is based on differentiated approach to operation of each component, allowing for its life, service loads, possibility of its heating and other requirements to the parts. Heat-hardenable high-strength aluminium alloys of 7xxx series (Al–Zn–Mg–Cu alloying system) are successfully used in aviation industry. They are the structural material for the wing, skin and inner structural elements of the airframe (spars, ribs, frames, etc.). Aluminium alloy AA7056 was developed as an alloy with characteristics of strength, corrosion resistance and fatigue life, improved relative to alloys AA7150 and AA7449. This alloy is used for manufacturing medium- and large-sized parts, such as upper panels of the wing in aircraft construction, which operate under alternating loading conditions. Modern welding technologies allow reducing the structure weight and lowering the operating costs, respectively, while providing the required strength and fatigue life values. The data on fatigue resistance characteristics of welded joints of AA7056 alloy are not available. Therefore, research in this direction is urgent, and producing a sound welded joint with high physico-mechanical properties is an important scientific and technological problem [4, 5].

Owing to high energy concentration in the electron beam, electron beam welding (EBW) allows producing welded joints with minimum dimensions of the HAZ and high weld depth-to-width ratio. EBW enables application of low heat input with small volume of pool molten metal and short-time thermal impact on the metal being welded. Application of a small amount of heat results in a marked reduction of item deformation. Welding in vacuum prevents saturation of the molten and heated metal by gases. As a result, a high quality of welded joints is achieved on such reactive metals and alloys as niobium, zirconium, titanium, molybdenum, etc [6].

The objective of this work is studying the level of softening, structural features, magnitude of residual postweld stresses, mechanical properties and regularities of fatigue resistance of EBW joints of heat-hardenable aluminium alloy AA7056 with higher zinc content.

High-strength aluminium alloy AA7056 (8.5–9.7 % Zn, 1.5–2.3 % Mg, 1.2–1.9 % Cu) was welded in heat-hardened condition T351. Plates of 12 and 30 mm thickness were EB welded in a vacuum chamber.

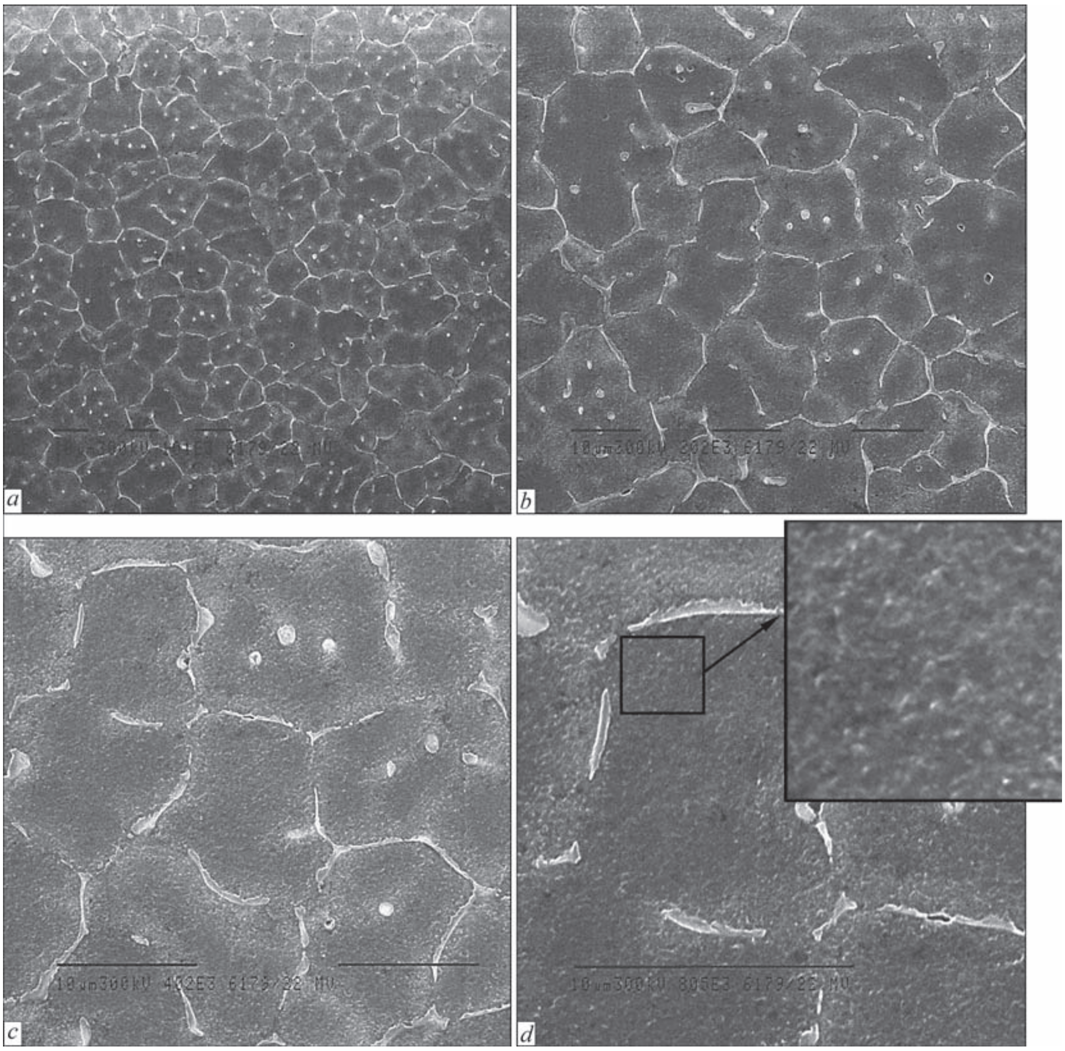

Figure 1. Metal structure of welded joint of alloy 7056-T351: *a* — ×1010; *b* — ×2020; *c* — ×4040; *d* — ×8080

EBW of specially prepared in keeping with the technological requirements plates of aluminium alloy AA7056-T351 12 and 30 mm thick was performed in UL-209M machine in vacuum. Computer-controlled UL-209M machine of PWI design is fitted with power unit based on ELA-60/60 and electron beam gun that moves in a vacuum chamber with internal dimensions of 3850×2500×2500 mm. Working vacuum was $3.54\cdot10^{-2}$ MPa in the chamber and $6.65\cdot10^{-3}$ MPa in the gun and was reached in 30 min. Electron beam gun with metal tungsten cathode together with the high-voltage power source ELA-60/60 provides the range of electron beam current I_b = 0–500 mA at accelerating voltage U_{acc} = 60 kW. The technology of EBW of aluminium alloy 7056-T531 was finalized using local scanning of the electron beam with up to 1000 Hz frequency and up to 4 mm amplitude.

Studying the structural features of butt welded joints of aluminium alloy 7056-T351 12 and 30 mm thick showed that the weld is characterized by uniform structure in absence of pores or cracks, the grains have an equiaxed shape with the size of 4–15 μm (Figure 1, *a*, *b*). Rather thin interlayers of phase formations (FF) 0.1–0.4 μm wide are observed on grain boundaries (Figure 1, *c*, *d*). Uniformly distributed disperse FF particles of 0.1–0.2 μm size are found in inner volumes of the grain structure and individual FF of larger size of 0.7–1.0 μm are also formed. Here, appearance of a substructural component is characteristic, the size of subgrains being 0.4–0.8 μm (Figure 1, *d*). At transition to the fusion line from the weld side, the grain structure practically does not change, and from the HAZ side — a banded structure with the same orientation forms, which is characteristic for base metal. Band width is 10–30 μm at FF increase to 2–3 μm (Figure 1). Thin FF interlayers up to 0.5 μm wide form on the boundaries of band component. Base metal is characterized by a structure with grain size of 6–10 μm at uniform orientation along the banded structure (up to 15 μm width) that forms under the conditions of directed deformation (rolling). Here, formation of a more fine-grained structure is also observed in the base metal. Thus, at EBW a uniform structure forms in the weld metal, fusion line and HAZ of welded

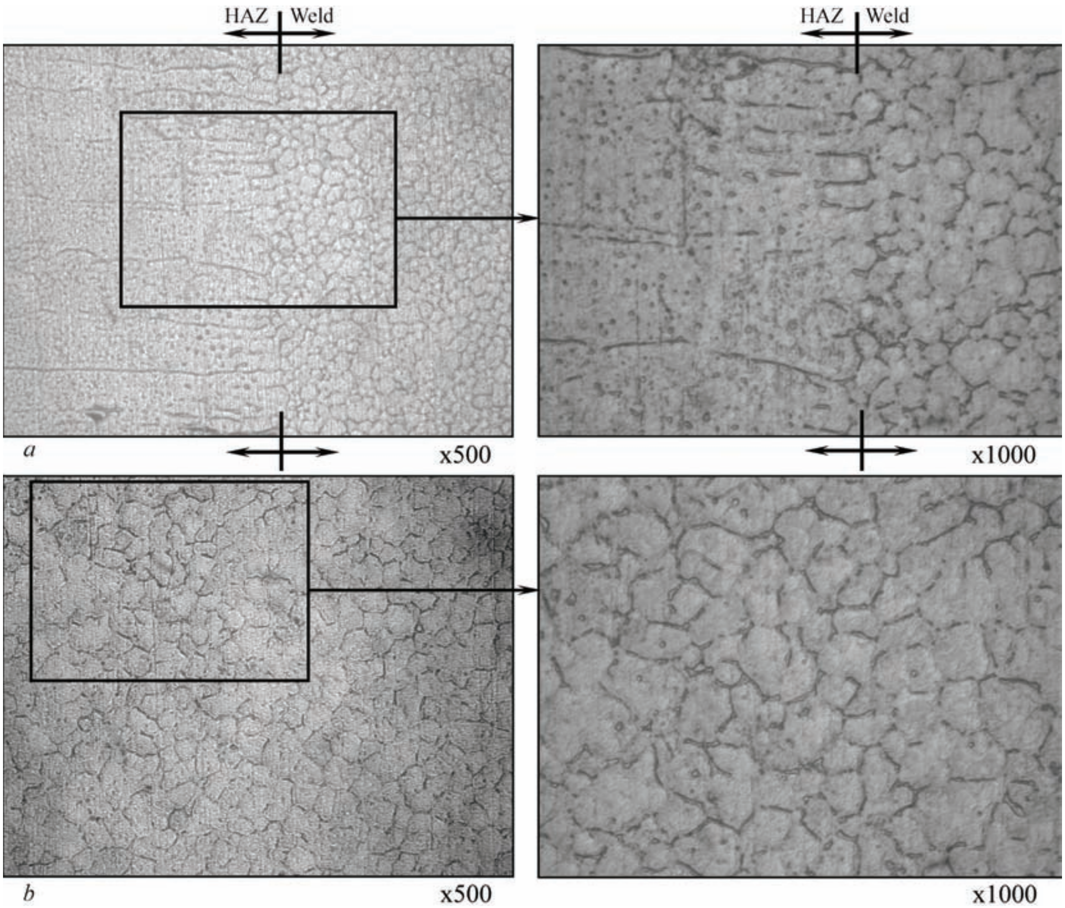

Figure 2. Microstructure of characteristic regions of the joint of alloy 7056-T351 in the fusion zone (*a*) and weld metal (*b*)

joints of aluminium alloy 7056-T351 at significant dispersion of both the grain structure and the phase formations. Pores or cracks are absent (Figure 2). In welding at nonoptimized modes considerable technological problems may develop, which are related to its increased proneness to formation of solidification cracks in the weld and partial melting of base metal grains. All these defects are due to structural and phase transformations, which proceed under the impact of thermal cycle in welding.

Degree of metal softening in the welding zone was assessed by the results of measurement of its hardness to GOST 9013–59 in Rockwell instrument with a steel ball of 1/16″ diameter and 600 N load. Figure 3 shows ball distribution in the welded joint of 7056-T351 alloy. Hardness of base metal of alloy AA7056-T351

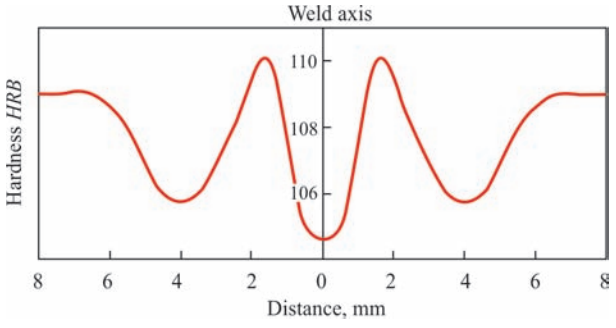

Figure 3. Metal hardness in welded joint of alloy 7056-T351

is on the level of *HRB* 108–109. In the welded joint the width of the softening zone is 15 mm, weld metal hardness being *HRB* 105–110.

Considering the small size of the weld, additional Vickers microhardness measurements were performed to GOST 2999–75. Weld metal microhardness values are 13 % lower than those of base metal, whereas in the fusion zone the microhardness is 9–13 % higher. Table 1 gives the generalized results of microhardness measurements.

The nature of distribution and levels of residual stresses, due to the welding process in the samples, were determined by the destructive method of unloading using resistance strain gauges and ISD-3 instrument [7], as well as nondestructive ultrasonic method, using UPKN instrument [8].

Measurements of residual stresses show that their maximum values reach their maximum in the longitudinal direction relative to the weld, and are almost two times smaller in the transverse direction. Here, maximum residual tensile stresses are in place in the sample center. Figure 4 shows the curves of residual stresses, obtained by ultrasonic method, in the welded plate ($\delta = 12$ mm) of alloy 7056-T351 of 500×240 mm size. Owing to smaller temperature input, the maximum values of longitudinal (σ_x) residual stresses are

Table 1. Microhardness of alloy 7056-T351 in the joint zones

Joint zone	Weld	Fusion line		HAZ	Base metal
		Weld	HAZ		
HV, MPa	1360	1600–1870	1690–1760	1700	1560

equal to just 90–95 MPa, and those of the transverse ones (σ_y) are 40–45 MPa.

Mechanical testing of samples was conducted in a universal servohydraulic machine MTS 318.25 with maximum force of 250 kN, in keeping with the adopted state standards. Base metal plates of alloy AA7056-T351 12 and 30 mm thick were used to prepare cylindrical samples of the IIIrd type of 8 and 10 mm diameter to GOST 1497–84 for determination of the main mechanical characteristics. Welded plates of rolled metal were used to prepare, in keeping with GOST 6996–66, proportional samples (of 6×28 mm cross-section and 270 mm length) for determination of strength limit at uniaxial tension. Average value of strength limit for the sample series was equal to 412–426 MPa that is equal to approximately 70 % of the respective base metal values (Table 2).

Flat samples of 30×6 mm cross-section with a weld in the sample center were cut out of 500×250×30 mm plates with a central weld of 500 mm length, in order to study the fatigue resistance of the joints of alloy 7056-T351. Corset-type samples of 250×30 mm size (20 mm in the test zone) were used for fatigue testing in keeping with GOST 25.502–79. Testing was conducted under the conditions of uniaxial cyclic tension

Table 2. Mechanical properties of base metal and welded joints of alloy 7056-T351*

Properties	Base metal	EBW
Proof stress $\sigma_{0.2}$, MPa	540–560	–
Strength limit σ_t, MPa	610–625	412–426
Relative elongation δ_5, %	14–16	2–5

*T351 — condition of heat-hardening, which consists of hardening, specified deformation and natural ageing.

with 8 Hz frequency at the value of the stress asymmetry coefficient of 0.1 and 0.4. Results of the conducted fatigue testing for each sample series, based on the established values of limited endurance limits, were used to plot the fatigue curves — regression lines in $2\sigma_a$–lg*N* coordinates. Fatigue curves were plotted for high-cycle fatigue region of 10^4–$2\cdot10^6$ stress alternation cycles.

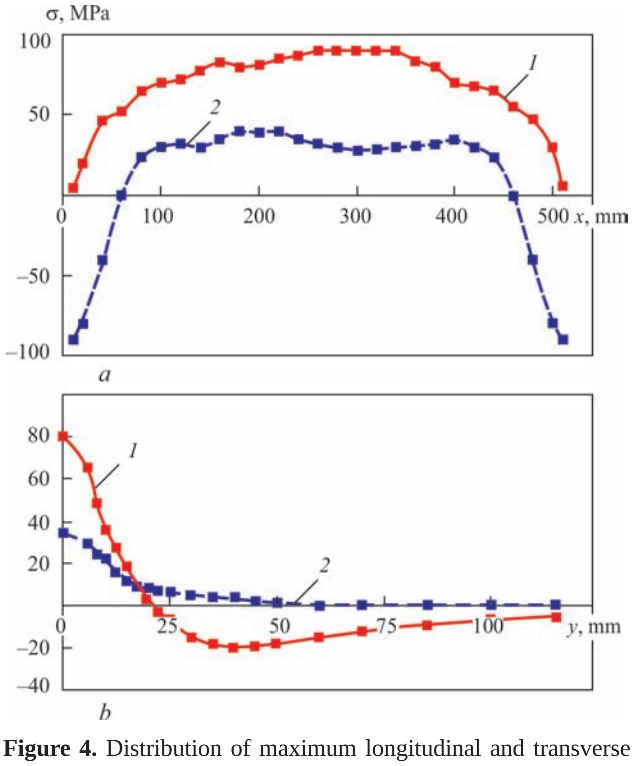

Figure 4. Distribution of maximum longitudinal and transverse residual stresses along the weld (*a*) and normal to the weld (*b*) of welded joint of alloy 7056-T351 12 mm thick: *1* — σ_y; *2* — σ_y

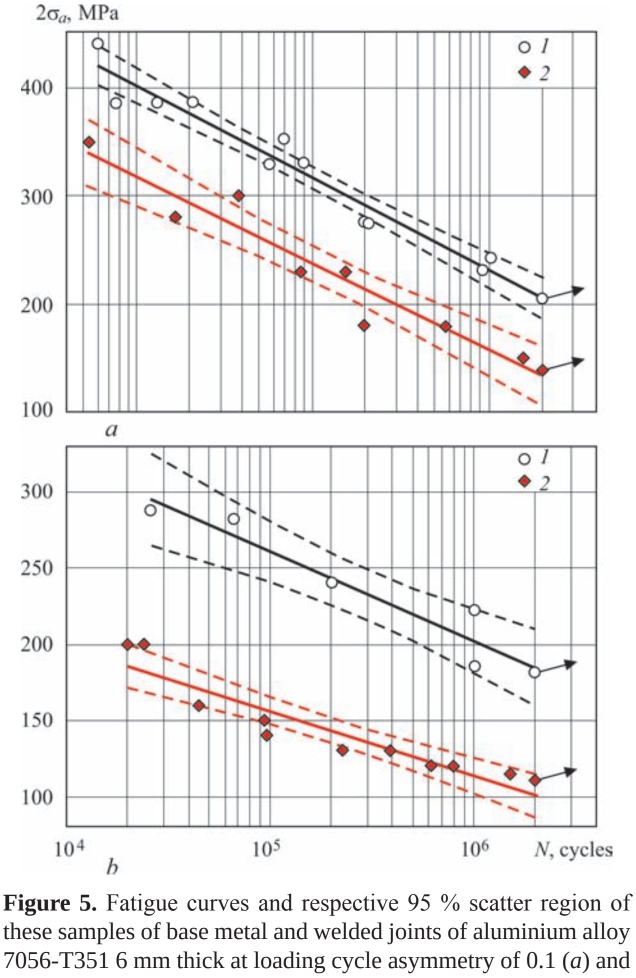

Figure 5. Fatigue curves and respective 95 % scatter region of these samples of base metal and welded joints of aluminium alloy 7056-T351 6 mm thick at loading cycle asymmetry of 0.1 (*a*) and 0.4 (*b*): *1* — base metal; *2* — welded joints

Limited endurance limit on the base of $2\cdot10^6$ cycles at loading cycle asymmetry of 0.1 and 0.4, is equal to 150 and 110 MPa, respectively, for the joints that makes up approximately 70 % of the respective base metal values (Figure 5). Slope of fatigue curves obtained at loading cycle asymmetry of 0.1 and 0.4 in the double logarithmic system of coordinates for the joints is equal to $m_{0.1}$ = 5.36 and $m_{0.4}$ = 6.99, whereas for base metal this value is $m_{0.1}$ = 6.92 and $m_{0.4}$ = 8.5, respectively. Here, sample fatigue life at the stage of fatigue crack propagation up to complete fracture is much smaller than the fatigue life of the stage before crack initiation that is attributable to low ductility of weld and HAZ metal.

Derived results are indicative of the good prospects for application of electron beam welding for producing quality joints of high-strength aluminium alloy 7056-T351 with higher zinc content.

Conclusions

1. Physico-mechanical properties of welded joints of high-strength heat-hardenable aluminium alloy 7056-T531 (δ = 12 and 30 mm) with higher zinc content (8.7–9.8 %) produced by optimized EBW technology, were studied. It is found that the strength limit of such joints is equal to approximately 70 % of the respective base metal values ($\sigma_{t\,bm}$ = 620 MPa).

2. Maximum values of residual longitudinal stresses in the welded plate of 500×240×30 mm size, produced by EBW technology, are equal to 90–95 MPa, and those of transverse ones are 40–45 MPa.

3. It is found that the limited $2\cdot10^6$ endurance limit of EBW joints at loading cycle asymmetry of 0.1 and 0.4 is equal to 150 and 110 MPa, respectively that makes up approximately 70 % of the respective base metal values.

4. At EBW a defect-free uniform structure forms in metal of welds, fusion line and HAZ, at dispersion of the grain structure and phase formations that ensures a high level of strength and fatigue life of welded joints of aluminium alloy 7056-T351.

1. Ishchenko, A.Ya. (2003) Aluminium high-strength alloys for welded structures. *Progresyvni Materialy i Tekhnologii*, **1**, 50–82 [in Russian].
2. Gureeva, M.A., Grushko, O.E., Ovchinnikov, V.V. (2008) *Welded aluminium alloys in structures of transport vehicles*. VIAM/2008-205182, **10**, 51–82 [in Russian].
3. Fridlyander, I.N., Sandler, V.G., Grushko, O.E., Bersenov, V.V. et al. (2002) Aluminium alloys as a perspective material in automobile industry. *Metallovedenie i Termich. Obrab. Metallov*, **9**, 3–9 [in Russian].
4. Martin, K., Ruzek, R., Novakova, L. (2015) Mechanical bahaviour of AA7475 friction stir welds with the kissing bond defect. *Int. J. of Fatigue,* 74(**5**), 7–19.
5. Eibla, M., Sonsinob, C.M., Kaufmann, H., Zhanga, G. (2003) Fatigue assessment of laser welded thin sheet aluminium. *Ibid*., 25(**8**), 719–731.
6. Nesterenkov, V.M., Kravchuk, L.A., Arkhangelsky, Yu.A., Orsa, Yu.V. (2017) Formation of welded joints of magnesium alloys in pulse multipass electron beam welding. *The Paton Welding J*., **4**, 35–38.
7. Kasatkin, B.S., Kudrin, A.B., Lobanov, L.M. et al. (1981) *Experimental methods of investigation of strains and stresses*. Kiev, Naukova Dumka [in Russian].
8. Gushcha, O.I., Smilenko, V.N., Kot, V.G., Brodovoj, V.A., Klochkov, I.N. (2009) Control of stresses based on application of subsurface acoustic waves. *Tekh. Diagnost. i Nerazrush. Kontrol*, **1**, 11–13.

Received 04.10.2018

DOI: http://dx.doi.org/10.15407/tpwj2019.01.04

DEPENDENCE OF HYGROSCOPICITY OF COATINGS OF LOW-HYDROGEN ELECTRODES ON COMPOSITION AND STRUCTURE OF LIQUID GLASS

A.E. MARCHENKO[1], V.V. TRACHEVSKY[2] and **N.V. SKORINA[1]**
[1]E.O. Paton Electric Welding Institute of the NAS of Ukraine
11 Kazimir Malevich Str., 03150, Kyiv, Ukraine. E-mail: office@paton.kiev.ua
[2]Technical Center of the NAS of Ukraine
13 Pokrovskaya Str., 04070 Kyiv, Ukraine. E-mail:tracev@imp.kiev.ua

Presented were the results of investigation of hygroscopicity of coatings of low-hydrogen electrodes depending on composition of liquid Li-, Na- and K-glasses as well as their binary mixtures, which were interpreted from point of view of evolution of a silicon-oxygen structure in the process of glass formation under effect of changing type and relationship of cations of alkali metals. Carried diagnostics of structure-functional self-organization of the silicon-oxygen anions in composition of the liquid glasses was performed based on data of a nuclear magnetic resonance. The spectra of nuclear magnetic resonance ^{29}Si were used. Generalized data were considered taking into account dominance of polycondensation mechanism. Correlation between the indices of coating hygroscopicity and relationship of bridge Q^4, Q^3, Q^2 and nonbridge Q^1 connectivities in structure of the silicon-oxygen anions were determined. 19 Ref., 2 Tables, 12 Figures.

Keywords: *arc welding, welding electrodes, coating hygroscopicity, production technology, liquid glass, structure of liquid metal, spectroscopy of nuclear magnetic resonance*

Atmosphere always contains some amount of water vapor, i.e. has a relative humidity. When reaching saturation the water vapor is condensed in form of dew, mist, hoarfrost, snowflakes or rain-drops depending on ambient environment.

In course of regular heat treatment of the electrodes in a temperature range of 150–400 °C the humidity (moisture content) of electrode coating is led to a level lower than equilibrium moisture content of the environment, i.e. coating is hygroscopic and characterized with the capacity to absorb moisture as many other dehydrated capillary-porous and colloidal materials.

Moisture which has penetrated the coating initiates with time chemical transformations of its constituents. After reaching specific concentration typical for that or another composition of the coating the absorbed moisture promotes significant deterioration of welding-technological characteristics of electrodes connected with change of appearance, formation of defects, decrease of coating strength and, as a result, formation of weld porosity and near-weld cracks (Table 1).

Welding engineering spends enormous resources [1, 2] on detection, removal, restoration of defective areas of the welds and verification of quality performance of repair operations.

For keeping electrode condition on humidity at the level of regulatory requirements the specific types of their packaging are used, and for condition restoration and further storage of the electrodes until application a fleet of drying-baking units is used. Performance of reanimation activities, list and sequence of performance of which is presented on Figure 1, also requires engagement of enormous resources.

In order to overcome the problems there is a need in development of technological methods which allow dramatically improve moisture resistance of the coating. One of the tasks is to keep such condition of coating of electrodes taken out of package, at which during at least eight-hours working shift content of

Table 1. Types and place of appearance of inadequacies caused by hygroscopic humidity of coating

Object of control	Type and nature of appearing inadequacies
Appearance of electrodes	Spots on coating surface
	Bulbs in the coating
	Core corrosion
Electrode coating	Reduction of strength
Welding — technological properties of electrodes	Deterioration of arcing stability
	Excessive spattering of molten metal
	Unsatisfactory weld formation
	Bad separability of weld crust
Weld	Porosity
	Hydrogen embrittlement
	Cold cracks

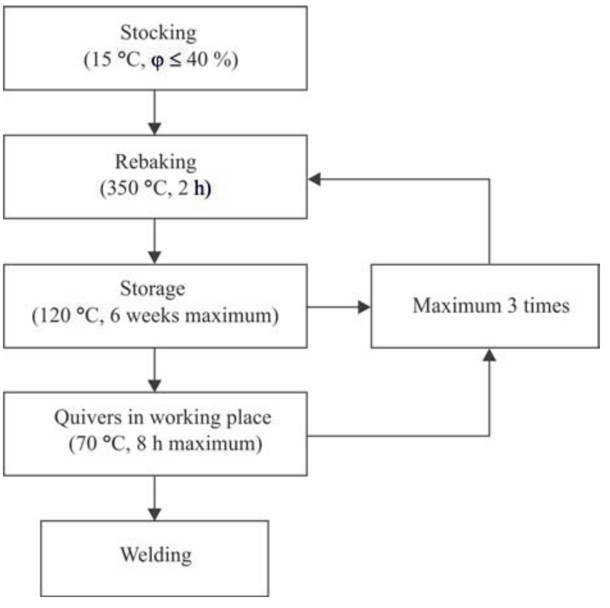

Figure 1. Scheme of regulation of preparation to welding and application of electrodes with low-hydrogen coating

hydrogen in the deposited metal remains within the regulatory limits. At the same time, without compromising welding-technological, metallurgical and sanitary-hygienic characteristics of the electrodes.

Such electrode manufacturers as ESAB [3, 4], Smith weld [5], Oerlikon [6], Metrode Product [7], Quasy Arc [8, 9], Thyssen Draht, Kobelco, Lincoln Electric, etc. as well as series of domestic SRO, including E.O. Paton Electric Welding Institute [10, 11] have dealt with this problem.

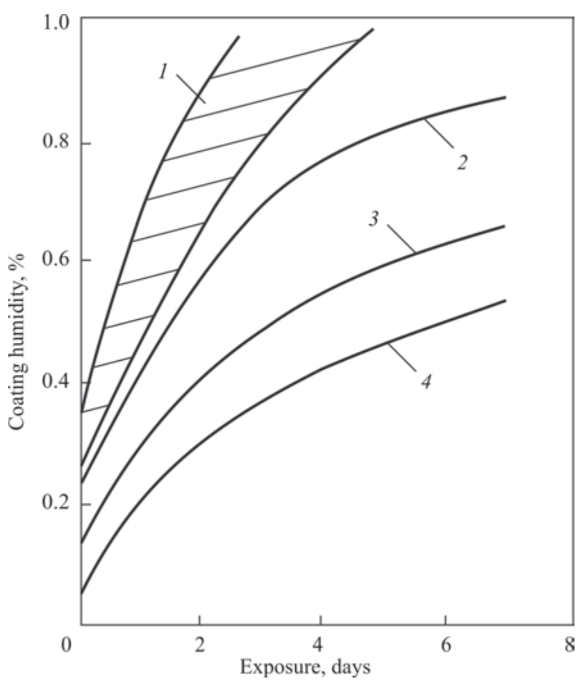

Figure 2. Hygrosorption resistance of electrode coatings depending on method of regulation of polymer condition of silicon-oxygen anions in liquid glass (φ = 75 %, T = 25 °C; designations *1–4* see in the text) [7]

As a result a range of technological procedures were developed for rising a hygrosorbtion resistance of the electrode coatings. The most important of them are based on a regulation of level of polymerization of alkali silicates in the binary liquid glass. They can be divided on 3 groups by efficiency (Figure 2).

Number 1 designates common electrodes, number 2 is the electrodes produced based on binary NaK liquid glasses with relationship of alkali ion-modifiers providing the minimum hygrosorption capacity of alkali hydrosilicate binder. Number 3 marks the electrodes with coating based on NaK glass, module of which was reached by means of regulation of molar ratio $SIO_2/(Na_2O + K_2O)$, including by addition in liquid glass of ammonia silicate. Number 4 marks the electrodes with the low hygroscopicity of the coating, reached due to additional modification of structural network of high-module silicate with cation-glass former.

The electrodes with high hygrosorbtion resistance of the coating are marked with R, MR, EMR, HMR or LMA symbols. The electrodes marked with that symbols satisfy the requirements to hygrosorption resistance of the coating mentioned above and allow getting significant economic result due to decrease of heating temperature, reduction of weld repair expenses, rebaking and maintenance of baked electrodes [1, 5, 11].

Reasons of hygroscopicity of electrode coatings are ambiguous. There are six types of adsorption isotherms, using each of which or their specific combination it is possible to characterize individual properties of any natural adsorbent, including the indices of absorption kinetics and limits of their saturation with moisture (equilibrium moisture content). Among them are mono- or biparametric isotherms of Henry ($x = kP$), Langmuir ($x = kP/(1 + kP)$), Freundlich ($x = kP^{1/n}$), BET, Zsigmondy and hysteresis shape given on Figure 3.

The hygrosorption characteristics of the electrode coatings do not match on shape with any of given isotherms. It is explained by the fact that the electrode coatings have several types of sorption centers. Among them are:

- grains of mineral gas-slag-forming materials, ferroalloys-deoxidizers and iron powder;
- dry residue of liquid glass in form of alkali hydrosilicates, contained in the space between them;
- particles of mineral plasticizers in form of kaolin, bentonite, mica, talc, carbonates of Na and K as well as alginates, CMC and other organic hydrocolloids;
- ash residues of thermo-oxidative degradation of organic hydrocolloids.

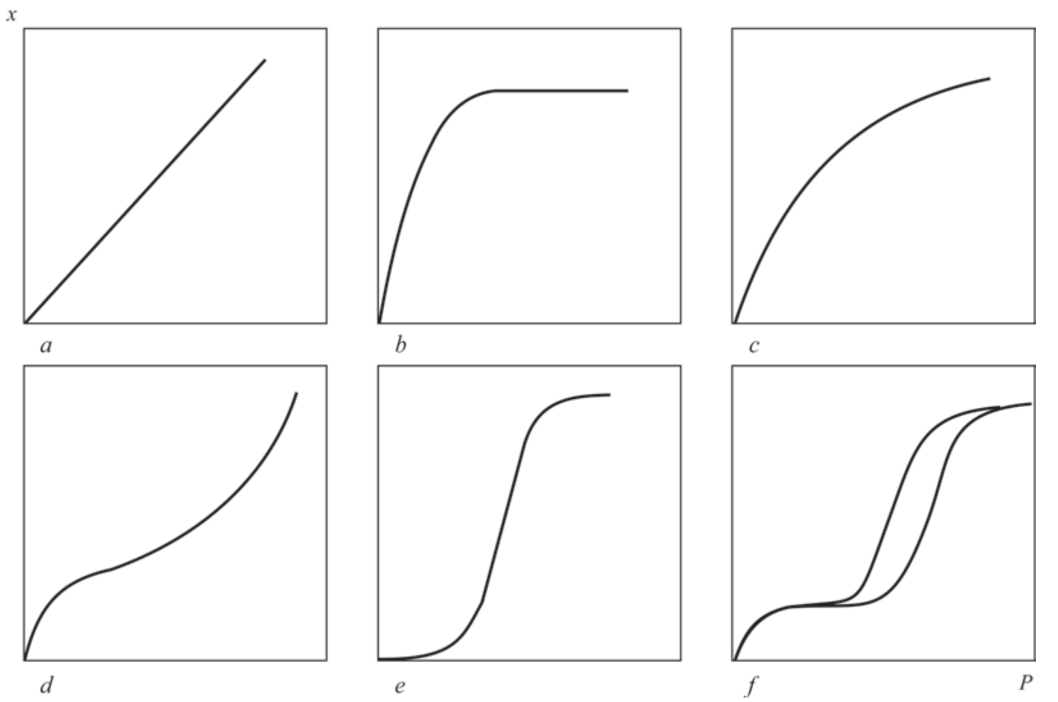

Figure 3. Typical variants of absorption isothermal curves [12]: *a* — Henry; *b* — Langmuir; *c* — Freundlich; *d* — BET; *e* — Zsigmondy; *f* — hysteresis shape

The moisture, absorbed from atmosphere, in course of time changes its physicochemical state in the coating, gradually transforming from capillary into chemically connected form.

Since moisture absorption isotherms of the electrode coatings can not be linearized, that allows determining the parameters necessary for matching the different coatings on hygroscopicity, they are compared by general view of hygrosorption curves obtained under standard conditions.

Procedure. The procedures based on this for determination of hygroscopicity of electrode coatings are divided on 3 groups by designation, namely:

• for investigation of nature and characteristics of hygrosorption process;

• for classification (certification) tests of the electrodes on capability of their coatings to resist absorption of atmospheric moisture;

• for technological control of electrode products.

In any case equipment includes a climatic chamber, designed to maintain of set (or standard, if we are talking about classification tests) climatic conditions, in which the electrodes are exposed during tests. It consists of humidistat and thermostat.

Humidistat is the box made of glass, plastic or another inert material, which contains:

• support with tested electrodes laid on it without connection with each other;

• thermometer;

• open tank with saturated salt solution, providing guaranteed atmosphere humidity with set value of partial pressure of moisture (relative humidity φ). Change of φ in course of testing is not allowed since measurement would provoke air circulation in the humidistat, which, respectively, would result in violation of results reproducibility.

Thermostat is made in a form of safely heat-insulated and tightly closed chamber, in which a temperature regulator by signal from the probe automatically, with ±1 °C accuracy keeps the set temperature and built-in fan uniformly distribute it over chamber workspace.

The International Institute of Welding (IIW) and International Organization for Standardization (ISO) developed the standards regulating the conditions, order of performance of classification tests and certification of low-hydrogen electrodes for resistance of coatings to atmospheric pressure absorption.

In the first of them a classification feature is coating limit humidity, reaching which the electrode shall be heat-treated for reconstruction of its condition. In the second, such a feature is an allowable content of hydrogen in the deposited metal, which as a result of humidity adsorption by coating in the climatic conditions regulated by standard (φ = 80 %, T = 27 °C, t = = 24 h) shall not be exceeded in any case. For keeping such conditions saturated solution of ammonia sulfate $(NH_4)_2SO_4$ is used.

IIW standard simultaneously regulates the conditions for preparation of the electrodes to tests, preservation of achieved hygrosorption humidity of the coating during testing, that is provided by use of transportable leak proof ampoules for the electrodes as well as order of treatment of electrodes during the

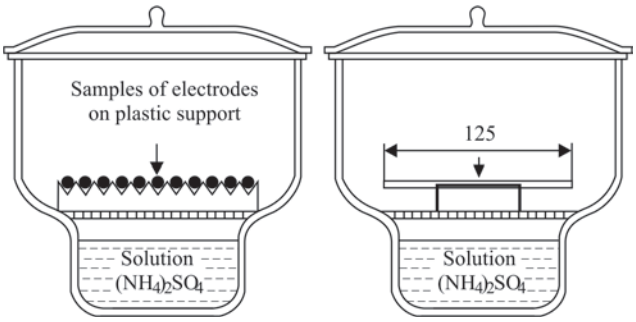

Figure 4. Humidistat for determination of hygrosorption capacity of electrode coating

procedure of measurement of hydrogen content in the deposited metal, corresponding to the provisions of ISO 3650 [13].

E.O. Paton Electric Welding Institute applies the procedure for evaluation of hygrosorption capacity of the electrode coatings to the maximum approached to these requirements. Kinetics of moisture sorption by coating immediately after electrode heat treatment is evaluated. Short-term (8 h) and long-term (14 days) exposure of the electrodes in atmosphere with $\varphi = 80$ % and $T = 27 \pm 1$ °C is used.

The essence of the procedure lies in the following:

• several electrodes are taken from the controlled batch and three samples of 125 mm length are cut out of them;

• cut out samples of the electrodes are baked at the modes prescribed in specification;

• after cooling on air to 20–30 °C samples of the electrodes are weighed on the analytical balances and at once transferred to the humidistat, being a standard glass exiccator (Figure 4), in which set climatic conditions are kept;

• humidistat with samples of the electrodes is placed in the work chamber of thermostat TVZ-25 (TU 64-1-619–76, heater power 300 W), in which 27 ± 1 °C temperature is kept.

• kinetics of moisture absorption by coating is controlled with weighing of each electrode on the analytical balances every 1, 2, 3, 5 and 8 h, and them after 1, 2, 3, 5, 8, 10, 12 and 14 days. During weighing the exiccator is removed from the thermostat. The electrodes are removed from it one by one and weighed. Duration of weighing of one electrode does not exceed 10 s;

• the calculations are made on formulae

$$x = \frac{(P_x - P_0)}{(P_0 - P_c)} 100, \qquad (1)$$

where x is the amount of absorbed by coating moisture in form of mass increment of adsorbent in course of humidification, %; P_0, P_x are the mass of electrode before and after hygrosorption humidification, g; P_c is the mass of electrode core, g.

Set relative humidity in the humidistat, if necessary, was changed using another salt diluted in a humidistat bath. The same is referred to the duration of process observation.

As it was mentioned above, when investigating hygroscopicity of electrode coatings it is assumed that increment of adsorbed substance mass is caused only by moisture absorbed from atmosphere. For electrode coatings such an assumption is not always true due to the fact that alkali hydrosilicate absorbs not only moisture, but also CO_2 in the case of long-term exposure. For this reason in the expert cases a check of the composition of adsorbed material, for example, by means of performance of special analyses using gas analyzer combined with DTA is carried out.

Role of combined liquid glasses in hygrosorption process inhibition. In electrode coatings made using binary (relatively ions-modifiers) liquid glasses, in variation of relationship of alkali constituents in the liquid glass, there was detected changes of hygrosorption characteristics [4, 10], which do not subject to additivity rule.

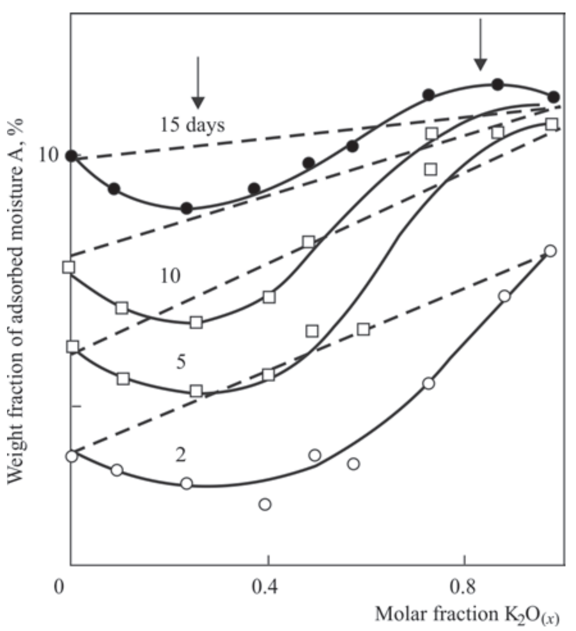

Figure 5. Effect of relationship of alkali oxides in NaK-liquid glass on hygroscopicity of electrode coating ($\varphi = 95$ %; $T = 25$ °C). The numbers show the exposure time of electrodes in humidistat [7]

Figure 5 compares dynamics of change of coating hygroscopicity of UONI 13/55 electrodes made on binary NaK liquid glasses depending on Na- and K-ingredients in the mixture. Modules of initial monoalkali glasses $M_{Na} = M_K = 2.9$, toughness 500 MPa·s. It can be seen that coatings on liquid glass with molar fraction of potassium constituent very close to 30–40 %, are characterized with minimum hygrosorption capacity. Coatings with larger fraction of potassium component than in the minimum point accumulate moisture more intensive than made based on glasses with smaller fraction of indicated component. Ascending (potassium) branches of the curves at short exposures is sharper than descending (sodium). Together with minimum, at 70–80 % of potassium constituent, the curve demonstrates the maximum of hygroscopicity (marked, as a minimum, by arrow). Rise of exposure aligns the slopes of ascending branches and a level of deviation of the extreme point from additive value reduces. Extremeness is studied for change of liquid glass toughness (maximum appears), and for water retaining capacity of dry residues of binary glasses and electrode coatings on their basis (the minimum appears as in hygroscopicity). This picture is changed under effect of type and module of solutions of alkali silicates, taken for preparation of binary liquid glasses [7, 10, 14, 15].

Figure 6 showed the nature of change of hygroscopicity of electrode coatings depending on relationship of initial sodium (Na_s) and potassium (K_s) constituents as well as module of made of them NaK liquid glasses, designed for electrode manufacture. In order to preserve similar Na_s/K_s relationship in the compared binary mixtures of glasses the authors [7] increased their module by addition of 5 % of ammonium silicate Quaram into the prepared mixture.

Accepted designations:

• 1 and 1′ are the electrodes directly after baking;

• 2, 3, 4 and 2′, 3′, 4′ are the electrodes exposed in humid medium during 24, 48 and 168 h, respectively;

• solid lines show the variants of the samples manufactured based on mixtures of glasses with lower, and dashed with larger values of module.

Humidity of the coating was determined after baking at 1000 °C (using IIW method).

Data given on Figure 6 verify that amount of moisture absorbed by electrode coating from corresponding atmosphere, has different effect on relationship of alkali constituents and their module depending on exposure duration. The minimum humidification is observed not at one fixed relationships of Na_s/K_s as it was determined in works [4, 10, 16]. According to Figure 6 a position of minimum of reached moisture contents in rise of the electrode exposure in humid condition can be displaced to the side of bigger or smaller from initial values.

Rise of module of liquid glass promotes decrease of moisture absorption in the minimum and point of minimum really displaces to the side of larger portion of potassium constituent in the mixture of liquid glasses. Asymmetry of the moisture absorption curves appears simultaneously, in the right i.e. potassium branch has more slope than sodium, particular in the case of long-term exposures.

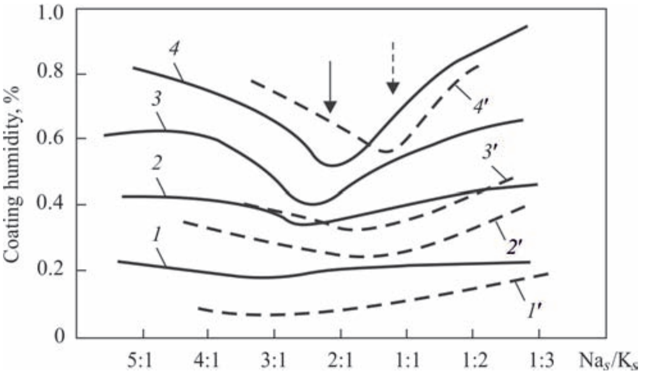

Figure 6. Dependence of amount of moisture absorbed by coating from relationship Na_s and K_s constituents, as well as module of binary liquid glasses (φ = 75 %; T = 25 °C, see description in the text) [7]

The pattern becomes more complex when binary mixtures are made of monoalkali solutions of silicates with larger difference of cation size than in K and Na. Figure 7 compares hygrosorption curves received during investigation of pilot variants of UONI 13/55 electrodes, marked with T-99 index. Coatings are manufactured using Li, Na and K liquid glasses with M = 3.2 and their binary mixtures. Electrode diameter is 4 mm.

It can be seen that during short-term exposure the coatings on liquid Li-, Na- and K-glasses absorbed 0.1, 0.3 and 2.0 % of moisture. Amount of absorbed moisture with rise of electrode holding to 14 days increases almost 3 times in Li- and K-variants, and in Na-variant in 5 times. At short-term exposure amount of moisture absorbed by coating monotonically grows with increase of fraction of second component in the liquid glass mixture. At long-term exposure the curve of coating moisture absorption of NaK-series contains the minimum and maximum, which are only displaced left and more expressed than in series of the electrodes manufactured based on liquid NaK glasses with 2.9 module (see Figure 5).

It is necessary to pay attention that effect on coating hygrosorption properties of the component added to lithium glass is significantly neglected by lithium constituent. In short-term exposure it only refers to potassium, and at long-term exposure to sodium constituent as well. The same pattern is observed in the case of effect of NaK-liquid glasses on coating hygroscopicity. At short-term exposures the sodium constituent suppresses hygroscopicity of potassium constituent and at long-term holding they almost equalize on the level of effect on coating sorption capacity as if modularity of the potassium component significantly rise due to some reason.

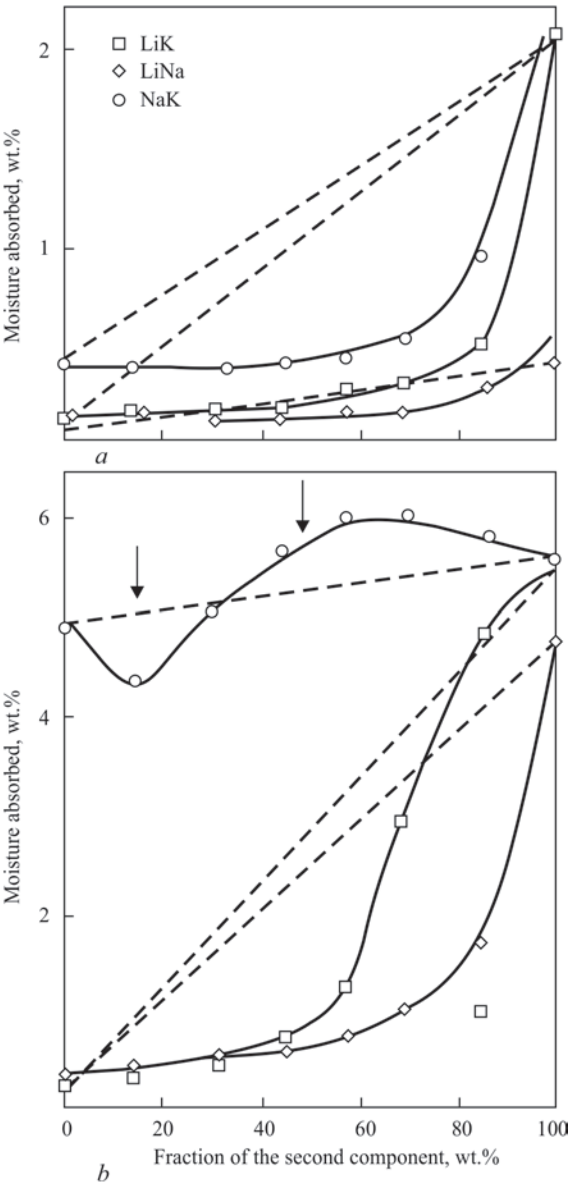

Figure 7. Effect of content of binary high module liquid LiNa-, LiK- and NaK-glasses on hygroscopicity of coating of pilot electrodes T-99: *a* — 8 h; *b* — 14 days

Based on mentioned above it can be concluded that change of hygroscopicity of electrode coatings in use of the combined liquid glasses has a complex nature. It can not be explained only by effect of increase of portion of more «hygroscopic» cations in the composition with less hygroscopic, if it is a priory supposed that change of integral hygroscopicity of cation constituent follows the linear law. A role of structure of anion constituent, apparently, shall also be taken into account since a structure of silicon-oxygen anions (SOA), which is changed under the effect of relationship of cation-modifiers, is essential in a synergism of toughness of the binary liquid glasses and in nonlinear change of water-retaining capacity of the binary mixtures of hydrosilicates at their thermal dehydration.

In this connection the paper studies the hygroscopicity of low-hydrogen electrode coatings ANV-35 in conjunction with SOA structure of liquid LiNa-, LiK- and NaK-glasses, which were prepared from monoalkali liquid Li-, Na- and K-glasses with the values of modules 2.8, 3.0 and 3.6, respectively. Composition of the initial glasses is given in Table 2 [17]. Toughness of the initial glasses made 350 MPa·s. Dose of glasses in the paste is 25, 26 and 23 %.

Monoalkali liquid Li-, Na- and K-glasses were used for preparation of pastes of pilot electrodes with the same consistency that in work [17].

In contrast to them binary glasses in advance were brought to the level of toughness of initial monoalkali glasses by means of dissolution with small additions of water in order to neglect the synergy effect. In LiK liquid glasses, containing from 16.3 to 50.0 wt.% of potassium constituent, in initial state the synergy burst reached 20800 MPa·s. Therefore, the level of their dissolution was significantly larger than in the rest samples of indicated series.

Produced electrodes were dried for 24 h on air, after what were hold for 1 h at 200 °C and then baked at 400 °C.

The values of chemical shift (δ, ppm) of ^{29}Si signals for samples of monoalkali and combined liquid glasses were determined at room temperature using NMR-spectrometer of AVANSE 400 model. A source of information on SOA structure of liquid glasses was a relative integral intensity of signals of corresponding structural groups Q_m in the primary ^{29}Si NMR analytical spectra. Procedure of work is outlined in [17]. The average value of connectivity Q_{av} was calculated using $\sum x_i Q_i$ expression, where Q_i is the index of chemical shift, characterizing connectivity *n*, and x_i is the partial value of this type of connectivities. The hygroscopicity of electrode coatings was investigated under conditions φ = 84 %, T = 25 °C. Figure 8 shows the results of evaluation of hygroscopicity.

As in the series of experiments T-99 the minimum hygroscopicity was revealed in a coating made based on lithium liquid glass. As it follows from Table 2 in structure of their SOA there is the highest fraction of bridge connectivities Q^4. During 4 hours the composition absorbed 0.1% of moisture, and 0.6 % of Na- and K-glass. However, after 14 days the sorption reached the values of 0.3, 0.5 and 5.5 % of H_2O, respectively, i.e. 3–10 times more. As can be seen, the hygrosorption capacity of the coating samples of these series is significantly higher in comparison with coatings T-99, made based on liquid glasses with M = 3.2.

It also follows from Figure 8 that hygroscopicity of the coatings with appearance of the second compo-

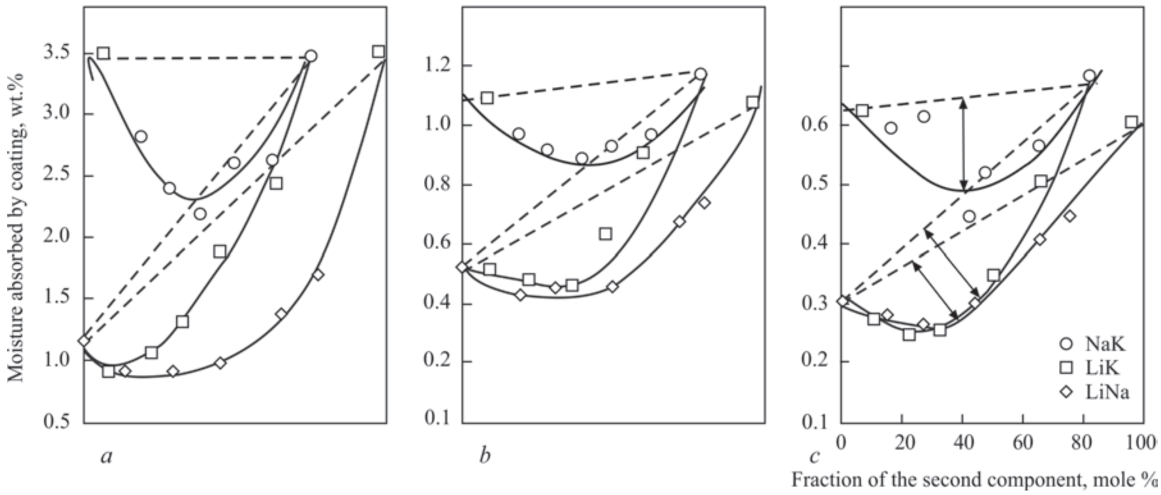

Figure 8. Dependence of amount of moisture absorbed by coating on content of liquid glass and duration of observation: *a* — 14 days; *b* — 24 h; *c* — 8 h

nent in the binary glasses is firstly below the expected one according to additivity rule. Then, after reaching the minimum, it monotonously grows, moreover for LiK-series it is significantly more intensive than for LiNa and NaK-series. Duration of electrode exposure in the humid medium has small effect on evolution of absorption capacity of the considered coatings.

Figure 9 shows the change of the weighted average value of connectivity index in SOA structure of the combined liquid glasses depending on concentration in them of the second component. Dependence of amount of moisture, absorbed by coatings, on index $Q_{av} \sum x_i Q_i$, is given on Figure 10.

Comparing meaningful aspects of indicated Figures, it is possible to assume that different hygrosorption capacity of the electrode coatings, made at combination of relationship of components of liquid glasses, is actually determined by tendency to hydration of ion-modifiers as well as, to significant extent, by structure of liquid glasses SOA dominating in specific conditions, which is formed under determining effect of corresponding cations.

At that the weighted average value of connectivities is changed. As a result, as it follows from data given on Figure 10, hygroscopicity of the coatings is, in particular, determined by Q_{av} index. At that, as it follows from Figure 11, Q_{av} rises due to increase of $Q^4/Q^2 + Q^3$ relationship.

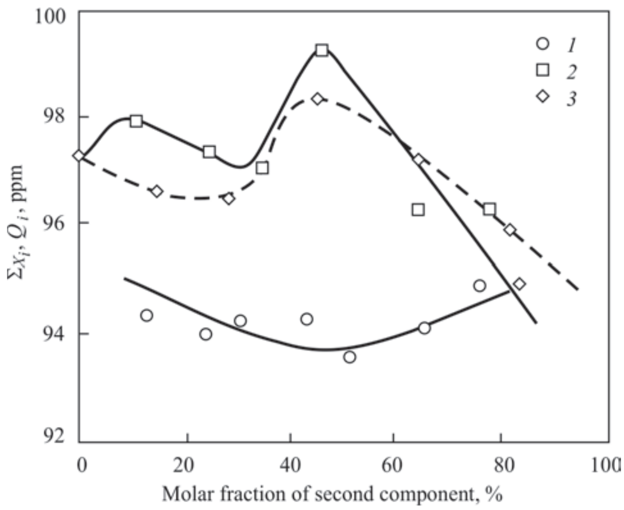

Figure 9. Change of Q_{av} depending on concentration of the second component in NaK (*1*), LiK (*2*) and LiNa (*3*) liquid glass

The results being out of general pattern are referred to three liquid LiK-glasses in composition of which molar ratios $K_2O/Li_2O \geq 1$.

Complete encapsulation of hygroscopic K-cations by high-module silicon-oxygen shall becomes impossible at that.

Effect of cation-glass former on hygroscopicity of electrode coatings. In liquid glasses, the results of investigation of which are outlined in the previous chapters, silicon is the single so-called cation-glass former determining variety of spatial constructions in the content of forming SiO_4^{-4}. Fine regulators of

Table 2. Composition, density and toughness of Li, Na and K liquid glasses

Type of glass	Module	Weight fraction, %				Glass properties		
		SiO_2	Li_2O	Na_2O	K_2O	ρ, kg·m^{-3}	η, mPa·s	Q^4, ppm
Li	2.77	25.52	4.60	–	–	1313	325	26.5
Na	3.09	28.54	–	8.40	1.70	1433	325	16.0
K	3.67	26.37	–	1.66	8.93	1422	360	13.5

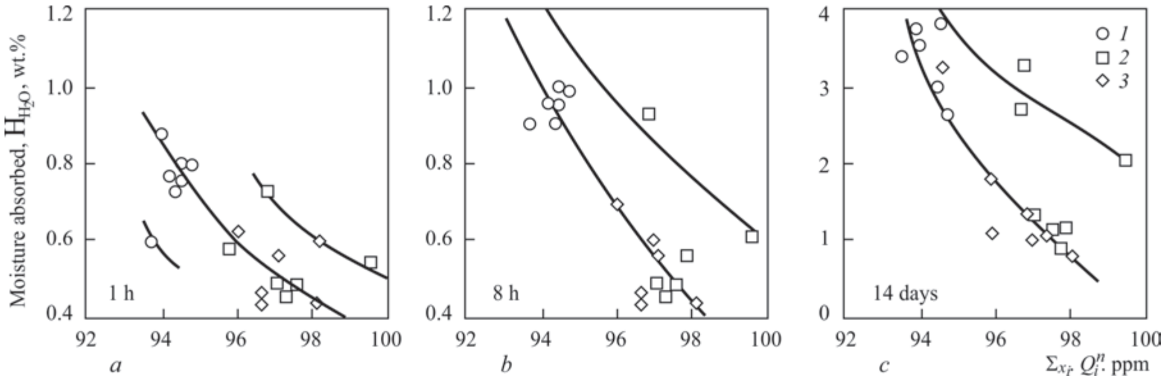

Figure 10. Dependence of amount of moisture, absorbed by coating from humid atmosphere, from Q_m of binary liquid glasses: *a* — 1 h; *b* — 8 h; *c* — 14 days (see designations on Figure 9)

structure of the forming SOA, and, as a consequence, physicochemical properties of liquid glasses, used in production of electrodes, are alkali cation-modifiers (Li^+, Na^+, K^+, NH_3^+ and rarely — Rb^+ and Cs^+). Even such, it would seem, limited list of the modifiers significantly expands the possibilities of rise of production efficiency, reaching set technical characteristics and indices of welding electrode quality.

Really, hygroscopicity of the coating can be significantly reduces with addition of ammonia hydrosilicate into a paste composition or liquid glass, promoting increase of its module and decrease of pH value [7]. The level of coating hygroscopicity reached at that can be provided by increase of electrode baking temperature from 400 to 450 °C, but it will require larger energy consumption than at introduction of modifying ammonium additive.

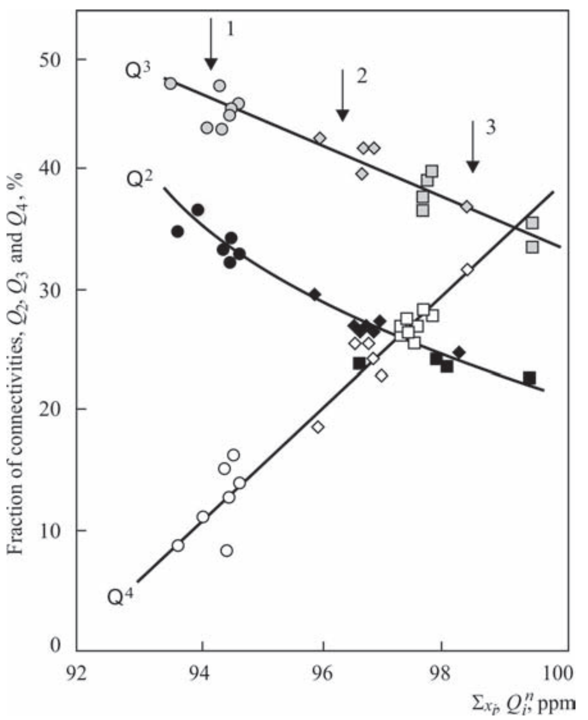

Figure 11. Change of relationship of connectivities in SOA structure of NaK (arrow 1), LiNa (arrow 2) and LiK (arrow 3) of liquid glasses depending on weighted average value of chemical shift

In the silicate technologies regulation of SOA structure of the silicate melts is carried out using modifiers in form of cation-glass formers (based on Al^{3+}, P^{5+}, etc.)[18]. Their effect of SOA structure can be performed by different mechanisms depending on force of corresponding cation being present in anionic part of modifying additive. Entering the silicate it tries to form its closest surrounding in new environment from nonbridge (Q^1, Q^2) and bridge (Q^3, Q^4) fragments.

At that the anion groupings with different level of polymerization are formed. Those of them, which were formed by stronger acids will be less polymerized in comparison with the anion groupings formed at participation of weaker acids. In any case, the re-

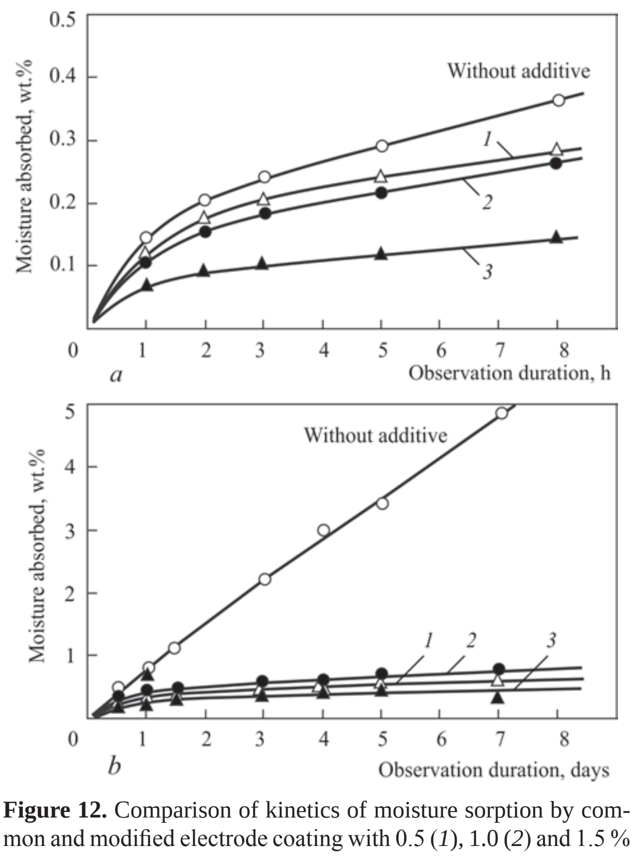

Figure 12. Comparison of kinetics of moisture sorption by common and modified electrode coating with 0.5 (*1*), 1.0 (*2*) and 1.5 % (3) of modifying additive based on cation-glass former. Exposure 1 (*a*) and 14 (*b*) days

sult is reached significantly larger than using cation modifier.

Figure 12 shows the results of testing of one of such additives in the coating of pilot electrodes UONI 13/55. It can be seen that hygroscopicity of electrode coating under its effect is reduced 5–10 times.

Let's note the following in the conclusion. SOA structure of a liquid glass intergranular film in the electrode coating in course of its heat treatment is formed on polycondensation mechanism.

Dehydration of alkali hydrosilicates is as deep as long molecules of water, precipitated in course of polycondensation reaction, are kept in a reaction zone and participate in the next acts of polycondensation transformation as original catalyst [19].

It can be assumed that different size SOA modifications, which appear in the modified liquid glasses, form dense, i.e. less permeable for precipitating water vapors packages than the packages from similar on size SOA — formations typical for non-modified liquid glasses.

Respectively, deeper dehydration in the dense packages provides reliable blocking of coarse, more susceptible to hydration cation-modifiers that rises hygrosorption resistance of electrode coatings, made based on the combined liquid glasses including using technical additives containing modifiers of different functional link.

Conclusions

1. Studied was a hygroscopicity of the low-hydrogen electrode coatings made based on liquid Li-, Na-, and K-glasses as well as composed of them binary LiNa-, LiK- and NaK-variants with different relationship of contained ion-modifiers. The lowest hygroscopicity has the coatings made based on liquid Li-glasses. It is explained by domination of fragments with Q^4 connectivities in the SOA structure of lithium liquid glasses.

2. Increase of coating hygroscopicity with rise of concentration in the binary mixture of glasses of the second differing by larger density of Z/r cation charge is not proportional to its concentration. Unfavorable from point of view of hygroscopicity effect of Na- and K-component is blocked in the binary compositions of lithium constituent, i.e. short-term exposure suppresses effect of dominating potassium and at long-term also sodium component. Sodium constituent in the content of binary liquid NaK-glasses at small exposures blocks increase of coating hygroscopicity, caused by potassium component and at long-term holding Na and K constituents effect the sorption capability of coating almost with similar level.

3. There is a tight connection between hygroscopicity of electrode coatings, on the one hand, and concentration of different forms of connectivities in SOA of the binary liquid glasses on the other hand. The higher the weighted average value of connectivities $Q_{av} \sum x_i Q_i^n$ the lower is hygroscopicity of the coating. It is true for mono- as well as binary liquid glasses. Indeed, in the first and the second case the hygroscopicity of coatings reduces with rise of module of liquid glass that is explained by increase of contribution of the higher connectivity forms into total SOA structure.

4. In the binary liquid glasses, in contrast to their monoalkali analogues, there are no static distribution of ion-modifiers. Cations with the lower values of Z/r, for example K^+, fill place in the surrounding of highly-polymerized fragments of SOA (Q^3 and Q^4), and cations with the larger Z/r (Na^+ or Li^+) in the environment of less polymerized SOA, i.e. with larger amount of bridge connectivities (Q^2 and Q^1). As long as the cation more susceptible to hydration is «blocked» by high module, i.e. less hygroscopic and less moisture permeable SOA forms, it, as surrounding SOA, has low susceptibility to moisture absorption and hydration. As a result, there is no single-valued connection between physical composition of the binary liquid glasses and average weighted value of the connectivities in SOA structure. More than two number of combinations Q_i^n correspond to the same Q_{av}, and, respectively, characteristics of liquid glasses and made of them filled compositions.

5. In short-term holdings the effect of potassium ion blocking by «high module» SOA is felt at weight fraction of Li_2O in the mixture with K_2O, in our experiments equal approximately 30 %, and sodium ions at even smaller dose. Q^2 and Q^3 connectivities prevail in the SOA structure of liquid NaK-glasses. Therefore, effect of encapsulation is revealed in smaller degree, and decrease of hygroscopicity in the minimum is expressed more obvious than in taken for comparison coatings on lithium-containing liquid glasses.

6. In liquid glasses with two cation-glass formers the cations also compete for place in SOA structure as cation-modifiers. Caused by such competition increase of inhomogeneity of distribution of nonbridge atoms of oxygen promote delay of the process of coating moisture absorption from atmosphere.

1. Smith, R. (1987) Improved consumables can change shop-floor practice. *Met. Construct*., 19(**5**), 282–283.
2. Barbin, L.M. (1977) The new moisture resistance electrodes. *Weld. J*., 56(**7**), 15–19.
3. (1983) LMA-a new quality concept for low hydrogen electrodes with low moisture absorption. *Svetsaren (A Welding Review)*, **2**, 3–5.

4. Almqist, G., Budgifvars, S., Lindström, L. et al. (1983) Some principles for low moisture absorption properties of basic MMA electrodes. In: *Proc. of 2nd Int. Conf. on Offshore Welding Structure* (London, 16–18 Sept. 1982). Abington, 1–6.
5. *Van* Nassau, L. Recent welding consumable improvements providing major handling advantages for offshore fabricators. *Smitweld International Report*, 00774.
6. Becker, H. von (1964) Über die Feuchtigkeitsaufnahme, die Auswirkung und die Zweckmässige Rücktrocknung bei Schweisselektroden. *Oerlikon Schweissmitteilungen*, 22(**52**), 12–19.
7. Marshal, F.W., Farrar, J.C.M. (1983) Progress in moisture/hydrogen control of lime-fluorspar and lime-titania electrodes. In: *Proc. of 1st Int. Conf. on Developments and Innovations for Improved Welding Production* (13–15 Sept. 1983, Abington). London, 28, 1–10.
8. Kaljee, J. (1978) Hydrogen in weld metal; causes and remedies. *Welding Reporter*, 14(2), 5–10.
9. Kaljee, J. (1986) Moisture resistant electrode coating. *FWP J.*, 26(1), 29, 30, 32–34, 38–40.
10. Marchenko, A.E., Skorina, N.V. (1989) Combined alkali silicates in manufacture of low-hydrogen electrodes. Metallurgical and technological problems of basic covered electrodes. In: *Proc. of 2nd Int. School for Countries-Members of CMEA* (Sofia, 1989). Kiev, Naukova Dumka, 123–130.
11. (2004) New electrodes for welding of carbon and low-alloy steels, demand and supply (in cooperation with I.R. Yavdoshchin et al.). In: *Proc. of 3rd Int. Conf. of CIS Countries on Welding Consumables. Development. Technologies. Manufacture. Quality* (Dnepropetrovsk, 1–-4 June 2004). Dnepropetrovsk, 64–67.
12. Hirai, Y., Minakawa, S., Tsuboi, J. (1980) *Prediction of diffusible hydrogen content in deposited metal with basic type covered electrodes*. IIW Doc. II-929–80.
13. *ISO 14372:2000 (E)*: Welding consumables — Determination of moisture resistance of manual metal arc welding electrodes by measurement of diffusible hydrogen.
14. Marchenko, A.E., Skorina, N.V. (1981) Synergism of toughness of combined liquid glasses and properties of electrode compounds. *CMEA: Inform. Materialy*, 20(**2**), 109–115 [in Russian].
15. Marchenko, A.E., Skorina, N.V. (1987) Water-retaining ability of alkali silicates and its effect on dehydration of electrode coatings. *Ibid*., 31(**1**), 43–60 [in Russian].
16. Schleyer, W.L. (1970) Welding electrodes and the properties of soluble silicates. *Weld. J*., 49(**12**), 918–924.
17. Marchenko, A.E., Skorina, N.V., Kiselev, M.O., Trachevsky, V.V. (2017) Nuclear magnetic spectroscopy study of the structure of liquid glasses for welding electrodes. *The Paton Welding J*., **1**, 41-45.
18. Anfilogov, V.N., Bykov, V.N., Osipov, F.F. (2005) *Silicate melts*. Moscow, Nauka [in Russian].
19. *Dent* Glasser, L.S., Lee, C.K. (1971) Drying of sodium silicate solution. *J. of Appl. Chemical Biotechnology*, 21(**5**), 127–133.

Received 30.10.2018

DOI: http://dx.doi.org/10.15407/tpwj2019.01.05

INFLUENCE OF MAGNETIC FIELD ON CRYSTALLIZATION OF WELDS IN ARC WELDING

A.D. RAZMYSHLYAEV[1] and **M.V. AGEEVA**[2]
[1]State Higher Education Institute Priazovsky State Technical University
7 Universitetskaya Str., 876500, Mariupol, Ukraine.E-mail: razmyshljaev@gmail.com
[2]Donbass State Machine Building Academy
72 Akademicheskaya Str., 84313, Kramatorsk, Ukraine. E-mail:maryna_ah@ukr.net

A review of publications on metallurgical and casting industry showed that when analyzing the properties of liquid metals and alloys, many authors proceed from the concepts of their cluster structure. Cluster structure of liquid is a hypothesis, but it is confirmed by studies of diffraction of X-rays, electrons and neutrons, reflected from its surface. The work considers the existing concepts of a cluster being a crystal-like concentration of atoms. Around the clusters a softening zone exists, which consists of disordered atoms. Its volume does not exceed 3–5 % and this provides the fluidity of many melts. The authors of publications have succeeded in explaining the forming structure of ingots, based on the cluster mechanism of the process of crystallization of liquid metals and alloys. The authors of this work suggested that the overheated liquid metal in the head part of the pool, which has smaller clusters, moves under the action of magnetic fields to its tail part, and provides a refinement of the primary structure of the weld metal. 20 Ref., 1 Figure.

Keywords: *welding, weld pool, magnetic field, cluster, weld structure, crystallization*

Application of controlling impacts of longitudinal magnetic fields (LMF), or transverse magnetic fields (TMF) in arc welding increases the process efficiency, refines weld structure, and improves welded item performance [1–3]. In [4] it is shown that there exist many hypotheses about the mechanism of weld structure refinement in welding with controlling magnetic fields (MF). Refinement of structural components of weld metal in welding with MF impact, probably, occurs at the stage of their initial crystallization. Known works on the mechanism of metal crystallization during its solidification pertain to casting processes, or to producing superpure single-crystals [5, 6]. Conditions of metal crystallization in the weld pool are known [7, 8] to differ from those described in [5, 6]. It should be also noted that in works [5, 6] and [7, 8] the process of melt crystallization is presented as that of melt atoms bonding with the solid substrate. In all the known works, brief review of which is given in [4], the process of crystallization of various metals and alloys is considered proceeding from the concepts described in [5–8]. Mechanism of crystal growth is represented as bonding of substance atoms from the melt to the solid phase (substrate), i.e. as a diffusion process. Here, the crystallization process is treated as a periodical one, with stopping at release of latent heat of crystallization. A thin solid-liquid interlayer forms on the boundary of the solidifying pool metal with the liquid metal, where diffusion processes (movement of atoms from the melt to the solid crystallized weld metal) develop. In this layer a region of concentration-induced densification δ is singled-out [8] and diffusion processes in this region (δ), as well as in the liquid and solid phase are considered [5, 6]. Such an approach was used in all the works, devoted to studying MF impact in arc welding on refinement of weld structure.

It should be noted that crystallization of weld metal is similar to crystallization of ingots in conventional casting processes in casting and metallurgical productions. At present there is a tremendous number of works (studies) on casting and metallurgical production, in which the mechanism of ingot crystallization is treated differently.

The objective of this work is analysis of published data on the cluster model of the structure of liquid metals and alloys for the case of pool metal crystallization in arc welding with the impact of controlling magnetic fields.

The model of cluster structure of liquid metals and alloys is taken as the base in works on ingot crystallization. The data of these works, in our opinion, are useful at consideration of weld crystallization in arc welding with MF impact.

Let us consider the essence of the problem in greater detail. Diffraction of X-rays, electrons and neutrons, reflected from liquid metals and alloys (also iron-based), revealed the presence of crystal-like components — clusters in the liquid [9–14].

A cluster is a crystal-like concentration of atoms [13]. Clusters form at melting of crystalline bodies [9,

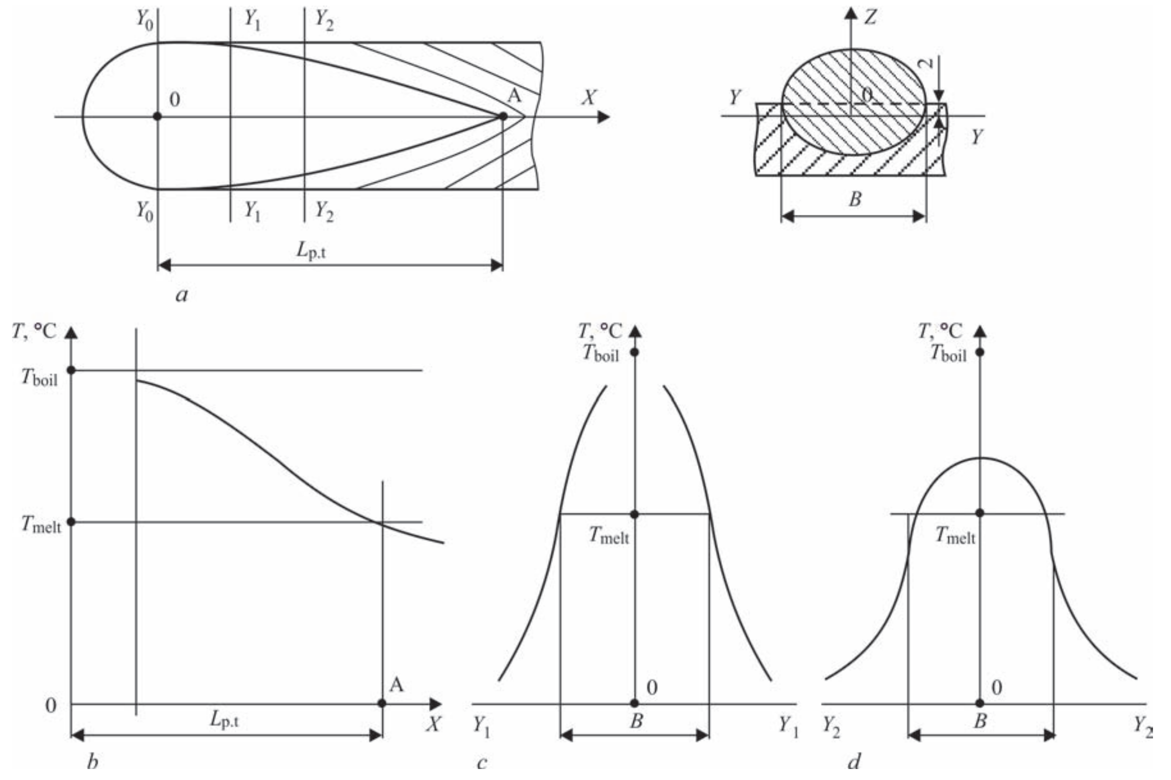

View of the weld pool (*a*) and scheme of temperature distribution in the weld pool ($Z = 0$): *b* — along the pool; *c* — along axis Y_1–Y_1; *d* — along axis Y_2–Y_2

10]. Cluster lifetime is equal to 10^{-7}–10^{-8} s, which is much greater than the period of atom oscillation in the crystalline lattice (10^{-14}–10^{-13} s). Clusters are short-lived, but quite stable atoms groups [10, 11]. A softened zone exists around the clusters (i.e. liquid metal atoms). One cluster of liquid metal (of iron-based alloy) contains about 10^2–10^3 atoms [12, 13]. The volume of the softened zone is equal to 2–5 % for many liquid metals and alloys [9, 10, 19]. The softened zone is an intermediate medium, through which the atoms pass from clusters to other clusters [12]. The publications on casting and metallurgical production consider the «solid-liquid metal» processes in detail, proceeding from the hypothesis of cluster structure of liquid metal [9, 14–18].

The mechanism of liquid metal crystallization is interpreted as follows. Researchers assume that the liquid already contains crystal-like groups (clusters). It is convincingly shown that the earlier used diffusion mechanism of crystallization does not stand scrutiny, as the process of crystallization is approximately 2 to 3 times faster that the rate of diffusion (self-diffusion) of atoms in liquid metals. The diffusion mechanism of crystallization implies formation of a monoatomic layer of the solid phase on the solid phase. It is proven, however, that at crystallization, the atoms form a step, the size of which is several orders of magnitude greater than that of the atom [9]. An elementary block of crystal growth is a certain larger formation, larger than the atom, namely a cluster [9, 10]. Crystal growth due to cluster bonding to the solid phase, does not exclude the possibility of simultaneous occurrence also of bonding of individual atoms. This process, however, is kind of complementary [10].

The above-mentioned crystallization mechanism is theoretically substantiated in works [15–19]. In the thesis [18] mathematical modeling confirmed this crystallization mechanism of iron-based alloys. Obtained model structures are attributed to presence of two stages of the alloy crystallization process. At the first stage clusters are formed in the boundary layer, and at the second stage their subsequent bonding to the cluster-rough surface occurs [18].

In our opinion, the mechanism of the impact of external (controlling) MF on the process of melt crystallization in the pool in arc welding can be explained as follows, on the base of the concepts of liquid metal (alloy) structure in the form of clusters. As is known, the liquid metal in the pool head part in welding iron-based alloys has the temperature of not less than 2500 °C (this temperature reaches the boiling temperature, T_{boil} under the arc). Metal temperature decreases smoothly in the direction of the pool tail part to melting temperature, T_{melt} ($T_{melt} \approx 1500$ °C). Measured by thermocouple immersion into the pool liquid metal in arc welding to the depth of 2 mm from the plate surface, the data of work [20] on the temperature of liquid metal in the pool are schematically given in the Figure. A temperature gradient of liquid metal is observed in the direction towards the tool tail part (Figure *b*). Temperature gradient is even more pronounced in the pool transverse sections (Figure, *c*, *d*). It should be noted that a similar temperature gradient is in place in the direction towards the pool bottom (along *OZ* axis in Figure, *a*). That is the process of crystallization of the pool liquid metal starts on the side walls and at the bottom of the pool, and moves to the pool tail part (up to point *A* in the Figure *a*, *b*, where $T = T_{melt}$). As was convincingly shown in [1], in welding with the impact of alternating LMF (and TMF acc. to our research) the pool liquid metal from the head part, overheated almost to $T = T_{boil}$, periodically moves to the pool tail part, and then to the pool head part. In [1], it is established that temperature gradient before the crystallization front reached 350 °C at some TMF frequencies.

In [9, 10, 12] it was found that at liquid metal overheating, the number of clusters in it becomes greater, and their dimensions become smaller. Considering the data of works [9, 10, 14–19] on cluster mechanism of crystallization and their competitive bonding to the pool solid substrate, it should lead to refinement of the primary structure of weld metal in welding with MF impact that is exactly what was observed in works [1–4].

Conclusions

1. Analysis of publications on metallurgical and casting production showed that many authors support the hypothesis of cluster structure of liquid metals, which was established by diffraction of X-rays, electrons and neutrons from their surface. Here, the ingot structure forms with participation of clusters in the liquid metal.

2. It was suggested that in arc welding with the impact of controlling magnetic fields, the overheated liquid metal from the pool head part, having finer clusters, periodically reaches the crystallization front in its tail part and leads to refinement of the primary structure of the welds.

1. Chernysh, V.P., Kuznetsov, V.D., Briskman, A.N. et al. (1983) *Welding with electromagnetic stirring*. Kiev, Tekhnika [in Russian].
2. Razmyshlyaev, A.D., Ahieieva, M.V. (2014) Features of arc surfacing process in a longitudinal magnetic field. *Appl. Mech. Mater*., **682**, 313–318.
3. Razmyshlyaev, A.D., Vydmysh, P.A., Ageeva, M.V. (2017) *Automatic submerged-arc welding under action of external magnetic field*. Mariupol, PGTU [in Russian].
4. Razmyshlyaev, A.D., Ageeva, M.V. (2018) On mechanism of weld metal structure refinement in arc welding under action of magnetic fields (Review). *The Paton Welding J*., **3**, 25–28.
5. Chalmers, B. (1968) Theory of solidification. Moscow, Metallurgiya [in Russian].
6. Flemings, M. (1977) *Processes of solidification*. Moscow, Mir [in Russian].
7. Bagryansky, K.V., Dobrotina, Z.A., Khrenov, K.K. (1976) *Theory of welding processes*. Kiev, Vyshcha Shkola [in Russian].
8. Frolov, V.V. (1988) *Theory of welding processes*. Moscow, Vysshaya Shkola [in Russian].
9. Gavrilin, I.V. (2000) *Melting and crystallization of metals and alloys*. Vladimir, Vladimir. Un-t [in Russian].
10. Tolochko, N.K., Andrushevich, A.A. (2013) Cluster structure of melts. *Litio i Metallurgiya*, 73(**4**), 59–63 [in Russian].
11. Zhukova, L.A. (2002) *Structure of metallic liquids: Manua*l. Ekaterinburg, UGTU-UPI [in Russian].
12. Skrebtsov, A.M., Ivanov, G.A., Sekachev, A.O. et al. (2006) New method for determination of number of atoms in metal melt cluster. *Visnyk Pryazov. DTU: Transact.*, **16**, 1–7.
13. Skrebtsov, A.M. Structure of liquid metals in liquidus-boiling temperature range. *Protsessy Litiya*, **3**, 3–7 [in Russian].
14. Najdek, V.L., Melnik, S.G. (2015) Clusters — the structural constituents of metal melts. *Metall i Litio Ukrainy*, 266(**7**), 21–33 [in Russian].
15. Aganaev, Yu.P. (2014) Formation of structure of metal alloys under conditions of energy inhomogeneity of phase interface in periodic crystallization. *Sovrem. Naukoyomkie Tekhnologii*, **9**, 6–10 [in Russian].
16. 16. Stetsenko, V.Yu. (2015) Clusters in liquid metals — stable nanocrystals. *Litio i Metallurgiya*, 79(**2**), 33–35 [in Russian].
17. Marukovich, E.I., Stetsenko, V.Yu. (2015) Main difficulties of modern theory of metal melt. Ways to overcome. *Litio i Metallurgiya*, 84(**3**), 24–27 [in Russian].
18. Ivanov, I.A. (2007) *Kinetic phase transition in crystallization of metals from melt:* Syn. of Thesis for Cand. of Phys.-Math. Sci. Degree. Moscow [in Russian].
19. Deev, V.B., Tsetsorina, S.A., Selyanin, I.F., Prikhodko, O.G. (2003) Some peculiarities of cluster model of metal melts. *Polzunovsky Almanakh*, **3**, 141–149 [in Russian].
20. Frumin, I.I. (1961) *Automatic electric arc surfacing*. Kharkov, Lit-ra po Chyornoj i Tsvetnoj Metallurgii [in Russian].

Received 23.10.2018

DOI: http://dx.doi.org/10.15407/tpwj2019.01.06

ROBOTIC WELDING ON TUBE NODES

S. KEITEL[1], **U. MÜCKENHEIM**[1], **U. WOLSKI**[1], **S. LOTZ**[1], **J. MÜGLITZ**[2] and **T. SIGMUND**[3]
[1]SLV Halle GmbH, Halle, Germany
[2]ZIS Industrietechnik GmbH, Meerane , Germany
[3]Ibs Automation GmbH, Chemnitz. E-mail: mail@slv-hall.de

Hollow-profile structures are significantly more stable than structures made using open profiles, which is the main reason for their use in truss and truss-like structures. The node intersections of such structures requires three-dimensional curved welded joints. Small and medium-sized enterprises usually weld tubular frame and truss structures manually, which is highly time-consuming and cost-intensive. In addition, this method requires personnel with corresponding qualifications to carry out the work as the welders need to adapt to constantly changing conditions in weld preparation and welding position, which obviously requires intensive training. Replacing this manual activity by mechanised welding processes would provide great relief to welders. 1 Ref., 2 Tables, 8 Figures.

Keywords: *hollow-profiles, robotsystem, sensor, MAG, productivity; 3D-welding; 3D-cutting*

One-off production still dominates in steel construction as there is hardly any standardisation in joints as applies in other applications, such as pipeline construction. This has kept series production on hollow profile nodes out of the focus in research and development. However, the situation has changed in recent years especially due to developments in offshore wind farms. These structures have frequently repeating joints at the nodes, so a process would be conceivable involving prefabricated nodes with beams welded in between the nodes on site using orbital welding processes. Node prefabrication using the corresponding equipment and manipulation automation would be realistic in view of the small size that nodes occupy compared to the overall structure. Even so, tube node joint welding has so far only been fully mechanised to a limited extent in practice. The equipment is almost only programmed using teach-in methods. Technological limits exist in applications such as those involving multilayer welds and excessive tolerances in semi-finished structures, especially in fully mechanised root welds. Hollow profile prefabrication, on the other hand, involves CNC-controlled thermal cutting using offline programming.

This was the point of focus in the research project, which used theoretical studies, systematisation, welding process development, software customisation, and experimental production on a test rig for industrial implementation towards developing a decision-making basis with presentable reference solutions.

Defining the general conditions. *Tube node geometries and dimensions*. The studies included lattice boom structures in crane construction, tube nodes in vehicle construction and nodes in offshore constructions. These industries all share similar node structures, albeit in varying dimensions. Diameters range from 40 mm to 300 mm in typical structures, with wall thicknesses varying from around 2 to 16 mm.

All the nodes shared a full joint to the socket on the entire wall thickness with added fillet welds. The following materials and tube dimensions were selected for the nodes as examples based on offshore construction applications:

- main tube: diameter 406.4×10 mm; socket: diameter 273×16 mm;
- material: S355;
- oblique joint: 45°, T-joint: 90°;
- bevel angle: 50°.

Weld preparation. Flame or plasma cutting may be used on tube sections in the offshore industry due to the materials and wall thicknesses used. Autogenous flame cutting is usually used in this thickness range, and was also used in the studies. The main reason for that is that flame cutting is suitable for very large cutting angles of up to 65°. Machining processes were also considered in weld preparation, beginning with considering a possible saving in costs especially with thin walls by eliminating the reworking required on thermally cut surfaces and higher accuracy of fit between the components to be joined, even with the increased costs of thin walls. Machining would reduce tolerances to about ± 0.5 mm as compared to about ±2 mm for flame cutting sockets at diameters of 273 mm. Sockets cut at angles of 90° and 60° to the main tube were first flame-cut at a dimensional tolerance of 5 mm, and then machined down. This involved setting the main tube contour at 3 mm away from the nominal inner diameter of the socket to achieve a high degree of accuracy, rather than at the inner diameter itself.

The selected K-node was shaped as a full joint throughout the largest part. The intersection contour in the remaining portion was joined using a multilayer fillet weld, but did not cover the whole material thickness of the socket. In contrast, the double T-node required a full joint around the whole circumference.

Welding processes, additives and auxiliaries. MAG welding (135) was used for deposition rates and suitability for difficult welding positions in agreement with representatives from industry. The intersection contour and frequent variations in roundness in the tubes cause different gap dimensions in positioning the connecting tubes to the main tube. One of the project's areas of focus was therefore to study automated root-run welding on varying gap widths. A number of process variants available on the market may be suitable for this problem, which required research. Several process control options were available using a suitable MIG/MAG power source from EWM. The studies were limited to one power source manufacturer so as to ensure the same equipment in the studies at Halle and on the larger tube nodes at the project partner ibs Automation GmbH in Chemnitz. Welding additive: DIN EN ISO 14341 – A – G4Si1; diameter 1.2 mm Inert gas: DIN EN ISO 14175 – M21 – ArC – 18; 15 l/min.

Design and construction of a test rig. Considerations on applicable component geometries included accessibility during welding, working space and load capacities of potentially suitable robots. Another important point was component positioning depending on weld characteristics with the various component geometries.

These general conditions led to the test rig design as shown in Figure 1.

- KR 15/2 robot with 15 kg load capacity;
- one manipulator with 5 m lift to move the robot;
- manually movable and fixable DKP-400 rotary tilting table on a linear axis positioned before the manipulator;
- one manually movable and fixable roller block on the linear axis;
- CNC control for the nine synchronised movable axes connected to a laser triangulation sensor for weld tracking.

The robot was equipped with Sinumerik 840D SolutionLine CNC control as options for integrating sensor systems, and therefore data connections to the tube blanks. CNC control has a more open structure for the integration required compared to robot controllers. The arrangement of the tilt-and-turn table's rotation axis in the lower part of the work space of the robot and the resulting steep angle of the robot's forearm minimised the risk of collision with the component. Apart from that, the main tube was rotated around its central axis on tracking the weld contour, so the contour on the intersection was effectively welded in a single plane allowing the horizontal rotated welding position.

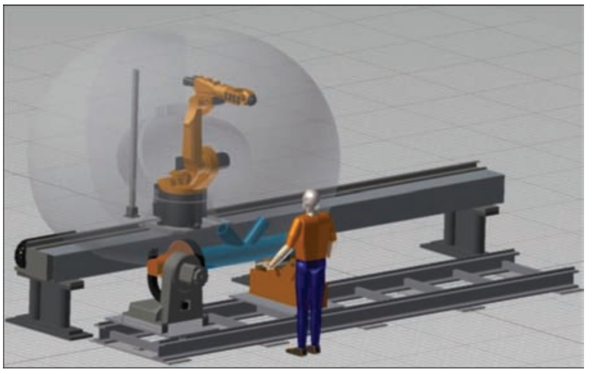

Figure 1. Test rig design with tube nodes

Table 1. Process parameters determined for oblique joint samples (pulsed root)

Gap, mm	I_s, A	U_s, V	v_D, m/min	v_s, cm/min	Comment
0	270–280	30,0	9,3	45	Stringer bead
2	140–150	23,0	4,5	40	Stringer bead
3	140–150	23,0	4,5	16	0,8 s pulse, 1.5 mm amplitude
4	140–150	23,0	4,5	11	0,8 s pulse, 3.0 mm amplitude

A fixed station with monitor, keyboard, mouse and a machine control panel and a hand-held controller as alternative options are available for CNC operation. An interface controller includes, among other things, safety components for an external emergency-stop circuit and access protection for the work space using a light curtain in automatic mode. Figure 2 shows a partial view of the system with the control components.

Developing welding technologies. Initial welding tests on 20 mm linear oblique weld samples using bevel-groove weld preparation alongside the development phase of the robot system were carried out with a 60° flame angle and 50° bevel angle for parameter determination on varying gap widths on a three-axis portal in horizontal rotated welding position. Gap widths of around 1 to 2.5 mm were bridged using a stringer bead root weld, but existing technology (standard process, no pulsing) was unreliable at welding root gaps of 3 mm. The root was unevenly welded through in parts; we were unable to weld a secure

Figure 2. Partial view of the robot system

Table 2. Macrosections for the root weld using the pulsed MAG process

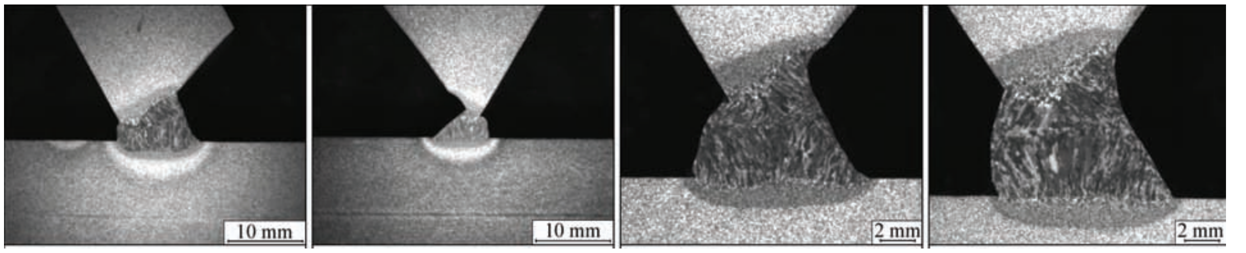

0 mm gap	2 mm gap	3 mm gap	4 mm gap

joint onto the chamfered side of the metal sheet. This bevel-groove weld preparation posed increased risk of incomplete fusion at the root. After starting up the robot work station and connecting a suitable power source using a suitable interface, we made more attempts on a 4 mm gap using methods including the pulse-controlled process and ColdArc light arc. The study focused on determining the parameters for the root weld up to a gap of 4 mm. Samples with gaps of up to 2 mm were still welded wire oscillation, while the torch required oscillation on gaps of 3 mm. We were able to determine suitable parameters for intermediate and outer layers in the preliminary tests on the three-axis portal. In summary, the pulse process proved to be the most suitable root-welding method as shown by detectable level of reliability in edge fusion. The process parameters ultimately defined for the root welds are listed in Table 1. The following Table 2 shows the macrosections for the root welds using the MAG pulse process. Wire oscillation is advisable for reliable fusion on the base plate or tube with root gaps of more than 2 mm. In summary, we opted for the pulse process for the root, intermediate and cover layers in the experiments on the tube nodes.

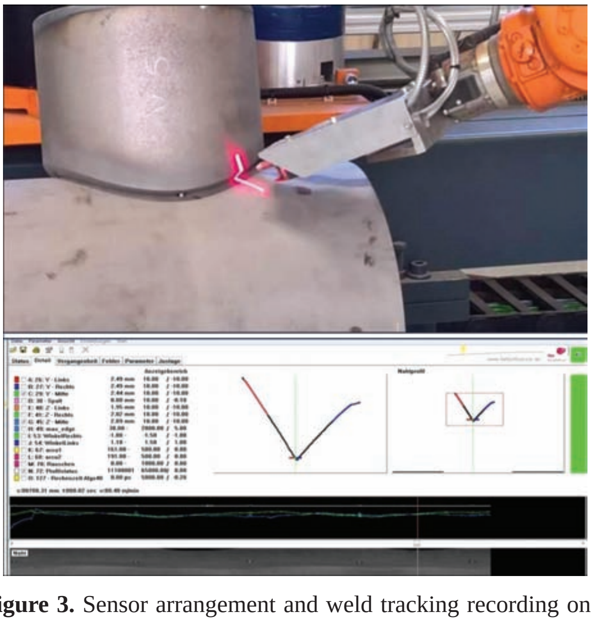

Figure 3. Sensor arrangement and weld tracking recording on a T-joint before welding the root

Control and sensor designs. The robot system's control concept was based on Sinumerik 840D SolutionLine CNC control with Sinumerik Operate 4.7 and Sinamics S120 drive technology from Siemens. These components were designed for operation with a KR15/2 robot and DKP-400 tilt-and-turn table.

The whole approach includes a sensor system consisting of an S7 laser triangulation sensor and a sensor computer from Falldorf. Together with Inspector software, this proved suitable for weld tracking and inspection. Weld tracking used the functions on the gap sensor to determine characteristics of the joint or parts of the joint not yet welded. The joint characteristics were transferred to the CNC controller and processed in real time while the sensor computer received information such as applicable parameters for weld tracking and current path speed from the controller. A Profinet interface was used for communication between the CNC control and sensor computer.

Weld preparation and layer structure required analysis in developing the sensor design. The important point here was to ensure reliable readings for geometric characteristics on the weld joint together with the appropriate evaluation algorithms in the sensor software. Existing geometric characteristics comprised the surfaces on the sheets or tubes, intersections between weld bead and sheet or tube, and intersections between weld layers. Preliminary tests showed evaluation algorithm No.40, T-joint Multimax, to be suitable, as it allowed two lines to be defined around the profile to be imaged. The intersection between the two lines was interpreted as the weld tracking position, and its coordinates were transferred to the CNC control. Additional adjustable offsets in two directions enabled torch position movement against the weld tracking point in addition to the positions of following weld layer on intermediate and cover layers during weld tracking. Smooth metal surfaces are unsuitable for the laser triangulation sensor as surface condition plays a critical role. Sandblasting or brushing the weld preparation or surface in the laser sensor's detection area provides a remedy. The option to decouple welding from measurement proved correct. Figure 3 shows the example of weld tracking on a tube node T-joint

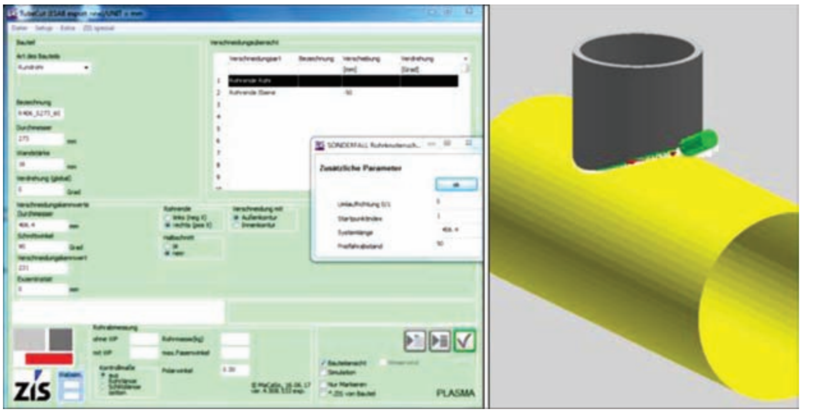

Figure 4. TubeCut input dialogue with rotating direction and starting point as well as a graphical rendering for the T-joint

recorded before a root weld. As the weld filled, usable areas were reduced with decreasing numbers of imaging points available; this made weld tracking more difficult for mathematically modelling the two intersecting lines, at least on the socket side. This evaluation method was unreliable for use on intermediate layers featuring several adjacent welds with a convex profile, which already arose after the third weld layer. Further progress in the multilayer weld saw increasingly varied geometry characteristics due to the uneven filling between the saddle and crown points during inspection tracking. Therefore, the path resulting from weld tracking on the non-welded joint was used for all the weld layers on the welds to the tube nodes and tracked using offset values derived from the layer structure of the oblique joint samples.

Test procedure. First, the weld path was generated using TubeCut CAM software (ZIS Industrietechnik GmbH) [1]. The direction of travel around the socket and the beginning of the path were selectable. A DXF file was suitable for setting the welding torch position and angle to the layer structure. The horizontal rotated welding position was used in welding the socket, which involved using the robot system to turn the tube nodes around the main axis of the tube in sync with the tool. The equipment configuration caused access problems for the welding torch while encircling the oblique joint at the acute angle of the joint. The parameter input dialogue in the customised TubeCut showed more favourable conditions for welding studies on the T-joint as shown in Figure 4.

TubeCut was used again to create the NC program for the T-joint, which only generated the path for the root weld. The path was then used to start weld tracking, the calculated path adjusted to match the actual process, and the coordinates of the path points stored in an NC file for further use. There was no algorithm for parameter adjustment on the widely fluctuating root gap at this point, so the weld preparation was additionally manually adjusted for a root gap from 0 to 0.5 mm. This made the root weld possible at fixed process parameters for a gap of 0 mm at a welding speed adjusted to 40 cm/min. T-joint nodes were also partly mechanically welded to compare cost-effectiveness; Figure 5 shows selected steps in the robot welding process flow.

The small amount of welding material missing at one point on the top layer in the first attempt was solved by minor adjustments in wire positioning; no external irregularities were recognisable in subsequent tests. Figure 6 shows an example image of a cover layer part of a T-joint with a flame-cut and manually altered weld preparation and a total of nine weld layers required.

Welders constantly need to change posture in partly mechanised welding, and each bead required welding in four individual sections (approximately horizontal rotated position). Achieving a favourable weld shape while minimising grinding effort on the intermediate layers required lowering the wire feed and welding current. However, this also required eighteen weld layers.

Results. Three macrosections each were obtained at different positions on the weld for metallographic tests

Figure 5. Steps in the process flow

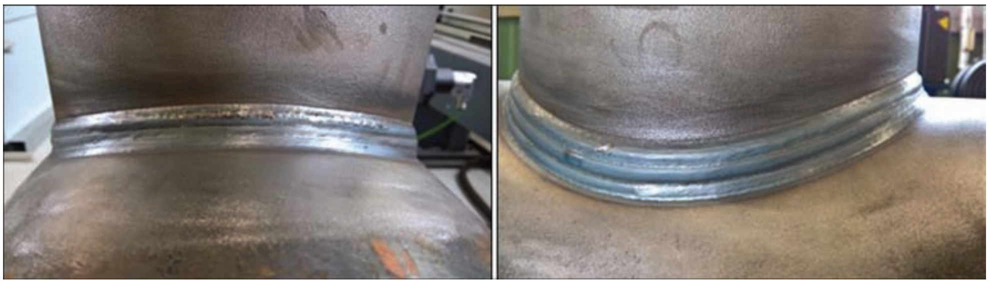

Figure 6. Tube node weld, T-joint (cover layer)

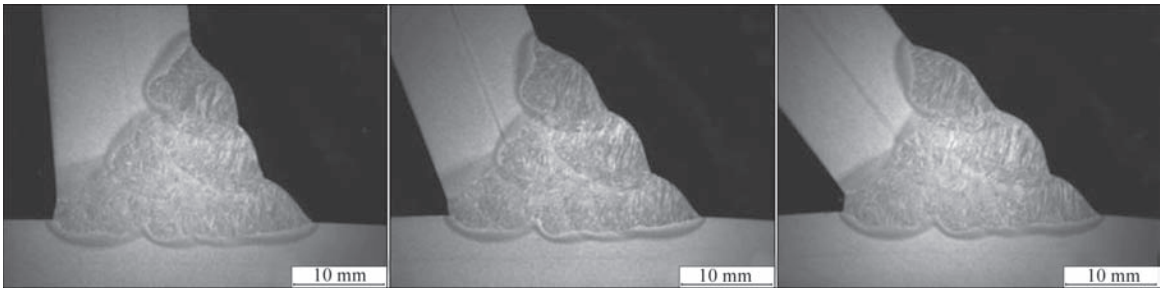

Figure 7. Macrosections on a robotic T-joint weld

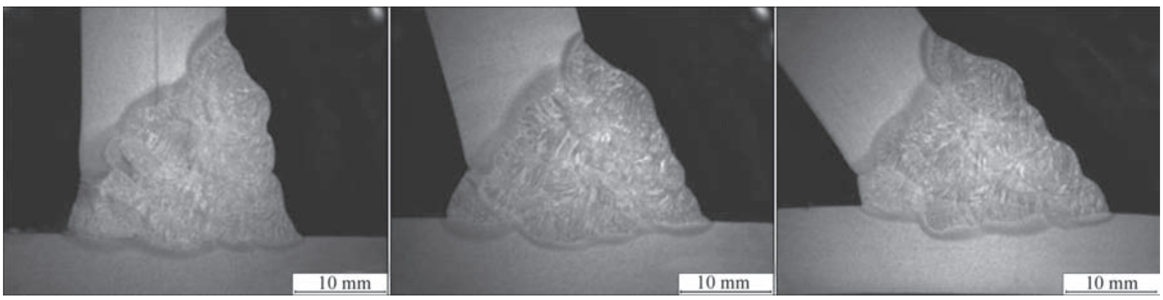

Figure 8. Macro sections on a manual T-joint weld

on the example tube node above in order to assess weld and root fusion quality, see Figure 7 and Figure 8.

The macrosections show that the root weld was not easy for the welder either; this type of work requires extensive training and experience as well as excellent judgement. The test also showed that automation may lead to a favourable outcome on constant gap dimensions. Constant welding speed combined with continuous component movement also increased the deposition rate, thus halving the number of weld layers.

Summary and outlook. The tests carried out in the project have shown that fully mechanised multi-layered MIG/MAG welding is possible on tube joints. The weld quality achieved represents a leap in both geometric and visual quality as well as in material properties, so the findings will be used in further studies planned for this topic. The research findings define the influencing factors determined and possible approaches in performing these complex welding jobs using robots. We intend to research approaches into more detailed issues such as root welding with varying gaps or welding on oblique tube nodes together with the project partners we have been working with so far and new project partners. Implementation on root welds with varying gaps or other joint types (oblique joints) promises a high level of potential in financial terms as shown in initial theoretical economic comparisons using the welded tube nodes as an example. Comparison between manual and robotic welding showed production time savings of around two-thirds. These studies and findings are also of great economic importance in demonstrating automation options as an alternative in view of the apparent lack of qualified welders on the market.

Acknowledgements. *We would like to express our gratitude to the German Federal Ministry of Economics and Technology (BMWi) and EuroNorm as the project owner for their support in our research. We would especially like to thank the companies that participated in these studies:*

- ZIS Industrietechnik GmbH;
- Ibs Automation GmbH;
- Falldorf Sensor GmbH;
- EWM AG.

1. http://www.zis-meerane.de/software/tubecut/

Received 13.11.2018

DOI: http://dx.doi.org/10.15407/tpwj2019.01.07

INFLUENCE OF MODES OF FLUX-CORED STRIP SURFACING ON THEIR WELDING-TECHNOLOGICAL PROPERTIES

A.P. VORONCHUK, A.P. ZHUDRA, A.V. PETROV and **V.O. KOCHURA**
E.O. Paton Electric Welding Institute of the NAS of Ukraine
11 Kazimir Malevich Str., 03150, Kyiv, Ukraine. E-mail: office@paton.kiev.ua

Influence of surfacing modes on welding-technological properties of different types of high-alloyed flux-cored strips was studied. Electrode metal melting, surfacing, loss factors, as well as the efficiency of electrode material melting and deposition rate, were determined. As the objects of study, the flux-cored strips PL-AN-101 and PL-AN-179 made on a shel strip-sheath, as well as the strip PL-AN-111 on the bes on nickel sheath, widely applied in industry, were selected. Surfacing of samples for investigations was performed in A-874N machine with AD-167 attachment and VDU-1201 power source in a wide range of modes: current of 600–900 A, voltage of 32–40 V, speed of 32–55 m/h. Obtained results are presented graphically. It is found that alongside the surfacing modes, the filler-powder composition and sheath strip material have a significant effect on the characteristics of welding-technological properties of flux-cored strips and chemical composition and hardness of deposited metal, respectively. In surfacing with PL-AN-111 strip with a nickel sheath, having a high ohmic resistance, the more intensive heating of the flux-cored strip at the stickout takes place, and, consequently, the coefficient of electrode material melting is increased. Melting efficiency was lower in surfacing with PL-AN-101 and PL-AN-179 strips. At current rise, losses for burn-out and spattering become greater for PL-AN-111 strip, and change only slightly for PL-AN-101 strip, while for PL-AN-179 strip they decrease abruptly in the current range of 900–1200 A because of the specifics of powder-filler composition. Values of melting and surfacing factors, as well as melting and deposition efficiency decrease with increase of process speed for all the strip types. For PL-AN-111 strip, however, these values change only slightly. 7 Ref., 1 Table, 3 Figures.

Keywords: *flux-cored strip, current, voltage, surfacing speed, melting and surfacing efficiency, losses for burn-out and spattering*

In the development of technological processes of restoration and hardening of parts with the use of flux-cored strip, an important tool for obtaining the desired effect is the selection of surfacing modes. A high coefficient of flux-cored strips filling allows conducting the process of surfacing with a high efficiency and producing the deposited layers with a high degree of alloying. Earlier, the attempts were made to study the processes of melting flux-cored strips and formation of deposited layer [1, 2]. But these works describe surfacing at the forced modes under a layer of flux. The specifics of melting flux-cored strips with an open arc required complex studies of influence of the technological parameters of surfacing process and a whole number of factors characterizing the formation and quality of the deposited metal. In previous works [3, 4], the effect of modes of surfacing using flux-cored strips of different compositions on geometrical parameters of the formed beads, chemical composition and hardness of the deposited metal was studied.

In the course of development of these works, the present paper describes the results of investigations on welding-technological properties of flux-cored strips, such as the electrode metal melting, surfacing, loss factors, as well as efficiency of melting the electrode material and efficiency of surfacing.

The mentioned parameters play a key role in the calculation of flux-cored strip compositions and affect the chemical composition, hardness and service characteristics of the deposited metal.

Three grades of flux-cored strips: PL-Np-300Kh25S3N2G2 (PL-AN-101) and PL-Np-400Kh20B7M7V2F (PL-AN-179) were investigated, made on the basis of steel strip-sheath, and also the strip PL-Np500Kh40N40S2RTs (PL-AN-111), which is made on the base of the nickel strip of the sheath [5–7]. The selection of flux-cored strip grades with a steel sheath is predetermined by the fact that the strip PL-AN-101 was made using a complex alloying in the composition of the powder-filler. The strip PL-AN-179 was made on the base of a mechanical mixture of refractory ferroalloys.

The experiments were carried out in the surfacing machine A-874N, equipped with the power source VDU-1201 and the attachment AD-167. Surfacing was performed in separate beads in a single layer at direct current of reverse polarity, at a constant value of stickout equal to 50 mm and a rigid external char-

Surfacing modes

Current, A	Voltage, V	Surfacing speed, m/h
600 ± 25	32 ± I	32 ± 1
750 ± 25	32 ± I	32 ± 1
900 ± 25	32 ± I	32 ± 1
1150 ± 25	32 ± I	32 ± 1
1200 ± *25*	32 ± I	32 ± 1
900 ± 25	24 ± I	32 ± 1
900 ± 25	28 ± I	32 ± 1
900 ± 25	36 ± I	32 ± 1I
900 ± 25	40 ± I	32 ± 1
900 ± 25	32 ± I	19 ± 1
900 ± 25	32 ± I	40 ± 1
900 ± 25	32 ± I	48 ± 1
900 ± 25	32 ± I	55 ± 1

acteristic of the power source. As the base metal, the plates from St3 with a thickness of 30 mm and a size of 300×400 mm were used. On each of the plates 6 beads were deposited with a length of 200–250 mm. To exclude the effect of preheating, each subsequent bead was applied after a complete cooling of the previous one. The surfacing modes using all the given strips are shown in the Table.

The coefficients of melting α_m and surfacing α_s were determined by the formulas:

$$\alpha_m = \frac{3600(m_{st} - m^1_{st})}{It},$$

where m_{st} is the mass of the strip before surfacing, g; $_{st}$ is the mass of the strip after surfacing, g; I is the current of surfacing, A; t is the time of surfacing, s;

$$\alpha\ = \frac{3600(m_p \quad m_p)}{It}$$

where m_p is the mass of the plate after surfacing, g; m^1_p is the mass of the plate before surfacing, g; I is the current of surfacing, A; t is the time of surfacing, s.

The loss coefficient K_l is determined by the formula

$$K_l = \frac{(m_{st} - m^1_{st}) - (m_p - m^1_p)}{(m_{st} - m^1_{st})}.$$

The efficiency of melting and surfacing (N, N') were determined by the formulas:

$$N = \frac{\Delta m \cdot 3.6}{t}, \quad N' = \frac{\Delta m' \cdot 3.6}{t},$$

where Δm is the difference between the masses of the strip segments before and after surfacing, g; $\Delta m'$ is the difference between the masses of the plates after and before surfacing; t is the time of surfacing, s.

Figure 1 presents data by coefficients of melting, surfacing and losses, as well as by efficiency of electrode melting and surfacing depending on current. The coefficient of melting of the electrode material

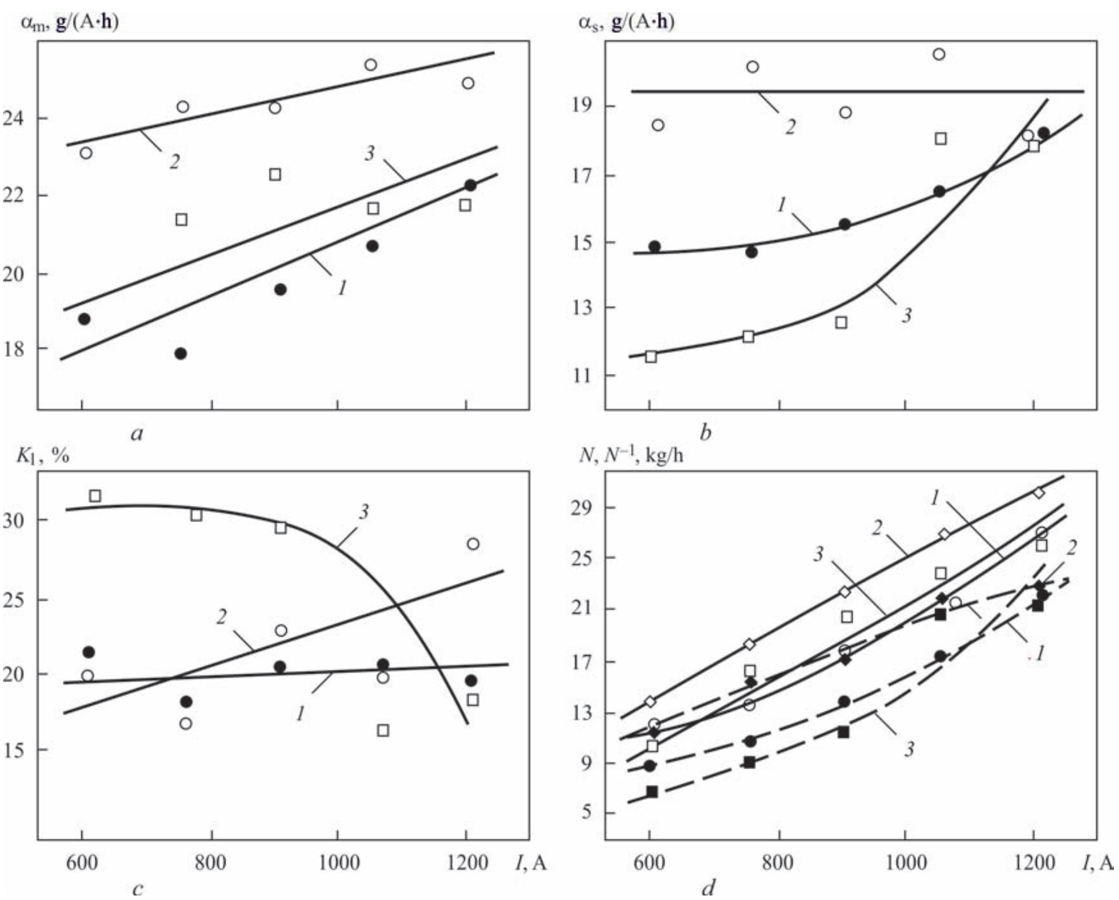

Figure 1. Characteristics of melting flux-cored strips depending on current: *a* — melting factors; *b* — surfacing factors; *c* — loss factors; *d* — efficiency of melting (solid) and surfacing (dashed) of flux-cored strips (*1* — PL-AN 101; *2* — PL-AN 111; *3* — PL-AN 179)

(Figure 1, *a*) increases with growing current for all tested flux-cored strips. At the same time, it should be noted that the coefficient of melting the flux-cored strip PL-AN 111 is significantly (by 2.5–4.0 g/A·h) higher than for the flux-cored strips PL-AN 101 and PL-AN 179. This is explained by differences in the nature of melting the electrode materials associated with the use of different strips-sheathes during manufacture.

Thus, the strip PL-AN 111 is manufactured with the use of nickel strip and, as was noted above, this causes its higher ohmic resistance, and consequently, the more intense heating of the electrode material at the stickout.

The deposition rate factor (Figure 1, *b*) for different strips with the increase in current from 600 to 1200 A behaves ambiguously. When using flux-cored strips PL-AN 101 and PL-AN 179, it increases, moreover, for the strip PL-AN 179 its growth is more pronounced. When using the flux-cored strip PL-AN 111, the change in the deposition rate factor with increasing current does not occur. This is explained by differences in varying losses with the increase in current from 600 to 1200 A (Figure 1, *c*). Thus, the relative value of losses for burn-out and spattering over the entire range of current variation for the flux-cored strip PL-AN 101 remains unchanged, and for the flux-cored strip PL-AN 111 it increases, and for PL-AN 179 it drops sharply.

Both the efficiency of melting flux-cored strips, as well as the efficiency of surfacing grows for all grades of tested flux-cored strips with the increase in current within the entire considered range (Figure 1, *d*).

Figure 2 presents data on characteristics of melting the flux-cored strips depending on the arc voltage. The coefficient of melting the flux-cored strips increases with growing arc voltage (Figure 2, *a*). For the flux-cored strips PL-AN 101 and PL-AN 179, as the arc voltage grows, the deposition rate factors also increase (Figure 2, *b*).

During surfacing using the strip PL-AN 111, a similar increase is observed when the voltage grows

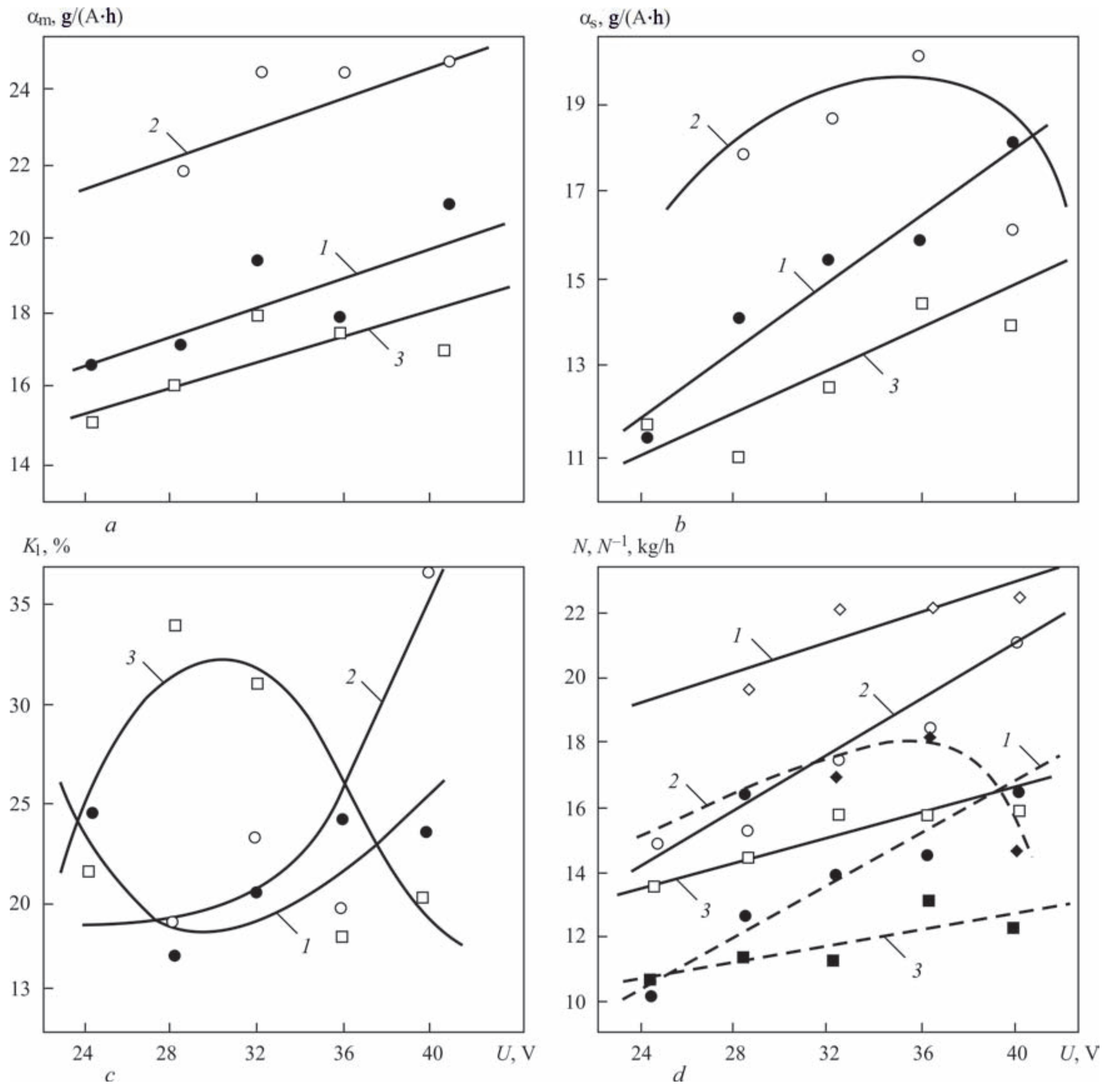

Figure 2. Characteristics of melting flux-cored strips depending on voltage (designations are the same as in Figure 1)

to 32–34 V. A further increase in voltage leads to decrease in the values of specified characteristics. At the same time, as is seen from the plot (Figure 2, *c*), the burn-out and spattering losses sharply increase, which, obviously, is first of all connected with the active oxidation of the electrode material components.

Figure 3 shows the coefficients of melting and surfacing, as well as the efficiency of melting and surfacing depending on the speed of arc movement for all the tested flux-cored strips.

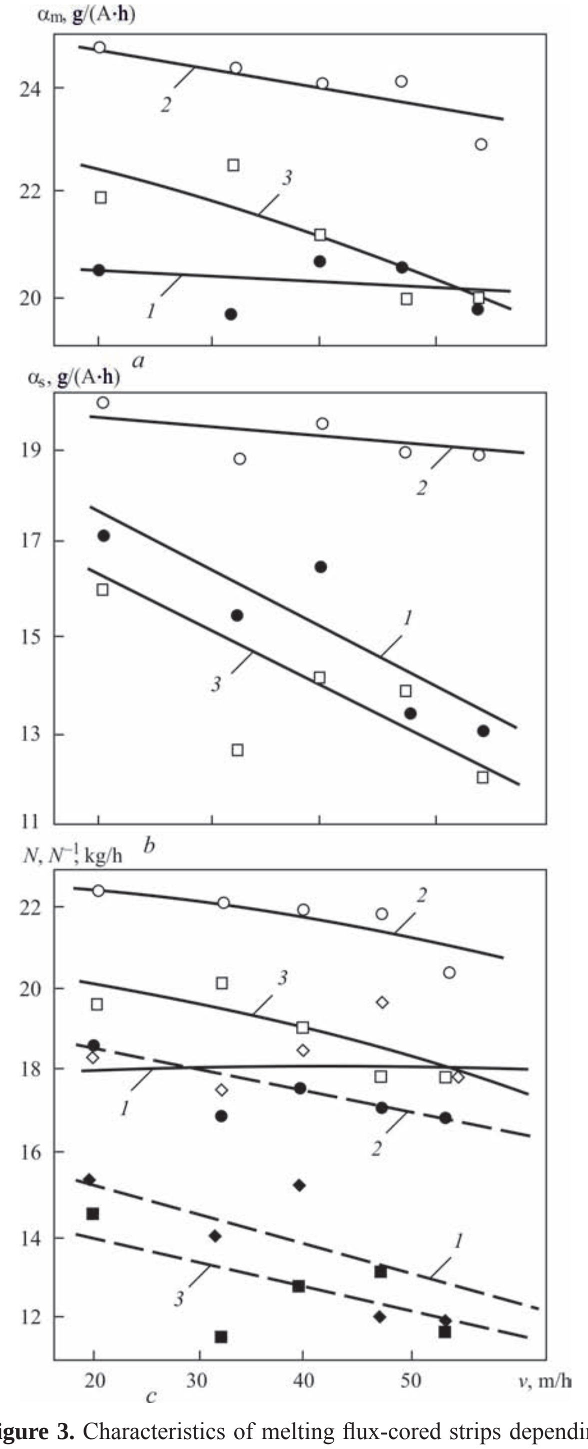

Figure 3. Characteristics of melting flux-cored strips depending on change in the rate of surfacing: *a* — melting factors; *b* — surfacing factors; *c* — efficiency of melting (solid) and surfacing (dashed) of flux-cored strips (*1* — PL-AN 101; *2* — PL-AN 111; *3* — PL-AN 179)

Considering the results obtained in general, the following should be noted. The characteristics of melting the flux-cored strips, and, consequently, the chemical composition and hardness of the deposited metal, in addition to surfacing modes, are significantly influenced by the composition of the powder-filler and the strip-sheath material. Thus, during surfacing using the flux-cored strip PL-AN 111, made on the base of nickel strip-sheath, all the studied characteristics are significantly different from the data obtained during surfacing using the flux-cored strips PL-AN 101 and PL-AN 179, made of steel strip-sheath. This can obviously be explained by a higher ohmic resistance of the nickel strip-sheath. At the same time, due to a higher voltage drop on the electrode stickout, a more intensive heating of the flux-cored strip on the stickout occurs, which, in turn, increases the efficiency of its arc melting, i.e. leads to a more efficient use of heat power of the arc. The resulting positive effect in the form of increasing coefficient of melting the electrode material, which is a decrease in the volume of the base metal, is leveled by increase in burn-out and spattering losses. It should be noted that the chemical composition of the metal deposited by the flux-cored strip PL-AN 111 with the simultaneous influence of the abovementioned factors, remains almost unchanged in the entire considered range of welding current. Increase in voltage leads to intensive oxidation of basic alloying components: carbon and chromium, which reduces the degree of alloying of the deposited metal and its hardness. During surfacing using the flux-cored strips PL-AN 101 and PL-AN 179, the efficiency of melting is somewhat lower than that in the flux-cored strip PL-AN 111, but at higher currents the amount of the deposited metal for all strips is approximately the same. This can be explained by difference in losses of electrode material for burn-out and spattering. Thus, the losses for the strip PL-AN 101 with an increase in current change very slightly, for the strip PL-AN 111, they grow, and for the strip PL-AN 179 they fall sharply in the range of 900–1200 A.

The drop of losses for the flux-cored strip PL-AN 179 is obviously connected with the nature of melting the powder-filler, which is characterized by the presence of a large number of refractory components. In addition, this strip is characterized by the highest filling coefficient among the tested strips, which is about 65 %. In our opinion, this causes large losses of electrode material at low currents because of the insufficient of heat power of the arc and insufficient preheating of the strip at the stickout.

Increase in voltage for all the flux-cored strips leads to decrease in the level of alloying the deposited layer. This is explained by both an increase in the volume of the base metal and an increase in burn-out losses. Moreover, the burn-out losses increase more, if the preheating at the electrode stickout is higher. Thus, they increase most strongly during surfacing using the flux-cored strip PL-AN 111.

The deposition rate has a less noticeable effect on the studied characteristics, which mainly depends on distribution of heat fluxes and heat power of the arc.

For a more complete explanation of the obtained results, it is of interest to further investigate the ohmic resistance of the tested flux-cored strips and to obtain data on their preheating at the stickout.

Conclusions

1. The coefficient of melting the electrode materials increases with rise both current as well as voltage for all the types of strips. This is especially evident during surfacing using the strip PL-AN-111 with nickel sheath, which has a higher ohmic resistance.

2. The deposition rate factor grows with the increase in current and voltage for the flux-cored strips PL-AN-101 and PL-AN-179. For the strip PL-AN-111, it is stable when the current grows, and with the increase in voltage to 36 V, it grows and then drops sharply, which is associated with the increase in losses for burn-out and spattering.

3. The efficiency of melting and surfacing of flux-cored strips increases with the growth of current and voltage for all types of flux-cored strips, however, when the voltage is higher than 36 V, for the strip PL-AN-111, the efficiency of surfacing drops sharply due to the increase in the coefficient of losses for burn-out and spattering.

4. The coefficient of losses depends little on the current and voltage for the strip PL-AN-101, but increases significantly with the growth of current for the strip PL-AN-111 and is especially high at the voltages higher than 36 V. For the strip PL-AN- 179, the coefficient of losses sharply decreases with the growth of current to higher than 800 A, and the voltage higher than 32 V. This is connected with the refractory strip core, for melting of which an increased heat power of the arc is required.

5. In the entire range of modes of the surfacing process, the values of melting and surfacing coefficients of all types of strips, as well as the efficiency of melting and surfacing decreases with the increase in deposition rate, but for the strip PL-AN-111 these values change insignificantly.

1. Kuznetsov, L.D., Kortelev, G.A., Nikolaenko, N.R. (1982) Peculiarities of process of flux-cored strip surfacing on forced modes of parts of construction and road machines. *Theoretical and technological principles of surfacing. Current methods of surfacing and their application*. Ed. by I.I. Frumin. Kiev, PWI, 12–15 [in Russian].
2. Kuznetsov, L.D., Kurkumelli, E.G., Nikolaenko, M.R. (1983) Peculiarities of structure and properties of metal in surfacing with strip electrodes on forced modes. *Wear-resistant and high-temperature steels and alloys*. Surfacing materials. Kiev, PWI, 24–28 [in Russian].
3. Zhudra, A.P., Voronchuk, A.P., Kochura, V.O., Fedosenko, V.V. (2017) Effect of flux-cored strip surfacing modes on geometric parameters of deposited beads. *The Paton Welding J*., **1**, 36–40.
4. Voronchuk, A.P., Zhudra, A.P., Petrov, A.V., Fedosenko, V.V. (2018) Influence of surfacing modes using flux-cored strips on chemical composition and hardness of deposited metal. *Ibid*., **4**, 35–38.
5. Danilchenko, B.V., Shimanovsky, V.P., Voronchuk, A.P., Kopylets, I.P. (1989) Surfacing of high-wear parts with self-shielding flux-cored strips. *Avtomaticheskaya Svarka*, **5**, 38–41 [in Russian].
6. Zhudra, A.P., Voronchuk, A.P. (2010) Wear-resistant surfacing with flux-cored strips. Svarshchik, **6**, 6–9 [in Russian].
7. Zhudra, A.P., Voronchuk, A.P. (2012) Cladding flux-cored strips (Review). *The Paton Welding J*., **1**, 34–38.

Received 21.11.2018

INTERNATIONAL INDUSTRIAL FORUM-2018

XVI International Forum took place on November 20–23 in Kyiv on the territory of the International Exhibition Center. This event starting from 2005 is included in the list of leading world industrial exhibitions, being officially certified and recognized by the Global Association of the Exhibition Industry (UFI) and year by year remains the largest exhibition event of machine-building topic in Ukraine.

The International Exhibition Center acts as the exhibition organizer. It provided excellent conditions for many companies and plants, which for many years choose Industrial Forum as an area for demonstration of their novel developments and place for meeting with wide range of specialists and potential partners.

352 enterprises and companies from 32 countries in the world have participated in the International Industrial Forum. In particular, China, Czechia and Turkey formed their national expositions. Total area of exposition made 22000 m^2, exhibition was visited by more than 12000 specialists.

In scope of the Forum the following international specialized exhibitions took place:

• Metal working (metal processing technologies, equipment);

• UkrVtorTekh (commission techniques and equipment);

• UkrCasting (equipment and technologies for casting production);

• UkrWelding (technology, equipment and materials);

• Hydraulics. Pneumatics;

• Bearings (rolling bearings, sliding bearings, free parts: balls, rolls, clamping sleeves, technologies, equipment and tools for bearing production);

• UkrPromAutomation (automation of production, automated systems for regulation of technological processes , automation of industrial objects);

• Lifting-transport, warehouse equipment;

• Samples, standards, templates, devices (control-measurement devices, laboratory and testing equipment, metrology, certification);

• Industrial safety (protective means, safety of working zone);

• National exposition of enterprises from Turkey.

First Vice-Prime Minister of Ukraine — Minister of Economic Development and Trade of Ukraine Stepan Ivanovich Kubiv visited the International Industrial Forum, made a speech during its opening and then attentively took a look at expositions of the enterprises of machine-building branch of Ukraine.

Enterprises of the domestic machine-building complex demonstrated in a worthy manner on their booths their products and developments. Metal working direction traditionally was presented by Avantis (Zhitomir), MIOS Company (Drogobych), Prigma-Press (Khmelnitsky), Motor Sich (Zaporozhie), Chernigov Mechanical Plant and others.

Micra LLC (Kyiv), Microl (Ivano-Frankovsk), Novotest (Novomoskovsk), Tekhnopolis Company (Kyiv) and other companies presented their developments in the field of instrument making and industrial automation. Krankomplekt plant (Zaporozhie), Alexandria Crane Systems, SPG Stankompromimport (Kharkov) and many

other manufacturers and designers of equipment and technologies can be outlined among the manufacturers of lifting-transport and warehouse equipment.

For the second consecutive year the Industrial Forum demonstrated the expositions of significant number of enterprise-manufacturers of laser equipment. It was presented on the booths of Jinan Bodor CNC Machine Co., Ltd (PRC), Abplanalp Ukraine (Kyiv), engineering subdivision ALISTA, Dnepropolimermash (Dnepr), Aramis (Cherkasy), El-Sel Group, Mashintech (Kyiv), Storozhuk (Kyiv).

Exposition of industrial tool traditionally impressed by perfect quality and variety of products, presented by permanent participants — Doss Instrument, ZCC Cutting Tools Europe (Germany), AV POLYSTAR (Kharkov), Industrial Company Golden Fleece, Ukraine (Kyiv), PKP Komkor (Dpenr), Microtech (Kharkov), Pnevmomaster (Kyiv), Praktyka Ukrayna (Dnepr), Tsentr Innovatsionnykh Tekhnologiy LM (Dnepr), Stankoinstrumentimport (Kyiv) and other manufacturers and suppliers of instruments.

Exhibition section «UkrWelding» of the Forum included demonstration of achievements in such directions:

- equipment and technology for welding and cutting;
- equipment for brazing, surfacing and related technologies;
- equipment for thermal treatment of materials and welded structures;
- equipment and technologies of welding consumables production;
- instruments and materials for welding, cutting, brazing;
- automation of welding processes.

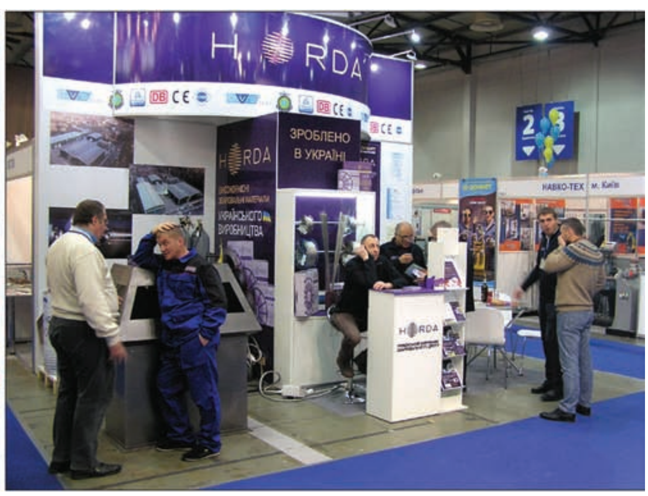



The participants of the exhibition, domestic and foreign presented significant number of equipment and materials for implementation of innovative technologies in welding branch. Demonstration of equipment operation for wide audience of specialists took place at the booths of Ideal (Odessa), Ukraine (Kyiv), Binzel Ukraine, Fronius Ukraine (Kyiv region) and series of others during all four days of the exhibition.

Among the domestic leaders in the field of welding and related technologies there were next companies, which presented their products and technology, namely Machine building factory Vistec (Bakhmut, Donetsk region), Vitapolis (Kyiv region), Autogenous equipment plant DONMET (Kramatorsk, Donetsk region), Energiya Svarka (Zaporozhie), Sumy-Electrode, Techvagonmash (Kremenchug, Poltava region), TM.Weltek (Kyiv), Triada Ltd. (Zaporozhie) and others.

For the first time among the participants of «UkrWelding» Exhibition there is Oliver (Minsk). It presented to the visitors a wide range of modern welding consumables (wires and coated electrodes) of Oliver production.

Robotics complexes at the booths of Binzel Ukraine (Kyiv region), KB Robotics Engineering (Kyiv region), Sammit (Dnepr), Techvagonmash (Kremenchug, Poltava region), Triada Ltd. (Zaporozhie), Fanuc Ukraine (Kyiv) continuously attracted attention of the specialists.

Equipment for plasma cutting was presented on the booths of Ukrainian production companies Artel Ltd. (Nikolaev), Zont, UG-Stankoservice (Odessa), Techmach (Odessa) as well as Favoryt AM (Lvov).

Comparing the Industrial Forum-2018 with earlier carried it is possible to note a rising attention to innovative technologies, experience of their implementation into domestic production and expansion of the sales market of the products in the European direction.

A.T. Zelnichenko, V.N. Lipodaev

INTERNATIONAL CONFERENCE «WELDING AND RELATED TECHNOLOGIES — PRESENT AND FUTURE»

On December 5–6, 2018 in Kiev at the conference-centre «DEPO» a representative International Conference «Welding and Related Technologies – Present and Future» was held, organized by the National Academy of Sciences of Ukraine, the E.O. Paton Electric Welding Institute, the International Institute of Welding and the International Association «Welding». The Conference was dedicated to the 100th anniversary of the National Academy of Sciences of Ukraine. In it more than 200 representatives of academic institutes, branch research institutes, universities, scientific, design and engineering centers, industrial and commercial enterprises, chiefs and managers of business structures, etc. took part. Among the Conference participants the foreign scientists from Austria, Bulgaria, Great Britain, Germany, Georgia, Israel, Kazakhstan, Canada, China, Poland, Slovakia and Switzerland participated. Among the honored guests of the Conference, Ms. Cecile Mayer, Executive Director of the International Institute of Welding, was present.

The beginning of the Conference was preceded by a musical greeting from the string ensemble «Kyiv Soloists» and greetings of Academician A.G. Naumovets, Vice-President of the NAS of Ukraine and Mr. Liao Bing, President of the Academy of Sciences of Guangdong Province (China).

During December 5 and the first half of December 6, 18 reports of scientists on the most important scientific and applied achievements in recent years in the field of welding and related technologies, as well as long-term development of these directions were presented and discussed at the plenary sessions.

Among the speakers there were well-known scientists Liao Bing (China), U. Reisgen (Germany), A. Pietras (Poland), L. Gelman (Great Britain), S.I. Kuchuk-Yatsen-

ko (Ukraine), L.M. Lobanov (Ukraine), I.V. Krivtsun (Ukraine), V.T. Nazarchuk (Ukraine), S. Keitel (Germany), J. Kleiman (Canada), M. Beloev (Bulgaria), V.V. Kvasnitsky (Ukraine), N. Enzinger (Austria), F. Kolenic (Slovakia), I.S. Gakh, Z.T. Nazarchuk, V.M. Nesterenkov, S.V. Akhonin (Ukraine).

The plenary report of B. E. Paton «Modern achievements and developments of the E.O. Paton Electric Welding Institute in the field of welding and related technologies» was presented by L. M. Lobanov.

On December 6, in parallel with the main reports of the Conference, at the youth section «Welding and related technologies» the reports of young specialists were presented.

On the afternoon of December 6, in the reading hall of the E.O. Paton Electric Welding Institute over 150 poster reports were presented. The exposition included the following sections:

• technologies, materials and equipment for welding and related technologies (52 reports);

• strength, stress-strain state, nondestructive testing, technical diagnostics (30 reports);

• surface engineering (28 reports);

• ecology, welding in medicine, new materials, certification and standardization of welding production (15 reports);

• section of young specialists (27 reports).

The exchange of opinions in discussing the scientific information was mutually beneficial.

By the beginning of the Conference, the plenary reports were published in the form of paired issues of the journal «Avtomaticheskaya Svarka» (Nos 11–12, 2018) and «The Paton Welding Journal» (Nos 11–12, 2018), and also in the Proceedings of the poster reports.

During the Conference, its participants were given the opportunity to familiarize themselves with the updated exposition of the demonstration hall of the E.O. Paton Electric Welding Institute.

Also, on December 6, the XX Council of the International Association «Welding» was held, at which the results of the work of the Association for the reporting period and the directions of future works were discussed. By the decision of the IAW Council, the authorities of Academician B.E. Paton, the President of the IAW Council and Dr. A.T. Zelnichenko, the IAW Director, were prolonged until 2020.

On December 7, for the participants of the Conference from Bulgaria and Poland a trip to the plant of the Company «Vita Polis» (Boyarka town, Kiev region) was organized, where they familiarized themselves with the production of welding wires of stainless and special steels, which were not previously produced in Ukraine.

A.T. Zelnichenko, V.N. Lipodaev

ROBOTIZATION OF WELDING PRODUCTION — ARGUMENTS «FOR»

In the recent past, in the engineering industry of Ukraine a persistent stereotype has emerged that industrial robots are expensive machines, which require a highly professional personnel and should be rationally applied in the conditions of mass or large-scale production. This myth is based on the following facts.

Robotic complex for welding of rear tail boards of dump trucks

Firstly, when calculating the effectiveness of implementing a robotic and technical complex (RTC), incomplete methods are often used. They take into account a direct piece-rate salary of welder, but at the same time the following items are missing:

• direct and indirect taxes on basic salary;

• additional salary;

• expenses for maintenance of back rooms (changing rooms, showers, toilets, canteens, etc.);

• coefficient, accounting for the probability of continuous operation of the RTC due to the absence of working shifts, vacations, sick leave, unproductive losses;

• reduction in costs for welding consumables (wire, shielding gas) and electricity;

• reduction in labor intensity for cleaning of welds;

• elimination of costs for training and recertification of qualified welders.

Secondly:

• unwillingness and inability of personnel at the enterprise to master the new technological processes. Hence, the forced administrative measures emerge, like additional inviting of new specialists to the existing staff, which threatens the recoupment of investments and creates antagonism in the team. Here it should be mentioned about the problematic nature of inviting the programmer-operator of the RTC of an appropriate level of training to the project.

Robotic complex for welding of transverse carriage beams

Thirdly:

• it is believed that robotic welding is intended for large volumes of products — for example, mass production of cars. At the same time, the model range should not change during several years;

Robotic complex for welding of container walls

• lack of flexibility of RTC. Most managers believe that their enterprises produce rather small batches of goods in order to invest in a robotic system.

Fourthly:

• robotic and technical complexes often break down, their repair is expensive and takes a lot of time. It is difficult to find specialists in repair and maintenance.

These are the main myths which make us think that industrial robots are expensive technologies which require a highly professional personnel and should be rationally used only in mass or large-scale production.

Now let us look how things on the outlined problems are going in reality.

On the first problem. By applying the real basic data on the cost-effectiveness of using RTC of the own enterprise, you will have the expected payback period of investments, which will help you to make a well-grounded decision. A recommendation is that basic data should reflect real values and not be «far-fetched».

As a result, you will receive a payback period on investments and can make a well-grounded decision.

Robotic complex for welding of heating boilers

On the second problem. Since the appearance of welding robots, manufacturers have constantly improved the process of writing working programs, striving to simplify it as much as possible and at the same time to make life for the future operator-programmer easier. Today, this problem has been solved with the help of the program Kinetiq, developed by the Robotiq Company (Canada), a fundamentally new program for training robots. The similar programs also exist at other developers. This technology allows the operator to manually move the welding torch of the robot along the entire weld line, and then, using the remote control, to entry the movement trajectory into memory and determine the welding parameters.

Robotic complex for welding of side boards of dump trucks

On the third problem. Modern RTCs are capable to quickly replace tools in automatic mode. Therefore, it is advisable to surround the robotic welding device with various removable tools. The robot can be programmed for all day operation only in position A with a specific set of tools, or alternately in positions A, B and C, producing small batches of each part. The sockets for tools are designed for quick replacement. The operator only needs a couple of movements to completely change one set to another. The robot stores many different programs in memory and it remains only to switch-over the program to make the robot start welding of a completely different part.

Here are just a few examples of RTC configuration.

You do not need to choose configuration and completing parts of the RTC on yourself. You need to correctly make a technical assignment for the required complex and contact the specialists.

The Scientific and Production Tekhvagonmash Company has been an integrator of the robots Fanuc in Ukraine for 10 years. As a rule, the proposal includes several options for solving the problem.

You will have only to make a choice in favor of one of them. Our company, in addition to the delivery of equipment, performs assembly and mounting, develops technology and trains the customer’s personnel.

On the fourth problem. Modern complexes, as a rule, are equipped with USB output, which allows transferring programs, created remotely using offline programming, to the robot memory. In addition, they are provided with a function of Internet connection for online communication with the supplier carrying out warranty or post-warranty support. As the practice shows, 99 % of failures of a complex occur because of the error of the operator or programmer of the RTC (a part is incorrectly installed in the RTC, a poor-quality assembly for welding, an error in creating a program, etc.). These errors are easily diagnosed and eliminated on site. The remaining 1 % is the failure of the program. Diagnostics and elimination are performed remotely without the time losses. In extremely rare cases, it is necessary that a specialist-integrator arrive to the site. Here the decisive factor is the geographical distance and the obligation of the supplier. The terms of warranty or post-warranty service should necessarily be taken into account in the contract for delivery.

A few more reasons in favor of the RTC effectiveness

Increase in efficiency

One of the main ways to justify the costs on a robot is to compare the efficiency of the RTC with the efficiency that you currently have, using manual or semi-automatic welding. In many cases, robot welding is performed 2–5 times quicker than using any other method. This means that for each hour you will produce 2–5 times more parts than you produce now. For example, the system of tandem MIG welding which simultaneously uses two arcs, combined by a robot, can increase efficiency by several times.

High reliability

Let us admit that hired workers are sometimes unreliable, they may not appear at work or they may have a bad day. Robots are reliable, they can work around the clock without a rest or a lunch break. In addition, having robots, you will forget about the staff turnover. They are loyal to your company and will not leave after their training by you.

Ability to increase volumes

When you sign a new contract, or wish to expand the range of performed works, robots will easily cope with the additional volume. And since they occupy less working space than people, during expansion of production, you will not have to worry about buildings, renting or purchasing additional areas. In most cases, robots are paid back within six months.

Guaranteed quality

Each time, robot will perform the same welding at the same point. Thus, it helps manufacturer to improve quality and efficiency. Having robots, the company invests in goods in advance without the need to correct defects after their occurrence as often happens in the case with manual or semi-automatic welding.

To check the welds, made by the robot, a visual inspection is usually sufficient. In semi-automatic or manual welding, additional tests may be needed, such as selective destructive testing, radiography or color flaw detection.

Savings on welding consumables

Buying a robot will reduce overlapping of a rather large weld, which often occurs during manual performing. During the work of electric welder the strength margin is already preset into each weld, which is made by him. As a result, he usually uses more filler metal than it is necessary and also makes an excessive weld reinforcement. The accuracy of the robot is much higher, it uses as much filler material as necessary. Moreover, in robotic welding, spattering is lower and, as a result, the consumption of welding wire is 10–15 % lower.

Reduced costs for training

As we have already mentioned, today it is very difficult to find a skilled worker. In changing economic conditions, it turns out that the labor market lacks qualified welders. Ever more young people are seeking for higher education. This means a shortage of young specialists who would replace the specialists of retirement age. The companies spend huge sums of money on search and training of welders, which are much higher than they realize themselves. Moreover, during the work requiring keeping in compliance with the rules of technical operation, welders should constantly pass retraining and prove their skills. Some enterprises even provided workers with their own training centers. As compared to the salary of a qualified welder, it is much cheaper to hire someone who will simply load and unload RTC.

Quality control during welding

The modern software of robots allows companies to improve the process of production control. For example, the software for arc tracking which monitors, records, and makes reports with welding data in real time mode. The data can be transferred to the central storage database via the Internet (local network). Other software automatically corrects errors and provides a quick solution to the problem in the case of an unexpected error of the robot, if it occurs. And finally, protection with the password and making the log of events will provide a current report of any changes in the process of robotic welding over a certain period of time. All these software packages are developed to help companies in maintaining a high standard of quality even in case of personnel replacement.

Conclusion

We hope that these arguments will help you to make a well-grounded decision in favor of robotization of your production. For most manufacturers, robotization and automation should only be a matter of time. If you are going to install a robot for the first time, choose a reliable integrator who in close cooperation with you will develop a system, corresponding to your individual desires. For any project on welding automation the technical support and training are also important. Remember that the tasks of automation and robotization are to reduce the production costs and improve the quality of welding.

Be sure, robots will help you to achieve these goals!

I.N. Shalaevsky, Head of Marketing Department.
Scientific and Production Company Tekhvagonmash

*Calendar of January**

January 1, 1932

Date of birthday of Anatoly Yakovlevich Ishchenko, a famous scientist, corresponding member of the NAS of Ukraine, Honoured Worker of Science and Technology of Ukraine. He made a significant contribution to the fundamentals of the theory of welding aluminum and magnesium alloys, in particular, concerning the problems of formation of oxide films, crystallization cracks during welding, interaction of the components of alloys with arc plasma, electron and laser beams.

January 2, 2009

Date of death of Daniil Andreevich Dudko, a prominent scientist in the field of welding and materials science, academician of the NAS of Ukraine, Honoured Worker of Science and Technology of Ukraine (1921–2009). He worked at the Electric Welding Institute, made a significant contribution to the research and development of processes of submerged-arc and carbon dioxide welding, electroslag welding, metallurgy, development of plasma-arc and microplasma welding methods and new spraying technologies. At the active participation of D.A. Dudko many developments were introduced in rocket production, electronics and power engineering. He is the author of more than 900 scientific papers.

January 3, 1927

One of the patents of the American Company «Harnischfeger Corporation» on modernization of the excavator was published. Applying modern technologies and welding, in 1935 this company for the first time in the world implemented the project of the first all-welded excavator. A year later, the company introduced the world's first all-welded hoisting crane with a box-type boom.

January 4, 2004

The construction of a missile boat of the Project 022 (Houbei class) was started, which is one of a series of 83 Chinese catamarans. This is the world's first missile-armed catamaran. It was designed according to the stealth technology. It is noteworthy that for creation of missile launch facilities, friction stir welding was applied.

January 5, 1935

Wilhelm Alert patented an improved method of thermit welding for railway tracks. In his device he applied a higher temperature, creating a special design which separated a welding zone with a high temperature from the base metal. Alert significantly simplified the system of joining and also used a preheating of the edges to be welded.

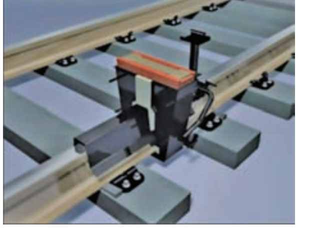

January 6, 1933

Date of birthday of David Mikhailovich Kaleko. He developed the scientific fundamentals of the technology of welding ferrous and nonferrous metals with a small section by an arc, burning during a discharge of capacitors, and the means for control of this process. He participated in creation of an installation for spot welding of aluminum alloys, automatic machines for percussion capacitor-type welding of parts of the electronics and radio industry. D.M. Kaleko also developed medical implants and tools of metal with a shape memory effect. He is the author of more than 172 scientific papers, including three monographs.

*The material was prepared by the company Steel Work (Krivoy Rog, Ukraine) with the participation of the editorial board of the Journal. The Calendar is published every month, starting from the issue of «The Paton Welding Journal» No.1, 2019.

January 7, 1935

Date of birthday of Valery Nikolaevich Kubasov (1935–2014), Soviet cosmonaut. On October 16, 1969, on the spacecraft Soyuz-6, the pilot-cosmonauts G.S. Shonin and V.N. Kubasov were the first in the world to perform welding in space. After depressurization of the inhabitant compartment, the cosmonaut-operator V.N. Kubasov, who sat in the descent vehicle, conducted experiments in automatic mode on plasma, electron beam and arc welding using consumable electrode.

January 8, 1910

The use of acetylene welding in the construction of pipelines for water supply was began, namely during the development of a natural water source in the United States. The construction of the three-kilometer pipeline was carried out by Central Colorado Power Co. The pipeline consisted of 200 sections of different diameters. The work took more than a year and a significant amount of carbide and oxygen was spent.

January 9, 1928

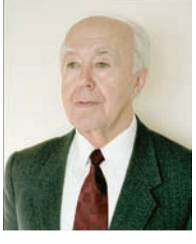

Date of birthday of Boris Alekseevich Movchan, an outstanding scientist in the field of materials science of metal and organic materials (amorphous, nanocrystalline, dispersion strengthened, laminated and porous) and protective coatings, as well as in the development and implementation of electron beam technologies and creation of new functional materials. B.A. Movchan is the academician of the NAS of Ukraine, the author of about 360 scientific papers and more than 100 patents for inventions.

January 10, 1972

Ship «Savannah», an experimental civilian vessel with a nuclear power unit, was taken off from the US Navy. It was created to demonstrate a potential for the peaceful use of nuclear energy. It was constructed in the late 1950s in the USA using the technology of arc welding with coated electrodes. The manufacturing process was controlled in detail using X-ray equipment. The vessel was in service since 1962 to 1972. It is one of four ever built merchant ships with a nuclear power unit. In 1981, «Savannah» was transferred to the exposition of the «Patriots Point Naval and Maritime Museum» in Monte Pleasant, South Carolina, USA.

January 11, 1805

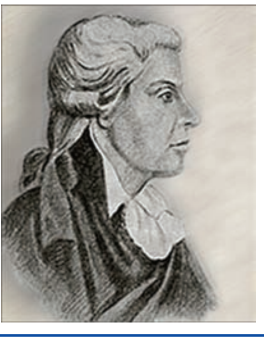

Date of death of Fontane Felice (1730–1805), Italian chemist and naturalist. He discovered a water (coke) combustible gas, which is produced from washing of burning hot coal with water and consists of hydrogen and carbon monoxide. Half a century later, this gas was actively used for heating the parts to be welded. In the 1930-1940s, forge welding and «water gas welding» were noted as separate varieties of the production process. In the same years, it was confirmed that the last of these methods can be used to weld sheets with a thickness in the range from 4 to 80 mm using a hammer or roller conveyers.

January 12, 1951

The scientists of Electric Welding Institute (N.G. Ostapenko, V.K. Lebedev, S.I. Kuchuk-Yatsenko, V.A. Sakharnov) for the first time in the world developed the method of flash-butt welding of rails using ring transformers applicable to joining of rails, pipes and other products. Flash-butt welding machines with ring transformers have 10–20 times lower short-circuit impedance in comparison with standard ones.

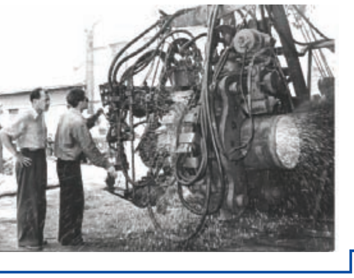

January 13, 1975

Beginning of Soviet-French Scientific Experiment ARAKS directed on investigation of ionosphere and earth magnetic field. An experiment technology has a lot of common points with the technology of electron beam welding as well as also uses kinetic energy of electrons in electron beam. The experiment is one of the world-known achievements of the PWI.

January 14, 1943

The patent was issued for a technology of tungsten electrode welding in helium to the staff members of Northrup Aircraft Inc. T.R. Piper, V.H. Pavleck and R. Meredith. Earlier at the end of 1941 R. Meredith developed a technology of argon TIG welding using direct current of reversed polarity and then using alternating current from IF transformer with high-frequency add-on.

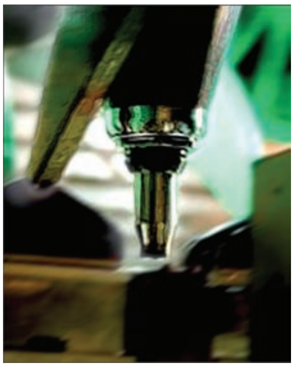

January 15, 1958

It was an order for US Navy atomic submarine Thresher (SSN-593). Later on it went down in the Atlantic ocean together with all crew. Thresher accompanied by rescue vessel ASR-20 Skylark put to sea for deep submergences. The aim of submergences was check of strength of vessel body at limiting for submarine depths (360 m). Due to the crack in the sea-water line weld an engine compartment of the submarine started to be filled with water. After loss of the submarine the investigation revealed numerous cases of technology violation, application of sub-standard materials and bad quality control of welds.

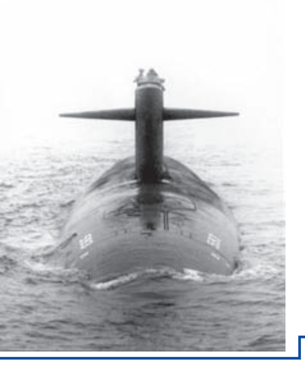

January 16, 1943

Tanker Schenectady fractured in two when returning to the base after a year of successful marine tests. The crack appeared in a sharp angle of the manhole on a deck, immediately passed through the deck and along the both shipboards until backbone. The message informed: «Schenectady tanker of 7320 t capacity fractured on smooth water at the wall of ship-building plant». Regardless the war, this event received wide publicity in the scientific press and served as a stimulus for development of the researches in the field of welding.

January 17, 1781

Birthday of Robert Hare (1781–1858) — American chemist. He designed a structure of oxygen-hydrogen torch. Works on development of reliable equipment were carried out in parallel with searching a gas composition for welding. First of all it was necessary to design the torch which would provide good mixing of gases with oxygen, high concentration of heat at the nozzle tip and explosion safety. Hare torch proposed in 1802 was one of the first devices deserving attention.

January 18, 1861

Birthday of Johann Wilhelm Goldschmidt (1861–1923) — well-known chemist. He entered the history as inventor of thermit welding method. The process taking place in this method sometimes is called «Goldschmidt reaction» or «Goldschmidt process». In 1898 Johann Goldschmidt for the first time performed thermit welding of two iron bars after their preliminary moulding and filling of the joint place with thermit mixture. After mixture burning the formed liquid pool was so overheated that provoked submelting of the edges and after solidification was transformed into the weld. Slag came to the surface and was easily removed from the place of joining.

January 19, 1833

Birthday of Henry Wilde — British scientist-engineer. In 1860th Henry Wilde welded the edges of wires of relatively large diameter with indirect electric arc applying the theories of Volta and Devy and primitive electric power sources. Henry Wilde was granted with a patent for his invention, which is known believed to be «electric welding patent».

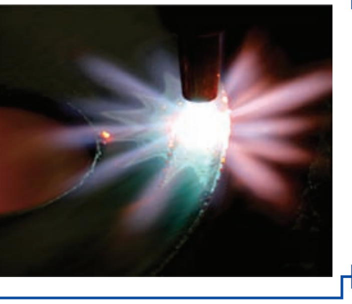

January 20, 1925

A.O. Smith Company registered one of their patents for welding of pipes. Company developed a method of resistance and flash welding and started practical application of the technology in production of longitudinally welded pipes with 5 mm wall thickness and 500 mm diameter, which were welded along the whole length (12 m) using machines of 5000 kV·A. In 1920th the engineers of the company developed a coating for welding rod, which they used in production till 1965 as well as the first method for arc welding of high-pressure pipes.

January 21, 1942

Fabrication of the first tank T-34, shell of which was for the first time welded using automatic welding. The welding technology was developed by the specialists of Electric Welding Institute. Efficiency of automatic welding was 10 times more than that in manual one.

January 22, 1971

Tamara Markovna Slutskaya (PWI) developed shelf-shielded activated electrode wires for arc welding. Addition of small quantities (5–7 wt.%) of salts of alkali and alkali-earth metals improves arcing stability in welding in CO_2 or its mixtures.

January 23, 1975

Boris Sergeevich Kasatkin, major scientist in the field of welding metallurgy, Corresp. Member of the NAS of Ukraine was awarded the E.O. Paton Prize of the NAS of Ukraine for a series of works on «Heat-hardened low-alloy high-strength steels for welded structures». Production of high-strength steels has been developed and mastered with his personal participation. These steels have been applied with success in manufacture of excavators, road bridges, mine skips, attachments, hydraulic works and other critical constructions. He is author of more than 300 scientific works, including eight monographs.

January 24, 1927

Birthday of Igor Konstantinovich Pokhnodnya, an outstanding scientist in the field of welding, academician of the NAS of Ukraine, Honoured Worker of Science and Technology. He made a significant contribution into the theory of welding processes (melting and transfer of electrode metal, absorption and desorption of gases by molten metal, influence of the electrode coating type on metal melting and transfer in welding). He participated in development of many grades of low-toxic and high-efficient electrodes and flux-cored wires; organized mass production of low-toxic welding consumables in several USSR enterprises. He is author of more than 900 scientific works, including 28 monographs.

January 25, 2004

«Opportunity» rover, delivered by rocket carrier Delta II, landed on Mars. This was the first rocket model, manufactured with application of friction stir welding. Pioneer Company Boeing started experimental application of the new joining method. Owing to its reliability, this method became applied in rocket construction.

January 26, 1946

Konstantin Konstantinovich Khrenov, major scientist in the field of welding, academician of the NAS of Ukraine, Honoured Worker of Science and Technology, was awarded the USSR State Prize «For development and introduction of the methods of electric welding and cutting under the water». During the years of World War II the laboratory led by K.K. Khrenov together with specialized teams performed a large scope of work on underwater repair of vessels, destroyed bridges and port facilities. He is author of more than 200 scientific works.

January 27, 1983

The longest undersea tunnel Seikan connecting the Japanese islands of Honshu and Hokkaido, has been completed. Final length of this railway tunnel was 53.9 km, including the underwater part of 23.3 km. The tunnel goes 100 m lower than the seabed level. The rails do not have any bolted butt joints; they are welded into one 54 km long section. This, apparently, is the longest welded railway track in the world.

January 28, 1951

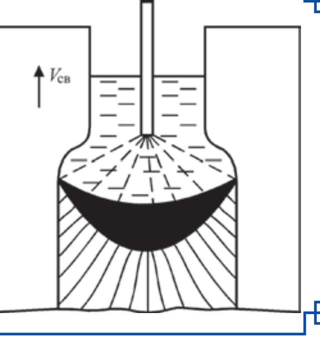

B.E. Paton and G.Z. Voloshkevich (PWI) for the first time created a fundamentally new process of electroslag welding of metals. It is designed for joining items of practically unlimited thickness in one pass. ESW became widely accepted in the USSR and abroad, fundamentally changing the technology of fabrication of thick-walled metal structures.

January 29, 1907

Swedish engineer, Oskar Kelberg, invented coated electrodes for welding and was granted a patent for the invention. His attention was drawn to welders' observation that the weld properties improve in those cases, when the electrodes or zones to be welded, were «stained» with lime, which contaminated the welding sites after making acetylene from calcium carbide. The same effect was produced by contamination, remaining on the wire surface after its drawing, which was conducted with application of lime.

January 30, 1991

John Bardeen, US physicist, died (1908–1991). After the end of World War II John Bardeen joined the Bell Company, where, working together with William Shockley and Walter Brattain, he participated in development of semiconductor devices, which can both rectify and enhance the electric signals. In 1956 Bardeen shared the Nobel Prize with Shockley and Brattain «for semi-conductor studies and discovery of the transistor effect». The transistor is one of the main components of the welding inverter.

January 31, 1964

Vladimir Ivanovich Trufiakov (PWI), known scientist in the field of bridge construction, Corresp.-Memb. of the NAS of Ukraine, Honoured Worker of Science and Technology of Ukraine, proposed and experimentally substantiated application of local explosion as a method of strengthening treatment of joints on large-sized structures. He also significantly developed the concepts of the effect of stress concentration, residual welding stresses, welding defects, frequency and kind of load on metal fatigue resistance. He is author of more than 240 scientific publications, including three monographs.

The journal Editorial Board will be grateful for additions and clarifications to the Calendar. Kindly send the materials to the following E-mail address: journal@paton.kiev.ua